Global satellite-based measurement of river and reservoir dynamics

by

Jiawei Hou

Submitted in fulfilment of the requirements for the degree of
Doctor of Philosophy
of the Australian National University

August 2020

Candidate's Declaration

This thesis contains no material which has been accepted for the award of any other degree or diploma in any university. To the best of the author's knowledge, it contains no material previously published or written by another person, except where due reference is made in the text.

This thesis is a **Thesis by Compilation**, as set out in ANU's Higher degree by research - thesis by compilation and thesis by creative works procedure (https://policies.anu.edu.au/ppl/document/ANUP_003405).

Jiawei Hou   Date: 28/08/2020

Acknowledgements

I would like to thank my supervisor Albert Van Dijk for offering me the opportunity to do a PhD project at my dream university, for getting me involved in such an amazing topic in satellite-based rivers, lakes, and reservoirs monitoring, for guidance and inspiration throughout the whole PhD journey, and for imparting me with a positive attitude towards life and work. I would also like to express my appreciation to Luigi Renzullo, and Robert Vertessy for guiding me in the completion of this work.

I am deeply grateful to all my co-authors: Norman Mueller, Hylke Beck, Yoshihide Wada, for your insightful suggestions and comments. Hylke Beck and Nathan Campbell are especially thanked for collating and sharing invaluable global in situ river discharge data and Australian reservoir storage data, respectively. I would also like to thank Zac Hatfield-Dodds and Pablo Larraondo for your friendly help in programming.

I will give a big thanks to Pietkiewicz family and Simon Walker for getting me involved in Australia's culture. I would also like to thank everyone at ANU Centre for Water and Landscape Dynamics, as well as staff and students at Fenner School of Environment & Society, for creating such a vibrant and friendly working environment.

Finally, to my partner Li Zhao, also a PhD "Endeavor", I must express my deepest appreciation. Thank you for all your love and encouragement on my life and work, and for your enthusiasm for experiencing a research career together. A special thanks also to my father, Kai Hou, and my mother, Libo Zhong. Thank you for raising me, and for the endless love and unconditional support for me.

Abstract

Knowledge of the dynamics of rivers and reservoirs is important to help manage the impacts of climate change and anthropogenic activities on water resources, which are intimately tied to human well-being, economic wealth and environmental health. However, ground-based measurements only capture a small fraction of water bodies, and in situ observed data are generally not publicly shared in most countries for a variety of reasons. Satellite remote sensing technology provides promising new opportunities to measure global water availability at different time and space scales. The objective of this study was to develop a global monitoring capacity to measure rivers, lake, and reservoir dynamics using satellite observation. In pursuit of this objective, I propose approaches to measure river discharge, river morphology, and lake (reservoir) storage based on remote sensing data. Satellite gauging reaches (SGRs) that can predict river discharge based on optical remote sensing are shown to be applicable to many rivers globally, especially in South America, Africa, and Asia. The river discharge prediction capability of SGRs in a certain river reach can be explained by its unique river morphology characteristics. Hydromorphological attributes, including spatial and temporal river width, flow regime and river gradient were produced for 1.4 million Australian river reaches, and can be used to improve river routing in models to better estimate river discharge. Finally, storage dynamics for 6,743 reservoirs worldwide for the period 1984-2015 were reconstructed based on satellite observations. The results indicate that some storages, particularly in southeastern Australia, central Chile, the USA, and eastern Brazil, have declined, accompanied by reduced reservoir resilience and increased vulnerability. Others have increased, mainly in the Nile Basin, Mediterranean basins and southern Africa. Multi-decadal changes in rainfall and hence streamflow were found to be the main reason for these changes. The techniques and data produced in this study provide components for a global monitoring capacity. The approaches developed can be used to process near real-time observations continuously. In future, the storage estimation method developed may be extended to lakes and wetlands. This study emphasizes the importance of increasing, or at least maintaining, the number of global gauging sites, which not only provide the historical context and current status of water resources under climate change, but also provide an indispensable basis to train remote sensing data in order to create a global water availability picture. Collaboration among different counties is urgently needed to share in situ river, lake, and reservoir data to tackle current and future water crisis, a challenge people worldwide face together. Considering the essential role of water resources for human well-being, new satellite missions are required that are specially designed for simultaneously measuring water extent and elevation in rivers, lakes, reservoirs, and wetlands at high spatial (e.g. 10 meters) and temporal (e.g. daily) resolution over the next decades.

Table of Contents

Chapter 1: Introduction

1.1 Background

Globally, rivers, lakes and reservoirs are the major sources of potable, irrigation and environmental water (Vörösmarty et al., 2010). Water exchange, laterally and vertically, between these water bodies and the atmosphere and the oceans play an essential role in the hydrological and biochemical cycles (Papa et al., 2008). Many rivers, lakes or reservoirs are highly dynamic at seasonal and inter-annual time scales, providing important ecosystem functions (Klein et al., 2017). Detailed measurement of inland surface water dynamics also provides basic and important information for policymakers, water managers, and researchers in a wide variety of disciplines (Sheffield et al., 2018).

Human activities and anthropogenic climate change have posed new threats to rivers, lakes, and reservoirs. Changes in lake extent and wetland flooding have been observed, for example in the world's saline lakes and endorheic basins (Wang et al., 2018, Wurtsbaugh et al., 2017), the declining number of lakes in the Arctic and on the Mongolian Plateau (Smith et al., 2005, Tao et al., 2015), decreases in spring and summer streamflow over California, USA (Barnett et al., 2008), and a shift in peak river flow to winter and early spring in snow-dominated regions (Barnett et al., 2005), to name a few. If of sufficient magnitude, such changes can alter global sea level rise and methane and carbon dioxide emissions (Chao et al., 2008), as well as threaten water availability and security, thereby causing economic damage and social instability (Schellekens et al., 2017). However, due to the lack of comprehensive river, lake and reservoir data, it is unclear whether such changes are part of a global trend or more local phenomena.

1.1.1 Limitations of in situ measurement

Since surface water is intimately linked to human well-being, economic wealth and environmental health, there is a need for mapping the distribution of water, quantifying storage and monitoring variations in river, lakes and reservoirs at local and global scales (Papa et al., 2010b). In situ measurement networks are highly unevenly distributed and in decline globally, and most gauging data are neither provided in real time nor publicly available. As a result, we have poor knowledge of the temporal and spatial dynamics of rivers and changes in water stored in lakes and reservoirs (Alsdorf et al., 2007). For instance, in northern high latitudes, 66% of the river gauging stations have stopped operating since 1985 (Birkinshaw et al., 2010, Nijssen et al., 2001). The density of river gauging stations in the eastern U.S. is two orders of magnitude greater than in the Amazon Basin, even though annual mean river discharge in the eastern U.S. is two orders of magnitude less in the Amazon Basin (LeFavour and Alsdorf, 2005). In situ lake data are rarely available, especially in areas that are inaccessible, remote or hindered by transboundary issues. Reservoir storage is presumably measured in most major dams, but not publicly shared in most countries for a variety of commercial, logistical, political and security reasons. All these

problems impede a better understanding of changes in rivers, lakes, and reservoirs affect our life and surrounding environment.

1.1.2 Opportunities of satellite remote sensing

Satellite remote sensing technology provides promising opportunities to measure and understand changes in water extent, level and volume in space and time. Recent years have seen vast improvements in the accessibility of remote sensing data (Tarpanelli et al., 2013). Establishing a global ground-based water monitoring network would require tremendous economic, technological and institutional support. In contrast, using remote sensing is a cost-effective way to acquire water information both at regional and global scales (Bjerklie et al., 2003).

There are three major types of remote sensing systems, i.e. optical remote sensing (visible radiation emitted from the sun and then reflected from the Earth's surface), passive microwave remote sensing (low frequency radiation emitted by the Earth's surface directly), and active remote sensing (emitted by the instrument and then reflected from the Earth's surface). Active remote sensing instruments, such as radar altimeters, are able to measure surface water elevation, but miss a large fraction of surface water bodies around the world because of the wide gaps between successive satellite orbits. Passive microwave remote sensing can provide imagery of spatial and temporal water extent variations at global scale under all weather conditions, but its spatial resolution is quite coarse. Optical remote sensing can not only provide high spatial resolution information of global surface water bodies (e.g. Landsat and SPOT), but also yield frequent and ongoing data (e.g. AVHRR and MODIS). Although cloud contamination limits the capability of optical sensors to detect surface water, optical sensors are still the most powerful means to produce consecutive spatio-temporal imagery over long time-spans. Therefore, my study is mainly based on optical remote sensing, from instruments such as MODIS and Landsat.

The Moderate Resolution Imaging Spectroradiometer (MODIS) is a mid-resolution optical sensor aboard the Terra (launched in 1999) and Aqua satellites (launched in 2002). Bands 1-2 in red and near-infrared wavelengths have a spatial resolution of 250 m and bands 3-7 in green, blue and the mid-infrared wavelengths have a spatial resolution of 500 m. MODIS has rich time-series data attributed to two observations per day for every point in the planet, which makes it useful to measure open water body dynamics, especially near-real time inundation, flood recurrence and large reservoir water extent. However, the capabilities of MODIS are limited by relatively low spatial resolution and cloud contamination. At a spatial resolution of 250-500 m, water bodies less than a pixel cannot be detected by MODIS. Moreover, floods regularly happen at the same time as cloud-borne rainfall events, which limits the amount of available data for peak floods.

The Landsat series of satellites operates since 1972 and continues to provide long-term space-based images of natural and human-influenced changes on the landscape at global scale. Landsat 1, Landsat 2, and Landsat 3 had an 18-day repeat cycle. The Multispectral Scanner (MSS)

provides 80 m spatial resolution images in the wavelength ranging from visible blue to near-infrared. Landsat 4 and Landsat 5 had a repeat cycle of 16 days. The improved Thematic Mapper (TM) provides 30 m spatial resolution images in the spectrum of the visible, near-infrared and shortwave infrared wavelengths. Landsat 6 failed to reach orbit. But the mission is continued by Landsat 7 and Landsat 8, which have the same orbit with Landsat 4 and Landsat 5. The Enhanced Thematic Mapper Plus (ETM+) on aboard Landsat 7 has same bands with TM while the Operational Land Imager (OLI) carried by Landsat 8 extend the shortwave infrared band. All these features enable Landsat to measure a large number of surface water bodies at different sizes and provide long-term dynamics information for trend analysis. The drawback of Landsat's application is low temporal resolution, which could be further worsen by cloud contamination.

1.1.3 Satellite-based river and reservoir measurement

Combining satellite and in situ observations, we have gained much knowledge of water resources on Earth. According to the HydroLAKES and the Global Reservoir and Dam database (GRanD), there are a total of 2.67×10^6 km^2 of natural lakes and 0.26×10^6 km^2 of human-made reservoirs with a surface water area greater than 0.10 km^2, and these water bodies cover about 2% of the global land area. The total shoreline length of reservoirs and lakes is approximately four times the global ocean shoreline (Lehner et al., 2011, Messager et al., 2016). According to the Global River Widths from Landsat (GRWL) Database, the total surface area of rivers and streams at mean annual discharge is roughly 7.73×10^5 km^2, which is about 0.58% of Earth's non-glaciated land surface (Allen and Pavelsky, 2018). However, we are facing challenges that employ satellite observations from two-dimensional applications, e.g. surface area, towards three-dimensional usage, e.g. to estimate river discharge and storage in lakes and reservoirs. For example, there are still technical and operational difficulties to produce bathymetric maps of rivers, lakes, or reservoirs, which currently require time- and cost-intensive survey methods (e.g. acoustic profiling). In addition, there is a widespread need of dynamic information, rather than static measurement.

The most common approach to estimate river discharge from space has been to use in situ river discharge measurements to train remote sensing imagery based on hydraulic geometry theory or at-a-station hydraulic geometry (AHG) (Leopold and Maddock, 1953), involving power-law relationships between discharges observed in situ and, remotely sensed river width (Pavelsky, 2014, Smith et al., 1996, Smith et al., 1995, Smith and Pavelsky, 2008), or river surface water height (Birkinshaw et al., 2010, Coe and Birkett, 2004, Kouraev et al., 2004, Papa et al., 2010a, Tourian et al., 2013). Recently, there has been a test of using at-many-stations hydraulic geometry (AMHG). Gleason and Smith (2014) found that the parameters of AHG are log-linearly related along a river, and were able to estimate river discharge from remote sensing (e.g. Landsat) derived widths at multiple river cross sections (Gleason and Wang, 2015, Shen et al., 2016). Alternatively, the ratio of the Advanced Microwave Scanning Radiometer (AMSR-E) passive microwave brightness temperature or Moderate Resolution Imaging Spectroradiometer (MODIS)

near-infrared reflectance between a wet measurement grid cell and its nearby dry calibration grid cell has become another pragmatic tool that can be trained using in situ data and used as a simple and computationally efficient approach to predict river discharge (Brakenridge et al., 2012, Brakenridge et al., 2007, Revilla-Romero et al., 2015, Tarpanelli et al., 2013, Van Dijk et al., 2016). A simpler automated statistical method that can be readily applied globally and provide near real-time information even also at ungauged reaches is required.

River width is an essential parameter associated with river morphology. It can be used to assess river conveyance, calculate river discharge, and improve river routing in hydrological and hydraulic models (Yamazaki et al., 2014). Lack of detailed data on river width is an impediment to improving river routing in state-of-the-art hydraulic and hydrologic models, as model development moves toward higher spatial resolution and larger spatial scale to better understand storage and flow of water across continents. River widths at mean discharge in the Mississippi Basin and across the globe were measured by Allen and Pavelsky (2015) and Allen and Pavelsky (2018), using RivWidth, a software tool (Pavelsky and Smith, 2008). Another automated analysis and mapping engine, RivMap, developed by Isikdogan et al. (2017), was used to estimate river width for North America. In line with these software tools, Yamazaki et al. (2014) developed an automated algorithm and used it to generate river width dataset for large rivers globally. However, none of these datasets provides information on temporal variability of river width or river width beyond overbank flow conditions.

Lake and reservoir storage variations can be estimated based on measurements of surface water level and inundation area, either or both of which can be derived from satellite observation (Busker et al., 2019, Crétaux et al., 2011, Gao et al., 2012, Medina et al., 2010, Tong et al., 2016, Zhang et al., 2014). There are several altimetry databases, including the Database for Hydrological Time Series of Inland Waters (DAHITI), the European Space Agency's (ESA) River and Lake data set, the French Space Agency Centre National d'Etudes Spatiales' (CNES) Hydrology by Altimetry, and Global Reservoirs and Lakes Monitor (G-REALM) from the United States Department of Agriculture Foreign Agricultural Service. But this approach is only suitable to a limited number of lakes and reservoirs worldwide due to wide gaps between the satellite altimetry tracks. Messager et al. (2016) estimated the volume of lakes and reservoirs with a surface area greater than 0.10 km^2 at global scale using a geo-statistical model based on surrounding topography information, but these estimates were not dynamic time series.

1.2 Objectives

The main objective of the research presented in this thesis was to develop elements of a global monitoring capacity that can provide spatial and temporal river, lake, and reservoir information derived from satellite observation. Such an information system should be a valuable platform for policymakers, researchers and society, to understand how climate change and anthropogenic activity affect global rivers, lakes, and reservoirs. It would allow any users to

access historical and current information on the state of water resources, either at global scale or in their region of interest. To pursue this objective, the research focused on measuring spatial and temporal river discharge, river morphology, reservoir storage based on remote sensing data, and aimed at answering the following research questions:

a) Can we use remote sensing to estimate river discharge at both gauged and ungauged river reaches globally?

b) What are the merits and drawbacks of using optical and passive microwave remote sensing, respectively, to predict river discharge?

c) What is the influence of river morphology on the application of remote sensing to measure river discharge?

d) Can we derive a satellite-based parameter to describe river reaches by the degree to which flow regime tends towards permanent, frequent, intermittent, or ephemeral?

e) What are the relationships between river width and contributing catchment area, river discharge, and reach gradient?

f) How do climate change and anthropogenic activities affect the flow in rivers and storage in reservoirs?

1.3 Structure

This thesis is a **Thesis by Compilation**, as set out in ANU's Higher degree by research - thesis by compilation and thesis by creative works procedure (https://policies.anu.edu.au/ppl/document/ANUP_003405). The content in each of **Chapter 2 to 5** is one paper published in, or submitted to, a peer-review journal. The first three chapters have been published and are included in their published version whereas the paper corresponding to the fourth chapter is currently under review. **Chapter 2 and 3** propose an approach to estimate global river discharge and answer research questions (a)-(c) above. **Chapter 4** produces river morphology data and addresses research questions (d) and (e). **Chapter 5** reconstructs global reservoir storage dynamics and discusses climate change and anthropogenic influences as per question (f). **Chapter 6** concludes the main findings of this study and outlines suggestions for future investigations. **Appendix 1 to 3** includes the supplementary material for **Chapter 2, 3 and 5**, respectively. Based on all data and methods developed in this study, **Appendix 4** propose a global near real-time river, lake and reservoir monitoring system. It was published as a conference paper.

Chapter 2: Using modelled discharge to develop satellite-based river gauging: a case study for the Amazon Basin

This chapter compares two methods to estimate river discharge at ungauged river reaches through a case study in the Amazon Basin and discusses the advantages and disadvantages of using optical and passive microwave remote sensing to measure river discharge. The content of this chapter was published in the journal Hydrology and Earth System Sciences as follows:

Hou, J., Van Dijk, A.I.J.M., Renzullo, L.J. and Vertessy, R.A., 2018. Using modelled discharge to develop satellite-based river gauging: a case study for the Amazon Basin. Hydrology & Earth System Sciences, 22, https://doi.org/10.5194/hess-22-6435-2018.

Using modelled discharge to develop satellite-based river gauging: a case study for the Amazon Basin

Jiawei Hou[1], Albert I. J. M. van Dijk[1], Luigi J. Renzullo[1], and Robert A. Vertessy[1,2]

[1]Fenner School of Environment and Society, Australian National University, Canberra, Australian Capital Territory, Australia
[2]School of Engineering, University of Melbourne, Melbourne, Victoria, Australia

Correspondence: Jiawei Hou (jiawei.hou@anu.edu.au)

Abstract. River discharge measurements have proven invaluable to monitor the global water cycle, assess flood risk, and guide water resource management. However, there is a delay, and ongoing decline, in the availability of gauging data and stations are highly unevenly distributed globally. While not a substitute for river discharge measurement, remote sensing is a cost-effective technology to acquire information on river dynamics in situations where ground-based measurements are unavailable. The general approach has been to relate satellite observation to discharge measured in situ, which prevents its use for ungauged rivers. Alternatively, hydrological models are now available that can be used to estimate river discharge globally. While subject to greater errors and biases than measurements, model estimates of river discharge do expand the options for applying satellite-based discharge monitoring in ungauged rivers. Our aim was to test whether satellite gauging reaches (SGRs), similar to virtual stations in satellite altimetry, can be constructed based on Moderate Resolution Imaging Spectroradiometer (MODIS) optical or Global Flood Detection System (GFDS) passive microwave-derived surface water extent fraction and simulated discharge from the World-Wide Water (W3) model version 2. We designed and tested two methods to develop SGRs across the Amazon Basin and found that the optimal grid cell selection method performed best for relating MODIS and GFDS water extent to simulated discharge. The number of potential river reaches to develop SGRs increases from upstream to downstream reaches as rivers widen. MODIS SGRs are feasible for more river reaches than GFDS SGRs due to its higher spatial resolution. However, where they could be constructed, GFDS SGRs predicted discharge more accurately as observations were less affected by cloud and vegetation. We conclude that SGRs are suitable for automated large-scale application and offer a possibility to predict river discharge variations from satellite observations alone, for both gauged and ungauged rivers.

1 Introduction

River discharge data are used to monitor the global water cycle, assess flood risk, and guide water resource management (Brakenridge et al., 2012). Example applications also include the assessment of the contribution of river flow to oceans and the distribution of river runoff on continents; the training of models to predict how water resources will be affected under climate change; the identification of where flood intensity and frequency is likely to increase; the provision of information for flood forecasting, monitoring, and warning systems; and the better formulation of water allocation plans for domestic, agricultural, and industrial uses (Van Dijk, 2015).

Over the past century, many ground-based gauging stations have been built to monitor river discharge across the world (Dai et al., 2009). However, the number of accessible gauging station records has decreased over the years due to the reluctance of contributors to share data, or the lack of financial and technical support to maintain gauging stations (Vörösmarty, 2001; Biancamaria et al., 2011; Brakenridge et al., 2012; Fekete et al., 2012). In addition, gauging station networks are sparse and unevenly distributed. For instance, there are few gauging stations on rivers with braided channels or wide floodplains, and on rivers located in remote areas (Smith et al., 1996; Alsdorf et al., 2003; LeFavour and Alsdorf, 2005; Calmant and Seyler, 2006). Finally, gauging sta-

tions are only representative for a single point along a river, which can make it difficult to obtain insight into hydrological conditions throughout river networks (Hunger and Döll, 2008; Stahl et al., 2012).

Remote sensing is a cost-effective way to acquire information on river dynamics both at regional and global scales (Alsdorf et al., 2007). Satellite observations can cover a river in the lateral dimension where there are wide channels or broad floodplains and in the longitudinal dimension in long and complex river systems (Smith, 1997; Bjerklie et al., 2003). Whereas gauging stations measure water level, remote sensing typically measures river extent or width with the exception of river altimetry (Birkett et al., 2002; Coe and Birkett, 2004; Kouraev et al., 2004; Zakharova et al., 2006; Papa et al., 2010). Such satellite-based measurements can be related to measured river discharges. The general approach has been to develop rating curves relating satellite observation where they coincide with in situ river discharge measurement, and to use the fitted rating curves to estimate river discharges with satellite observations only (e.g. Revilla-Romero et al., 2014).

Optical and microwave satellite imaging can provide continuous spatial observations of surface water extent along the entire river channel. Both inundation–discharge and width–discharge relationships can be developed using ground measurements of river discharge and satellite optical or synthetic aperture radar (SAR) imagery (Smith et al., 1995, 1996; Papa et al., 2008; Smith and Pavelsky, 2008; Pavelsky, 2014). In addition, Brakenridge et al. (2007), Tarpanelli et al. (2013), and Van Dijk et al. (2016) demonstrated that the ratio of a calibration and measurement pixel remote sensing signal for Moderate Resolution Imaging Spectroradiometer (MODIS) near-infrared reflectance or AMSR-E passive microwave brightness temperature can be an indicator of variations of river discharge, which provides opportunities to monitor river discharge at a global scale with medium spatial resolution and high temporal resolution. However, optical remote sensing requires a clear view of the water surface, unobscured by cloud or a dense vegetation canopy. While radar and passive microwave remote sensing are not affected by these factors to the same extent, radar is susceptible to wind-induced waves and vegetation above surface water, whereas the resolution of passive microwave imagery is too coarse for many rivers. As an alternative to the rating curve approach, open-channel hydraulic equations such as the Manning equation can be used to estimate river discharge from remotely sensed data. However, in addition to remotely sensed data, additional field data including river depth and roughness coefficient are needed to apply this method and can introduce large uncertainties, which limits its predictive performance (Te Chow, 1959; LeFavour and Alsdorf, 2005; Jung et al., 2010; Woldemichael et al., 2010; Michailovsky et al., 2012).

The main disadvantage of all methods described above is that in situ measurements are still necessary, which makes it impossible to apply them at ungauged sites and unsuitable for automated large-scale applications. An alternative is to use hydrological models to estimate river discharge throughout river networks and to relate these estimates to satellite imagery. In this paper we investigate whether satellite gauging reaches (SGRs) can be established at both gauged and ungauged rivers and applied to provide continuous, consistent, and up-to-date river discharge monitoring over a large area. A SGR, analogous to an in situ gauging station, is constructed based on an automated statistical method which relates hydrological model simulated river discharge to optical or passive microwave-derived surface water extent fraction for a region that includes the river reach. The concept of a SGR is similar to that of a "virtual station" used in satellite altimetry (Calmant and Seyler, 2006), but acknowledges that river surface water extent is measured along a river reach rather than at a single cross section. In the first part of this paper, we design and compare two methods to construct SGRs, and then choose the best method and evaluate its performance. In the second part, we construct SGRs based on optical or passive microwave observations and simulated river discharges, then compare river discharge estimates from optical and passive microwave observations and from the hydrological model to in situ river discharge measurements. We hypothesize that SGRs may perform better than the hydrological model if the model has poor timing, or worse if the model is already quite good. In the latter case, however, SGRs may still be useful for monitoring river discharge in the absence of a real-time hydrological model or gauging stations.

2 Data and methods

The fundamental assumption in our methodology is that there exist strong, monotonic relationships between remote sensing signal, surface water extent, river channel storage, and river discharge. Surface water extent fraction (hereafter, *water extent*) was previously derived from Global Flood Detection System (GFDS) passive microwave and MODIS optical remote sensing signal by Van Dijk et al. (2016). River storage and discharge were estimated by the World-Wide Water (W3) model version 2 (Van Dijk et al., 2018). First, we designed two alternative methods to develop SGRs with the aid of hydrological model estimates and compared performance of these methods on rivers of different sizes. We then applied the method that performed best across the Amazon Basin. Second, SGRs were constructed across the Amazon Basin based on MODIS and GFDS water extent. The derived river discharge estimates from the SGRs and from the W3 model were evaluated against in situ river discharge measurements at 31 stations. The overall methodology is shown in Fig. 1.

2.1 Study region

We chose the Amazon Basin as a case study in this research. The Amazon Basin serves as a suitable test bed for
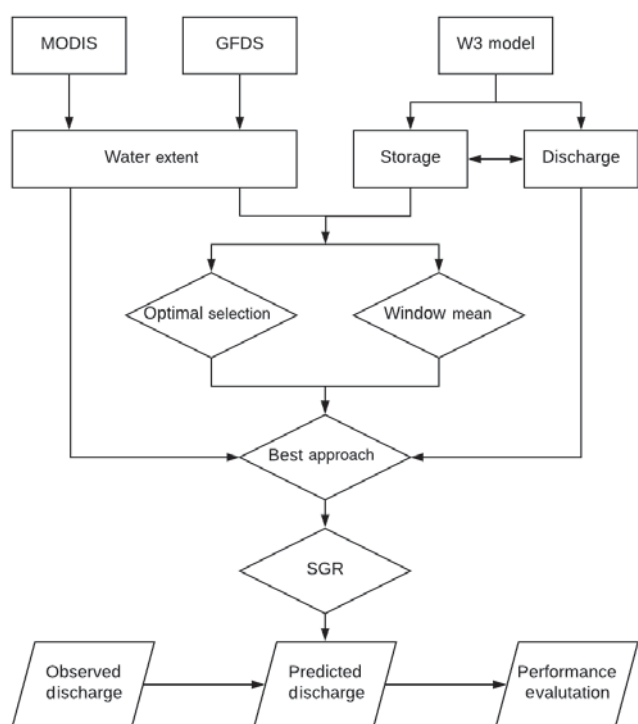
Figure 1. Workflow of the overall methodology (rectangle: data; diamond: method; parallelogram: validation).

our method in that it contains numerous inaccessible river reaches surrounded by dense tropical rainforests, frequently flooded areas, extremely wide river floodplains, and braided river channels. Moreover, it has unregulated rivers of widely varying size, which provides an opportunity to assess the sensitivity of spatial resolution in remote sensing to river size. In addition, because rainfall estimates across the Amazon Basin are generally poor, it is meaningful to test whether modelled discharge can be improved through remote sensing. A challenge is that MODIS observations are often affected by cloud cover. Van Dijk et al. (2016) found strong correlations between optical and passive microwave-derived water extent estimates and station discharge observations in the Amazon Basin, from which we infer that there may be further opportunities to develop satellite-based river gauging using modelled discharge at ungauged sites.

2.2 Data

2.2.1 Remote sensing

The Global Flood Detection System (GFDS) was developed to monitor floods and is operated by the Joint Research Centre of the European Commission, in collaboration with the Dartmouth Flood Observatory. De Groeve et al. (2015) proposed a discharge signal, s, as the ratio of brightness temperatures between a targeted wet pixel (measurement pixel) and a nearby dry pixel (calibration pixel), which allows tracking of relative changes in surface water extent within a river reach. The discharge signal s was calculated from brightness temperature recorded at 36.5 GHz in the H polarization by the Japanese Space Agency's AMSR2 and TRMM TMI sensors and NASA's AMSR-E and GPM instruments. The GFDS raster data product used here, named "merged 4-day average datasets", provides daily s as an average value of the signal for the current day and the signal from the last 3 days, with a spatial resolution of $0.09° \times 0.1°$ over the period of 2000–2014.

MODIS is an optical sensor aboard the NASA's Terra and Aqua satellites, which provide two images per day for almost every point on the planet. The surface observing capability of MODIS is limited by cloud cover, but this can be mitigated by using MODIS 8-day or 16-day composites which reduce the influence of cloud contamination. The MODIS data used here are the shortwave infrared (SWIR) spectral band 7 (2105–2155 nm) data from the MCD43C4.005 product which contains 8-day nadir BRDF (bidirectional reflectance distribution function) adjusted reflectance (NBAR) composites of imagery over the period of 2000–2014. The optical data were aggregated to a spatial resolution of $0.05° \times 0.05°$. The method to calculate surface water extent fraction from GFDS and MODIS data was described by Van Dijk et al. (2016). We calculated both 8-day and monthly GFDS- and MODIS-derived surface water extent fraction across the Amazon Basin.

2.2.2 Hydrological model

The World-Wide Water (W3) model version 2 (Van Dijk et al., 2018) is a global implementation of the Australian AWRA-L model, a grid-based, one-dimensional water balance model with semi-distributed representation simulating soil, groundwater, and surface water stores (Van Dijk, 2010). AWRA-L is used operationally by the Australian Bureau of Meteorology to estimate the daily water balance component across Australia at a spatial resolution of $0.05° \times 0.05°$ (Frost et al., 2016). Each grid cell has three soil layers (top, shallow, and deep soil layers) and one unconfined groundwater layer, and hydrological processes considered in the model include (1) net precipitation and interception losses; (2) saturation excess overland flow, infiltration excess surface runoff, and infiltration; (3) soil water evaporation, drainage, and interflow; (4) groundwater evaporation and base flow; (5) vegetation transpiration and cover adjustment; (6) surface water evaporation, inflows from runoff and discharge, and catchment water yield. Details about the W3 model including input data, parameterization, calibration, and validation can be found in Van Dijk et al. (2018). The model was not calibrated against gauging data used in this study. Daily simulated river channel storage and discharge in $0.05° \times 0.05°$ grid cells were used in this research and averaged to 8 days to relate them to remote sensing data. The W3 model estimates of river chan-

nel storage, rather than discharge, are compared with optical and passive microwave-derived water extents because conceptually they are more closely related. However, river channel storage has a linear relationship with discharge within the W3 model structure.

2.2.3 In situ river discharge measurement

Monthly in situ river discharge measurements were collected from two datasets developed by Beck et al. (2015) and Dai (2016) respectively. The former dataset was established to combine global unregulated river discharge data from the Global Runoff Data Centre (GRDC) and the USGS GAGES II (Geospatial Attributes of Gauges for Evaluating Streamflow) databases. The same data were used in a precursor to this study (Van Dijk et al., 2016). The latter dataset was developed to compile river flow data from the farthest downstream gauging stations of the world's largest 925 rivers. Among these two datasets there are 31 gauging stations located inside the Amazon Basin with records that were fully or partially overlapping with the remote sensing and model simulation records.

2.3 Method

2.3.1 Satellite gauging reach designs and performance evaluations

In developing SGRs, we tested two alternative methods to correlate remotely sensed water extent with modelled river channel storage. Method A finds the most strongly correlated water extent over a search window, which we refer to here as *optimal grid cell selection*. Method B calculates the spatial average water extent within a search window, referred to here as the *window mean*. We experimented with different window sizes: $0.15° \times 0.15°$, $0.35° \times 0.35°$, $0.55° \times 0.55°$, $0.75° \times 0.75°$, and $0.95° \times 0.95°$ (Table 1). These 10 experiments (two methods for each of the five search windows) were applied for each grid cell of the W3 model along a river channel across the Amazon Basin, using 8-day MODIS- and GFDS-derived water extent estimates, respectively. For each grid cell, the steps are as follows: a search window centres on a target grid cell of the W3 model, and simulated storage time series for the target cell and all water extent time series located within the search window are selected. Next, in method A, the storage time series is compared with each water extent time series, and the one with the strongest correlation is chosen to develop the SGR. In method B, spatial average water extent time series across the window is calculated and used to develop the SGR.

To test which of the two methods best estimates storage for different river sizes, we divided river reaches into four categories based on their mean simulated discharge over the period 2000–2014. The four categories of river were defined as small (10^2–10^3 m^3 s^{-1}), medium (10^3–10^4 m^3 s^{-1}),

Table 1. Experiment design (window size) for two methods to develop SGRs.

| Experiments	I	II	III	IV	V
Optimal selection	0.15°	0.35°	0.55°	0.75°	0.95°
Window mean	0.15°	0.35°	0.55°	0.75°	0.95°

large (10^4–10^5 m^3 s^{-1}), and very large ($> 10^5$ m^3 s^{-1}) rivers (Fig. 2). We did not consider rivers where discharge is less than 10^2 m^3 s^{-1} as we assume that they would have channel widths that could not be resolved using our sensing and modelling methods. The most suitable window overall and the SGR selection method were subsequently decided upon based on performance statistics.

The superior method was applied to construct SGRs across the Amazon Basin, using 8-day MODIS and GFDS water extent, respectively. For method A, the time series was split into training and validation periods to ensure independent validation. Data for the training period were used to select the best correlating pixel for each model grid cell, while data from the validation period were used to evaluate SGRs' performance. We evaluated the results from three experiments: (I) training: 2005–2014, validation: 2000–2004; (II) training: 2000–2004 and 2010–2014, validation: 2005–2009; and (III) training: 2000–2009, validation: 2010–2014 (Table 2). The mean result was adapted as the overall evaluation statistic. For method B, spatial average water extent for the whole period of 2000–2014 was compared to storage directly, as this produces the same results as using the cross-validation method. The performance of SGRs was assessed using Spearman's rank correlation (ρ), since the relationship between water extent and storage is often non-linear.

2.3.2 Evaluations of satellite gauging reaches and the W3 model

A Spearman correlation $\rho > 0.6$ in a grid cell ($0.05° \times 0.05°$) was used to identify a potential river reach for developing a SGR. We constructed a SGR for this river reach based on water extent and modelled discharge. The developed SGR was used to estimate river discharges using satellite observations only. We used the same training and validation periods described in Sect. 2.3.1 (Table 2). In the training period, both model and remote sensing data were used to establish a relationship between water extent and discharge. Remote sensing data for the validation period were used to estimate river discharge from SGRs using the developed relationship. To ensure the relationship can be transferred from the model simulation to the SGR, it was necessary to eliminate systematic differences between the two time series. Because the distribution of discharge is non-Gaussian, a simple transform by the first two statistical moments produced poor results. Better results were achieved through cumulative distribution func-
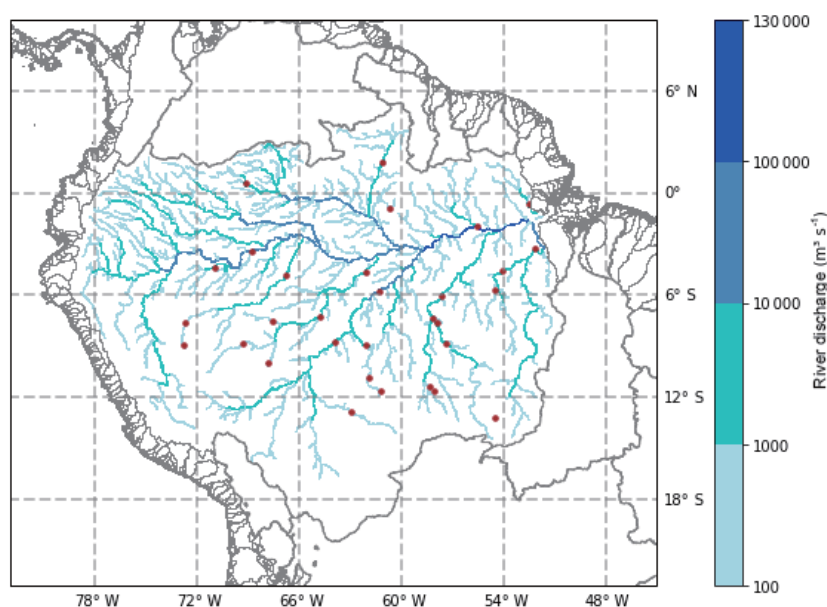
Figure 2. The W3 model simulated mean river discharges ($> 100\,\mathrm{m^3\,s^{-1}}$) in the Amazon Basin (grey line: basin boundary; brown dot: gauging station).

Table 2. Training and validation periods for the cross-validation method.

Periods	I	II	III
Training period	2005–2014	2000–2004 & 2010–2014	2000–2009
Validation period	2000–2004	2005–2009	2010–2014

tion (CDF) matching. Following the approach of Van Dijk et al. (2016), we used a rank-based look-up-table approach to estimate river discharge from mapped water extent. Estimates of water extent in the validation period are ranked relative to the estimate water extents in the training period, and CDF matching is then used to provide corresponding river discharge estimates over the validation period. The combination of river discharge estimates from the three validation periods was lumped to represent performance over the whole study period of 2000–2014. Overall, we obtained three river discharge estimates from MODIS, GFDS, and the model. All were then validated and evaluated against monthly in situ river discharge measurement (daily in situ data were not available for most stations).

3 Results

3.1 Evaluations of satellite gauging reach designs

The 10 experiments described in Sect. 2.3.1 for relating remotely sensed water extent to simulated river channel storage were compared, using MODIS and GFDS water extent, respectively. For MODIS, irrespective of window size or SGR selection method, the mean ρ between water extent and storage increases and the range of ρ narrows as discharge becomes larger (Fig. 3). For the small rivers (10^2–$10^3\,\mathrm{m^3\,s^{-1}}$), the optimal selection method (method A) achieved mean $\rho < 0.6$, while the window mean method (method B) resulted in mean $\rho < 0.3$. In contrast, in the main Amazon River channel, method A produced mean $\rho > 0.7$, while method B resulted in mean $\rho > 0.5$. Across all categories of discharge (Fig. 3a–d), method A produced ρ that increases as the window size increases, and method B produced inconsistent results. In the same way, the mean ρ in GFDS cases also increases as discharge rises (Fig. 4). Both methods showed similar results as the mean ρ grows as the window size becomes larger (Fig. 4a–d). For small rivers, both methods produced mean $\rho < 0.5$, while they achieved mean $\rho > 0.4$ in the main Amazon River channel. Overall, MODIS performed better than GFDS, and method A performed better than method B. Although the $0.95° \times 0.95°$ window size produced better results, larger windows increased the risk of selecting pixels over nearby rivers rather than the target river. We found that using method A with a search window of $0.55° \times 0.55°$ was the best overall approach for developing satellite-based river gauging.
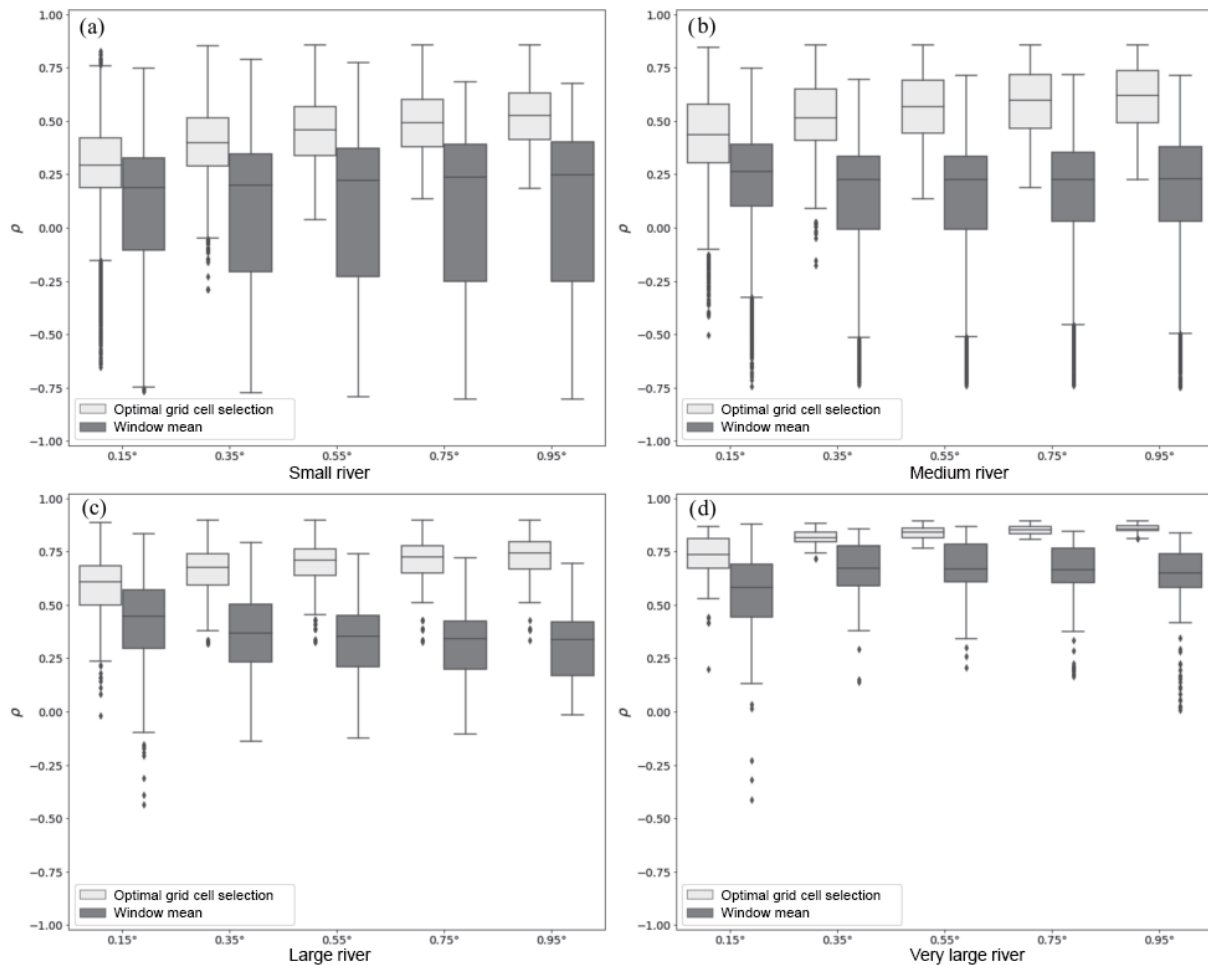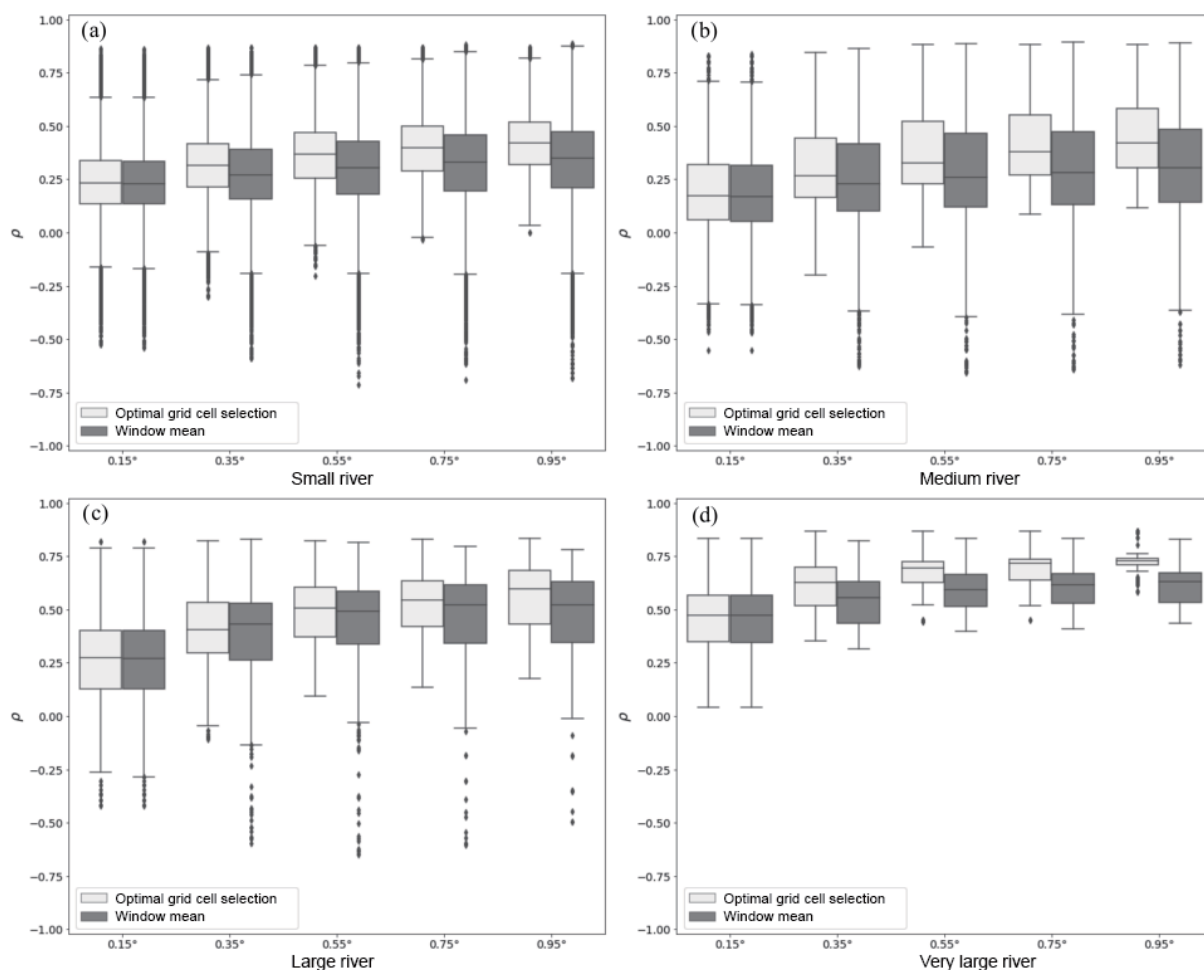
Figure 3. Distributions of Spearman's rank correlation between MODIS water extent and simulated storage using different window sizes (0.15° × 0.15°, 0.35° × 0.35°, 0.55° × 0.55°, 0.75° × 0.75°, and 0.95° × 0.95°) and two approaches (light grey: optimal grid cell selection (method A); dark grey: window mean (method B)) in four categories of river flow across the Amazon Basin. Outliers are data beyond the distance larger than 1.5 times the interquartile range from the first and third quartiles.

This approach was applied across the Amazon Basin using MODIS and GFDS water extent respectively (Fig. 5a–b). For MODIS SGRs, there were strong relationships ($\rho > 0.6$) between water extent and storage in most reaches of the main river channel and its large tributaries, particularly in the larger channels ($\rho > 0.8$), while there were weak correlations ($\rho < 0.4$) in upstream tributaries. The overall performance of the MODIS SGRs was superior to the GFDS SGRs. For GFDS SGRs, there were more river reaches with low correlations ($\rho < 0.4$) in upstream tributaries, and the lower reach of the Amazon River did not show continuous high correlations ($\rho > 0.8$).

3.2 Performance of satellite gauging reaches and the W3 model

We defined river reaches where ρ between water extent and storage is greater than 0.6 as potential locations for developing useful SGRs (Fig. 5). While there were 31 gauging stations in the Amazon Basin, only 10 gauging stations coincided with MODIS potential SGR sites and 5 with GFDS sites. Thus, we only assessed river discharge estimates for these 15 cases. Monthly river discharge estimates from MODIS, GFDS, and the model for the period of 2000–2014 were compared against monthly in situ river discharge measurements (Fig. 6). We focused on flow pattern comparisons between predicted and observed discharges, so different vertical axes were chosen to bring them close to each other (observations from gauging stations are shown on the right axis and river discharge estimates derived using remote sensing

Figure 4. Distributions of Spearman's rank correlation between GFDS water extent and simulated storage using different window sizes ($0.15° \times 0.15°$, $0.35° \times 0.35°$, $0.55° \times 0.55°$, $0.75° \times 0.75°$, and $0.95° \times 0.95°$) and two approaches (light grey: optimal grid cell selection (method A); dark grey: window mean (method B)) in four categories of river flow across the Amazon Basin. Box plots are defined as in Fig. 3.

and model on the left axis). The W3 model yielded good estimates, with Pearson correlation (R) generally greater than 0.8 across most sites. A total of 7 of the 10 MODIS SGRs estimated river discharge with R above 0.7, and the SGR for gauging stations G12 and G31 performed best, with R close to 0.9. Overall, MODIS SGRs estimates were not as skilful as the model, with the exception of the one for gauging station G12. While there were fewer potential sites for GFDS SGRs, they were similarly or more skilful than the MODIS SGRs. For gauging stations G12 and G19, GFDS produced better river discharge estimates than either MODIS or the W3 model. Overall, estimated river discharges from the SGRs and the model showed similar flow fluctuations to in situ river discharge observations. The performance of daily, 8-day, and monthly MODIS and GFDS SGRs are compared and discussed in the Supplement (Fig. S1).

4 Discussion

The relationship between remote sensing signal, water extent, river channel storage, and discharge enabled the estimation of river discharge from optical or passive microwave remote sensing. We showed that satellite gauging reaches (SGRs) can be developed without gauging station records, based on MODIS or GFDS water extents and W3 model estimated discharges. The optimal selection method (method A) with a search window of $0.55° \times 0.55°$ produced the best results. In total, we calculated Spearman correlations between modelled river channel storage and MODIS and GFDS water extent for 11 752 grid cells across the Amazon Basin (Figs. 3–5). The results suggest there are 3427 potential grid cells (ca. 17 135 km river reaches) to construct MODIS SGRs and 1447 grid cells (ca. 7235 km river reaches) to develop GFDS SGRs. The original MODIS data used in this research
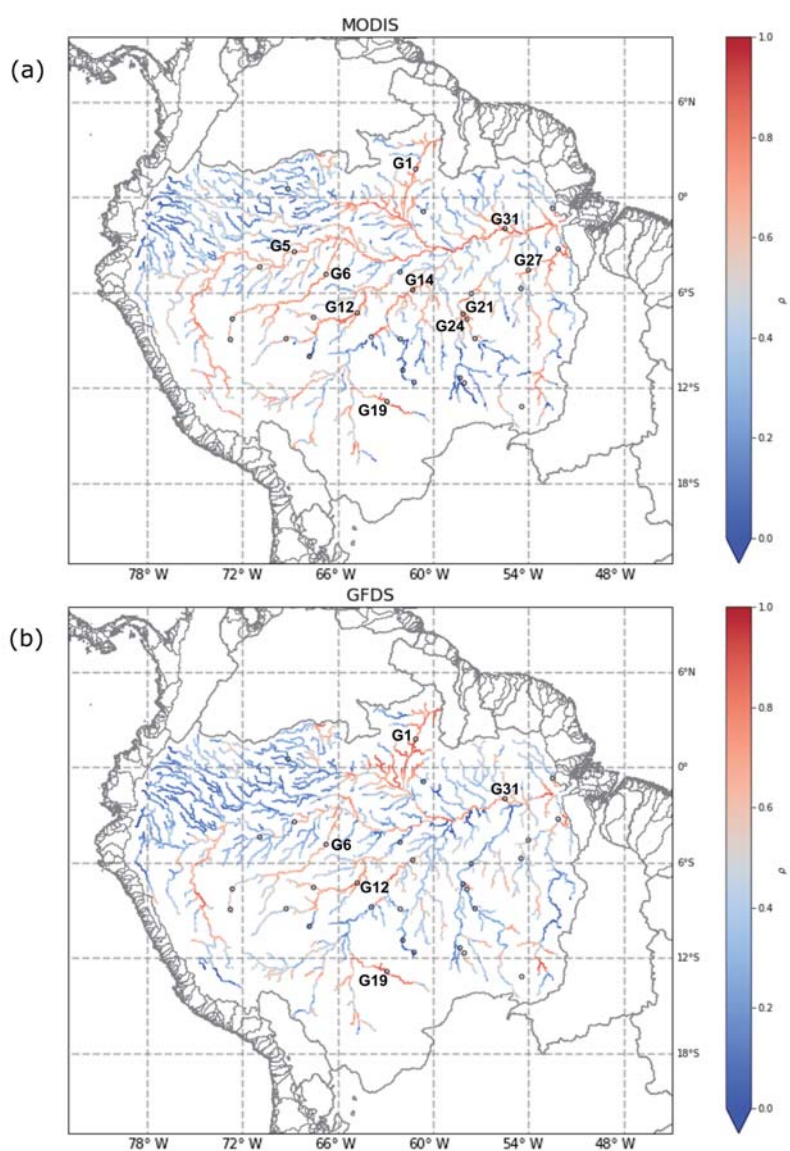
Figure 5. Spearman correlation (ρ) between modelled river channel storage and MODIS **(a)** and GFDS **(b)** water extent using the optimal grid cell selection method (method A) with a search window of $0.55° \times 0.55°$ (circle: gauging station; circle with label: potential SGR sites where gauging data are available).

have a spatial resolution of $0.05° \times 0.05°$, which is higher than the GFDS data ($0.09° \times 0.1°$). As such, MODIS should have better detection ability for river reaches with relatively small surface water extent. The performance of the method appears to be particularly related to the size of river reach. From upstream to downstream reaches in the Amazon Basin, ρ between water extent and storage increases as river width increases, because MODIS and GFDS remote sensing are more sensitive to river reaches with larger surface water extent. Thus, the best locations for developing SGRs at the coarse resolution considered here are the lower reaches of the Amazon system.

The performance of SGRs over the Amazon Basin is generally good, as most river reaches have unregulated flows, and these river reaches normally have wider river channels and large floodplains, as also remarked upon by Revilla-Romero et al. (2014). However, the performance of SGRs varies, even for rivers of similar size. The relationship between water extent and storage or discharge also depends on local river characteristics and floodplain channel geometry (Moffitt et al., 2011; Brakenridge et al., 2012; Khan et al., 2012). Even though GFDS is suited for fewer river reaches than MODIS, the results showed that GFDS sometimes yielded better estimates of river discharge. A likely reason for this is that MODIS optical remote sensing is limited
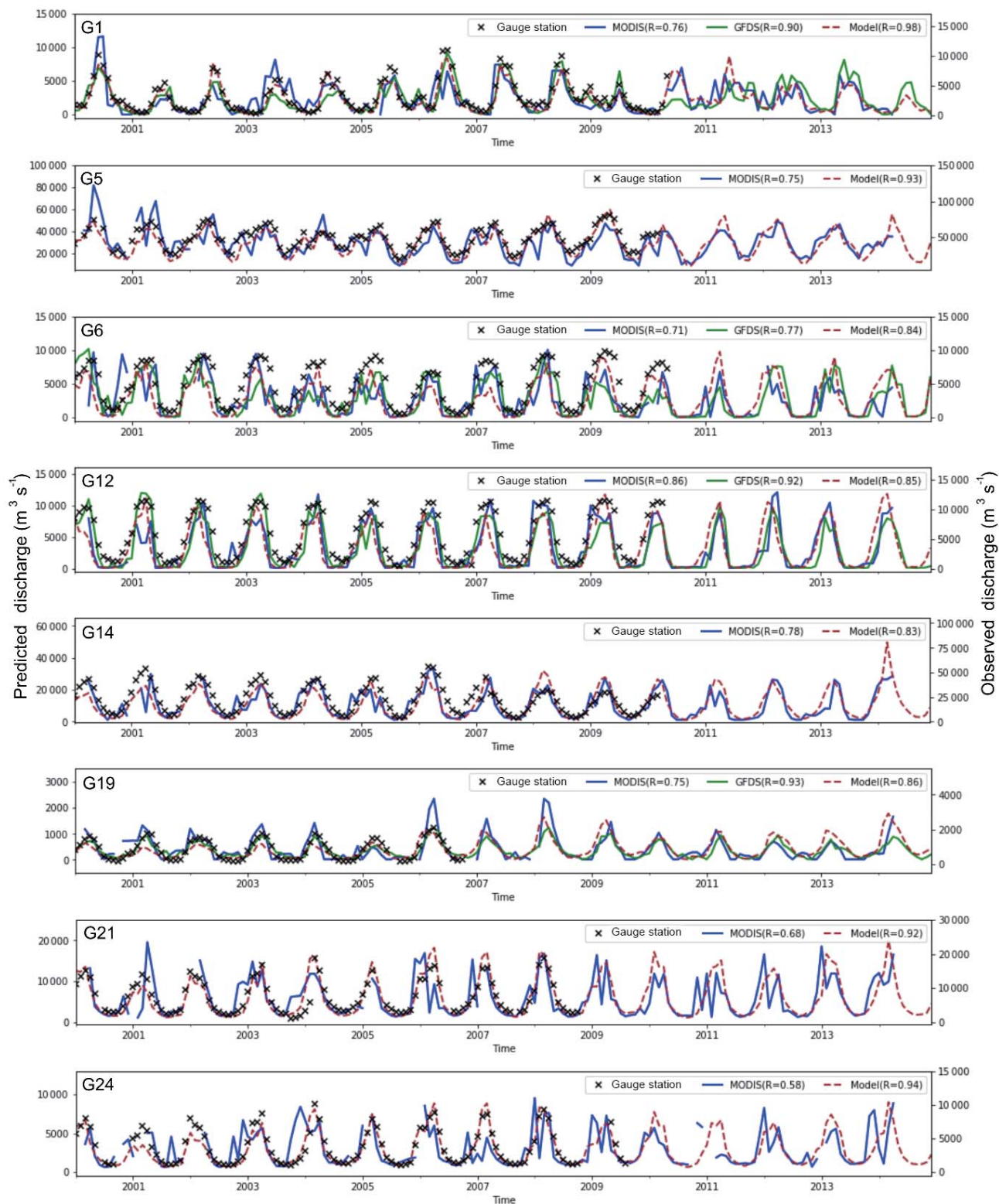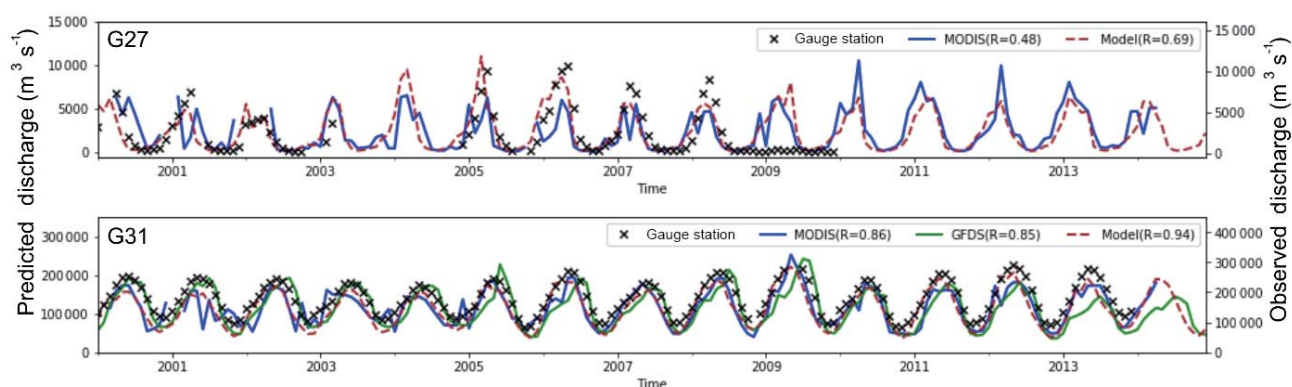
Figure 6.

Figure 6. Comparisons between observations (right axis) from gauging stations (black x) and river discharge estimates (left axis) derived using MODIS SGRs (blue line), GFDS SGRs (green line), and the W3 model (brown dash).

to clear-sky conditions, whereas GFDS passive microwave remote sensing is much less affected by this. River floodplains in the Amazon Basin are often covered with dense vegetation, and flood waters may spread below vegetation. Such flooding may be difficult to detect with optical imagery, but is still readily discernible with passive microwave remote sensing (Van Dijk et al., 2016). This is consistent with the results presented in Figs. 3 and 4. The window mean method (method B) produced similar results to the optimal selection method (method A) for GFDS, but worse results for MODIS. We suspect that this is because more MODIS grid cells within the search window are influenced by cloud or vegetation cover.

Gauging stations are usually located in single, narrow, and stable river reaches, while SGRs can be constructed in multiple, broad, and unstable river reaches provided variations can be detected by remote sensing. With that caveat, there were less than one-third of gauged river reaches that were feasible to develop MODIS SGRs and one-sixth to construct GFDS SGRs. Limited validation reaches with gauging stations do imply an underestimate of the percentage of successful SGRs. We focused on qualitative analysis rather than quantitative analysis for the performance of SGRs and the model. Qualitative metrics, such as Pearson correlation and Spearman's rank correlation, indicate the degree to which the estimates and observations show the same relative patterns, while quantitative metrics, such as RMSE, reflect the differences between estimates and observations. The SGRs were based on the model, so we would expect that the developed SGRs should have the ability to reflect flow patterns better than absolute flow values due to model biases. Tolerable errors and bias are contingent on the application for the data. For instance, for near-real-time drought and flood monitoring, it may be sufficient to know relative flows, whereas water resource assessments require estimates that are bias-free as much as possible. For the 10 gauging stations analysed here, the model showed a bias between −53 % and 57 % compared

to the gauge records, with a median of −35 %. This model bias propagates into the SGR estimates but could be removed easily where in situ data are available.

Based on comparison between gauging station records and river discharge estimates from MODIS, GFDS, and the W3 model for period of 2000–2014, we conclude that if the W3 model performs quite well in terms of river discharge estimation, then SGRs can perform with a similar level of accuracy. In certain cases, the SGRs were able to perform better than the W3 model in reproducing the timing of peak flows. For instance, at gauging station G19, the satellite-derived peak flows from both MODIS and GFDS over the period 2000–2005 were closer to gauged peak river discharges than those estimated by the W3 model (Fig. 6). However, there are also instances where the SGR estimates of discharge are inferior to those produced by the W3 model, e.g. for gauging stations G21 and G24. It is possible that in these instances MODIS has failed to measure water extent in small rivers or was affected by cloud cover. In other cases we suspect that poor results are attributable to data errors. For instance, the discharge observations at gauging station G27 were extremely low from late 2008 to 2009, suggesting a gauge measurement error or other artefact. Other performance problems may be attributable to the calibration processes and period, which were necessarily short. If SGRs were calibrated during a dry period, they may fail to estimate river discharge well during a wet period (and vice versa). For example, at gauging station G27, the SGR was not able to estimate peak flows accurately for the wet years from 2005–2009, and subsequently estimated much larger river discharges than the model during the dry years 2010–2014. This would be avoided if the full period had been used for SGR construction, which would be a pragmatic approach for operational implementation but would prevent independent evaluation in the context of the present study.

Previous research demonstrated that both gauging data and hydrological modelling can be used to calibrate the re-

Table 3. Performance comparisons between gauge-based SGRs, model-based SGRs, and the W3 model (Pearson correlations between predicted and observed discharges).

		G1	G5	G6	G12	G14	G19	G21	G24	G31	Mean
MODIS SGRs	Gauge-based	0.75	0.77	0.74	0.86	0.77	0.88	0.48	0.6	0.92	0.75
	Model-based	0.76	0.75	0.71	0.86	0.78	0.75	0.68	0.58	0.86	0.75
GFDS SGRs	Gauge-based	0.88		0.85	0.96		0.95			0.85	0.9
	Model-based	0.9		0.77	0.92		0.93			0.85	0.87
Model		0.98	0.93	0.84	0.85	0.83	0.86	0.92	0.94	0.94	0.9

mote sensing signal for estimating river discharge (Brakenridge et al., 2012; Revilla-Romero et al., 2014). Van Dijk et al. (2016) developed gauge-based SGRs using optical and passive microwave-derived water extent observations, which is valuable to gap-fill and extend gauging discharge records. In addition to that, we demonstrated that SGRs can be also developed using hydrological modelling. We compared our model-based SGRs to gauge-based SGRs from previous research (Van Dijk et al., 2016) for all gauging reaches, except gauging station G27 due to its seemingly unreliable record (Table 3). Both gauge-based and model-based GFDS SGRs at gauging station G12 and G19 have higher Pearson correlations than the model, which suggests opportunities for data assimilation to improve the model. At gauging station G1, G5, G21, and G24, the model performs much better than both gauge-based and model-based SGRs, which suggests that uncertainties in SGRs at these locations mainly arise from remote sensing, e.g. due to cloud and vegetation obstruction. Errors and uncertainties in the model, such as from input data, routing, and conceptual structure, can also affect the performance of SGRs. For instance, for GFDS at gauging station G6 and MODIS at gauging station G31, gauge-based SGRs produced higher Pearson correlations than model-based SGRs. Compared to gauge-based SGRs, the main advantage of our method is the practical applicability in both gauged and ungauged rivers. Our results show that the model outperforms SGRs in most cases. Nonetheless, we consider SGRs as an alternative, simple and automated approach for river discharge prediction using satellite observation only. SGRs would be useful as an alternative if the model was unable to provide real-time estimates, e.g. due to delayed rainfall gauge observations. As we used a model to train SGRs, poor model simulations might reduce the performance of SGRs. If more accurate and reliable hydrological models are available, SGRs can be redeveloped to estimate river discharge with greater accuracy. Overall, SGRs performed well in this case study in the Amazon Basin. The W3 model, MODIS and GFDS remote sensing all provide information with global coverage. Therefore, there is further potential to develop satellite-based river gauging elsewhere.

The further development of the SGR methodologies could benefit from combining optical and passive microwave remote sensing. With higher spatial resolution, optical remote sensing is more suitable for measuring surface water extent in reaches without dense vegetation and when clear-sky conditions prevail. Passive microwave remote sensing compensates for the limitations of optical remote sensing, but suffers from having lower spatial resolution. The main constraint in developing SGRs in this study was that the spatial resolutions of both MODIS and GFDS data were not high enough to detect changes in river dynamics in small rivers. New satellite imagery emerging from Sentinel-1 and Sentinel-2 provides further opportunities to develop satellite-based river gauging at a global scale. The spatial resolution of Sentinel-1 reaches 5 m with C-band synthetic aperture radar working in all weather and both day-time and night-time conditions. The Sentinel-2 A and B multispectral instruments have 13 spectral bands at 10–60 m spatial resolution and, combined with Landsat observations, this means that revisit times in the order of days are now achievable. These developments offer great promise for the future development of SGRs.

5   Conclusions

We proposed and tested two methods for relating MODIS- and GFDS-derived water extent to modelled river channel storage. For the Amazon Basin, river reaches with Spearman's rank correlation (ρ) between water extent and storage exceeding 0.6 were identified as suitable sites for developing SGRs. SGRs were then constructed across the Amazon Basin based on MODIS and GFDS water extent and modelled discharge, and river discharge estimates were evaluated using in situ river discharge measurements at 10 stations. Our main conclusions are as follows:

1. The optimal grid cell selection method performed better than the window mean method to relate W3-model-simulated river storage and discharge to MODIS- and GFDS-derived surface water extent fraction, and a window size of $0.55° \times 0.55°$ was considered a reasonable window size for identifying the best remote sensing pixels for each model grid cell.

2. There were strong correlations between modelled storage and both MODIS and GFDS water extent across the Amazon Basin. The optimal selection method is mainly limited by the size of river reach, as correlation generally increased from upstream to downstream reaches as river width increased.

3. In total, 17 135 km of river reaches in the Amazon Basin was assessed as suitable for constructing MODIS SGRs, and 7235 km of river reaches was deemed suitable for developing GFDS SGRs. The best locations for developing SGRs were mostly situated in the lower channels of the Amazon River and its main tributaries.

4. There were more potential SGRs derived using MODIS than GFDS, most likely because MODIS has higher spatial resolution than GFDS. However, GFDS SGRs predicted river discharges with more accuracy as GFDS was much less affected by cloud and dense vegetation than MODIS.

5. Although the W3 model performed very well in terms of river discharge estimates in the Amazon Basin, MODIS and GFDS SGRs can still be useful for estimating river discharge in the absence of a real-time hydrological model or gauging stations.

6. SGRs are suitable for automated development at a global scale. Remote sensing with higher spatial resolution can help improve river discharge estimation capabilities of SGRs. This also creates potential opportunities to assimilate remote sensing observations, or derived discharge estimates, into hydrological models to improve river discharge estimation, and based on these, streamflow forecasts.

Author contributions. JH and AIJMVD conceived the idea. AI-JMVD, LJR and RAV guided the study. JH carried out the analysis and wrote the manuscript with contributions from all the co-authors.

References

Alsdorf, D., Lettenmaier, D., and Vörösmarty, C.: The need for global, satellite-based observations of terrestrial surface waters, EOS T. Am. Geophys. Un., 84, 269–276, https://doi.org/10.1029/2003EO290001, 2003.

Alsdorf, D. E., Rodriguez, E., and Lettenmaier, D. P.: Measuring surface water from space, Rev. Geophys., 45, RG2002, https://doi.org/10.1029/2006RG000197, 2007.

Beck, H. E., de Roo, A., and van Dijk, A. I. J. M.: Global Maps of Streamflow Characteristics Based on Observations from Several Thousand Catchments, J. Hydrometeorol., 16, 1478–1501, https://doi.org/10.1175/jhm-d-14-0155.1, 2015.

Biancamaria, S., Hossain, F., and Lettenmaier, D. P.: Forecasting transboundary river water elevations from space, Geophys. Res. Lett., 38, L11401, https://doi.org/10.1029/2011GL047290, 2011.

Birkett, C. M., Mertes, L. A. K., Dunne, T., Costa, M. H., and Jasinski, M. J.: Surface water dynamics in the Amazon Basin: Application of satellite radar altimetry, J. Geophys. Res.-Atmos., 107, 8059, https://doi.org/10.1029/2001JD000609, 2002.

Bjerklie, D. M., Dingman, S. L., Vorosmarty, C. J., Bolster, C. H., and Congalton, R. G.: Evaluating the potential for measuring river discharge from space, J. Hydrol., 278, 17–38, https://doi.org/10.1016/S0022-1694(03)00129-X, 2003.

Brakenridge, G. R., Nghiem, S. V., Anderson, E., and Mic, R.: Orbital microwave measurement of river discharge and ice status, Water Resour. Res., 43, W04405, https://doi.org/10.1029/2006WR005238, 2007.

Brakenridge, G. R., Cohen, S., Kettner, A. J., De Groeve, T., Nghiem, S. V., Syvitski, J. P. M., and Fekete, B. M.: Calibration of satellite measurements of river discharge using a global hydrology model, J. Hydrol., 475, 123–136, https://doi.org/10.1016/j.jhydrol.2012.09.035, 2012.

Calmant, S. and Seyler, F.: Continental surface waters from satellite altimetry, C. R. Geosci., 338, 1113–1122, https://doi.org/10.1016/j.crte.2006.05.012, 2006.

Coe, M. T. and Birkett, C. M.: Calculation of river discharge and prediction of lake height from satellite radar altimetry: Example for the Lake Chad basin, Water Resour. Res., 40, W10205, https://doi.org/10.1029/2003WR002543, 2004.

Dai, A.: Historical and future changes in streamflow and continental runoff: a review, in: Chapter 2 of Terrestrial water cycle and climate change: natural and human-induced impacts, edited by: Tang, Q. and Oki, T., Geophysical Monograph, Am. Geophys. Un., 17–37, 2016.

Dai, A., Qian, T., Trenberth, K. E., and Milliman, J. D.: Changes in continental freshwater discharge from 1948 to 2004, J. Climate, 22, 2773–2792, https://doi.org/10.1175/2008JCLI2592.1, 2009.

De Groeve, T., Brakenridge, G. R., and Paris, S.: Global flood detection system data product specifications, JRC Technical Report, available at: http://www.gdacs.org/flooddetection/Download/Technical_Note_GFDS_Data_Products_v1.pdf (last access: 20 September 2018), 2015.

Fekete, B. M., Looser, U., Pietroniro, A., and Robarts, R. D.: Rationale for monitoring discharge on the ground, J. Hydrometeorol., 13, 1977–1986, https://doi.org/10.1175/JHM-D-11-0126.1, 2012.

Frost, A. J., Ramchurn, A., and Smith, A.: The Bureau's Operational AWRA Landscape (AWRA-L) Model, Technical Report, Bureau of Meteorology, Melbourne, 2016.

Hunger, M. and Döll, P.: Value of river discharge data for global-scale hydrological modeling, Hydrol. Earth Syst. Sci., 12, 841–861, https://doi.org/10.5194/hess-12-841-2008, 2008.

Jung, H. C., Hamski, J., Durand, M., Alsdorf, D., Hossain, F., Lee, H., Hossain, A. K. M. A., Hasan, K., Khan, A. S., and Hoque, A. K. M. Z.: Characterization of complex fluvial systems using remote sensing of spatial and temporal water level variations in the Amazon, Congo, and Brahmaputra Rivers, Earth Surf. Proc. Land., 35, 294–304, https://doi.org/10.1002/esp.1914, 2010.

Khan, S. I., Hong, Y., Vergara, H. J., Gourley, J. J., Brakenridge, G. R., De Groeve, T., Flamig, Z. L., Policelli, F., and Yong, B.: Microwave satellite data for hydrologic modeling in ungauged basins, IEEE Geosci. Remote S., 9, 663–667, https://doi.org/10.1109/LGRS.2011.2177807, 2012.

Kouraev, A. V., Zakharova, E. A., Samain, O., Mognard, N. M., and Cazenave, A.: Ob' river discharge from TOPEX/Poseidon satellite altimetry (1992–2002), Remote Sens. Environ., 93, 238–245, https://doi.org/10.1016/j.rse.2004.07.007, 2004.

LeFavour, G. and Alsdorf, D.: Water slope and discharge in the Amazon River estimated using the shuttle radar topography mission digital elevation model, Geophys. Res. Lett., 32, L17404, https://doi.org/10.1029/2005GL023836, 2005.

Michailovsky, C. I., McEnnis, S., Berry, P. A. M., Smith, R., and Bauer-Gottwein, P.: River monitoring from satellite radar altimetry in the Zambezi River basin, Hydrol. Earth Syst. Sci., 16, 2181–2192, https://doi.org/10.5194/hess-16-2181-2012, 2012.

Moffitt, C. B., Hossain, F., Adler, R. F., Yilmaz, K. K., and Pierce, H. F.: Validation of a TRMM-based global Flood Detection System in Bangladesh, Int. J. Appl. Earth Obs., 13, 165–177, https://doi.org/10.1016/j.jag.2010.11.003, 2011.

Papa, F., Prigent, C., and Rossow, W.: Monitoring flood and discharge variations in the large Siberian rivers from a multi-satellite technique, Surv. Geophys., 29, 297–317, https://doi.org/10.1007/s10712-008-9036-0, 2008.

Papa, F., Durand, F., Rossow, W. B., Rahman, A., and Bala, S. K.: Satellite altimeter-derived monthly discharge of the Ganga-Brahmaputra River and its seasonal to interannual variations from 1993 to 2008, J. Geophys. Res.-Oceans, 115, C12013, https://doi.org/10.1029/2009JC006075, 2010.

Pavelsky, T. M.: Using width-based rating curves from spatially discontinuous satellite imagery to monitor river discharge, Hydrol. Process., 28, 3035–3040, https://doi.org/10.1002/hyp.10157, 2014.

Revilla-Romero, B., Thielen, J., Salamon, P., De Groeve, T., and Brakenridge, G. R.: Evaluation of the satellite-based Global Flood Detection System for measuring river discharge: influence of local factors, Hydrol. Earth Syst. Sci., 18, 4467–4484, https://doi.org/10.5194/hess-18-4467-2014, 2014.

Smith, L. C.: Satellite remote sensing of river inundation area, stage, and discharge: A review, Hydrol. Process., 11, 1427–1439, https://doi.org/10.1002/(SICI)1099-1085(199708)11:10<1427::AID-HYP473>3.0.CO;2-S, 1997.

Smith, L. C. and Pavelsky, T. M.: Estimation of river discharge, propagation speed, and hydraulic geometry from space: Lena River, Siberia, Water Resour. Res., 44, W03427, https://doi.org/10.1029/2007WR006133, 2008.

Smith, L. C., Isacks, B. L., Forster, R. R., Bloom, A. L., and Preuss, I.: Estimation of discharge from braided glacial rivers using ERS 1 synthetic aperture radar: First results, Water Resour. Res., 31, 1325–1329, https://doi.org/10.1029/95WR00145, 1995.

Smith, L. C., Isacks, B. L., Bloom, A. L., and Murray, A. B.: Estimation of discharge from three braided rivers using synthetic aperture radar satellite imagery: Potential application to ungaged basins, Water Resour. Res., 32, 2021–2034, https://doi.org/10.1029/96WR00752, 1996.

Stahl, K., Tallaksen, L. M., Hannaford, J., and van Lanen, H. A. J.: Filling the white space on maps of European runoff trends: estimates from a multi-model ensemble, Hydrol. Earth Syst. Sci., 16, 2035–2047, https://doi.org/10.5194/hess-16-2035-2012, 2012.

Tarpanelli, A., Brocca, L., Lacava, T., Melone, F., Moramarco, T., Faruolo, M., Pergola, N., and Tramutoli, V.: Toward the estimation of river discharge variations using MODIS data in ungauged basins, Remote Sens. Environ., 136, 47–55, https://doi.org/10.1016/j.rse.2013.04.010, 2013.

Te Chow, V.: Open-channel hydraulics, McGraw-Hill, New York, 1959.

Van Dijk, A. I. J. M.: The Australian Water Resources Assessment System. Technical Report 3. Landscape Model (version 0.5) Technical Description, CSIRO: Water for a Healthy Country National Research Flagship, available at: http://www.clw.csiro.au/publications/waterforahealthycountry/2010/wfhc-aus-water-resources-assessment-system.pdf (last access: 20 September 2018), 2010.

Van Dijk, A. I. J. M.: Water resources, climate change and energy, in: Climate, Energy and Water: Managing Trade-offs, Seizing Opportunities, edited by: Pittock, J., Hussey, K., and Dovers, S., Cambridge, Cambridge University Press, 6–27 pp., 2015.

Van Dijk, A. I. J. M., Brakenridge, G. R., Kettner, A. J., Beck, H. E., De Groeve, T., and Schellekens, J.: River gauging at global scale using optical and passive microwave remote sensing, Water Resour. Res., 52, 6404–6418, https://doi.org/10.1002/2015WR018545, 2016.

Van Dijk, A. I. J. M., Schellekens, J., Yebra, M., Beck, H. E., Renzullo, L. J., Weerts, A., and Donchyts, G.: Global 5 km resolution estimates of secondary evaporation including irrigation through satellite data assimilation, Hydrol. Earth Syst. Sci., 22, 4959–4980, https://doi.org/10.5194/hess-22-4959-2018, 2018.

Vörösmarty, C., Askew, A., Grabs, W., Barry, R. G., Birkett, C., Döll, P., Goodison, B., Hall, A., Jenne, R., Kitaev, L., Landwehr, J., Keeler, M., Leavesley, G., Schaake, J., Strzepek, K., Sundarvel, S. S., Takeuchi, K., and Webster, F.: Global water data: A newly endangered species, EOS T. Am. Geophys. Un., 82, 54–58, https://doi.org/10.1029/01EO00031, 2001.

Woldemichael, A. T., Degu, A. M., Siddique-E-Akbor, A. H. M., and Hossain, F.: Role of Land–Water Classification and Manning's Roughness Parameter in Space-Borne Estimation of Discharge for Braided Rivers: A Case Study of the Brahmaputra River in Bangladesh, IEEE J. Sel. Top. Appl., 3, 395–403, https://doi.org/10.1109/JSTARS.2010.2050579, 2010.

Zakharova, E. A., Kouraev, A. V., Cazenave, A., and Seyler, F.: Amazon River discharge estimated from TOPEX/Poseidon altimetry, C. R. Geosci., 338, 188–196, https://doi.org/10.1016/j.crte.2005.10.003, 2006.

Hydrol. Earth Syst. Sci., 22, 6435–6448, 2018

www.hydrol-earth-syst-sci.net/22/6435/2018/

Chapter 3: Global satellite-based river gauging and the influence of river morphology on its application

This chapter examines the capacity of the best method, of those proposed in Chapter 2 above, to predict river discharge at global scale and compares the performance of its application based on model and gauging data. The study also analysed how river morphology affects the performance of the river discharge prediction method and suggested an approach to assess whether the method can be applied in any given river reach based on high-resolution inundation regime data derived from remote sensing. The content of this chapter was published in the journal Remote Sensing of Environment as follows:

Hou, J., Van Dijk, A.I.J.M. and Beck, H.E., 2020. Global satellite-based river gauging and the influence of river morphology on its application. Remote Sensing of Environment, 239, https://doi.org/10.1016/j.rse.2019.111629.
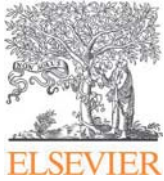
Global satellite-based river gauging and the influence of river morphology on its application

Jiawei Hou[a],[*], Albert I.J.M. van Dijk[a], Hylke E. Beck[b]

[a] *Fenner School of Environment and Society, Australian National University, Canberra, Australian Capital Territory, Australia*
[b] *Department of Civil and Environmental Engineering, Princeton University, Princeton, New Jersey, USA*

ARTICLE INFO

ABSTRACT

In the face of a sparse global river gauging station network in decline, new approaches are needed to reconstruct and monitor river discharge from satellite observations. Where *in-situ* river discharge measurements are not available, it may be possible to use discharge estimates from a hydrological model, provided the model simulations are of sufficient quality, to construct satellite-based discharge gauging. We tested this approach by developing model- and gauge-based satellite gauging reaches (SGRs) using 0.05° MODIS optical remote sensing at ~10,000 gauged and ~370,000 ungauged river reaches globally. Model-based SGRs are aimed to infer temporal flow patterns and reflect unusually high or low river discharge behavior (*i.e.* flood or drought conditions), if not necessarily absolute discharge volumes. The model-based SGRs achieved a discharge prediction skill that was often similar to gauge-based SGRs, and sometimes better than the model itself. Our results showed promising opportunities to develop model-based SGRs in sparsely gauged basins in South America, Africa, and Asia. We selected river reaches, with mean widths ranging from 67 to 3105 m, representing both poor and successful SGRs in different environments for case studies to analyze conditions for successful SGR development. River size and morphology were the main factors determining the performance of SGRs. Wide channels with strong temporal variations, broad floodplains and multiple braided or anastomosing channels provided the best conditions for SGRs. The probability of constructing a successful SGR could be predicted from high-resolution inundation summary data available globally, and can thus be predicted anywhere. Ongoing increases in the spatial and temporal resolution of remote sensing will further increase the number of river reaches for which satellite-based discharge gauging will become possible.

1. Introduction

River discharge measurements provide fundamental information for water resources management and help understand the influence of climate change and anthropogenic activities on the terrestrial water cycle. River discharge records are also the basis for designing flood control, irrigation and hydropower systems and transboundary water agreements, while real-time discharge data are needed to operate water infrastructure and manage flood and drought risk (García et al., 2016; Sheffield et al., 2018).

Most drainage basins around the world are poorly gauged or ungauged (Hannah et al., 2011). Gauging station networks are unevenly distributed and sparse, and their number has declined since the 1980s (Biancamaria et al., 2011; Davids et al., 2019; Fay et al., 2017). Except for some countries (*e.g.*, United States, Australia), measurements from many of the remaining stations are not made available in near-real

time, cover only a few years, or have records that end decades ago (Sheffield et al., 2018). These various issues currently pose challenges to tracking river discharge globally.

Remote sensing provides a complementary source of surface water extent and level observations, creating opportunities to derive river discharge information where and when *in-situ* data is not available (Alsdorf et al., 2007; Bjerklie et al., 2003; Smith, 1997). Empirical relationships between discharge and, respectively, remotely sensed water level (Birkinshaw et al., 2010; Coe and Birkett, 2004; Huang et al., 2018a; Kouraev et al., 2004; Papa et al., 2010; Paris et al., 2016; Tourian et al., 2017; Tourian et al., 2013), river width (Pavelsky, 2014; Smith et al., 1996; Smith et al., 1995; Smith and Pavelsky, 2008), and inundation extent (Papa et al., 2008) have all been used with considerable success (Table 1). In theory, the combination of satellite-derived river width, level, and slope can be used to calculate discharge without calibration based on Manning's equation, but in practice *in-situ*

Table 1

Summary of relevant approach to estimate river discharge through satellite observation.

Method	Study	Spatial scale	Remote sensing	Ancillary data	Strength & limitation
1. Discharge-height rating curve	Coe and Birkett (2004)	1 site	Altimetry	*In-situ* river discharge	+ readily automated
	Kouraev et al. (2004)	1 site			+ suited to monitoring
	Tourian et al. (2013)	9 sites			− only for broad rivers
	Birkinshaw et al. (2010)	6 sites	Altimetry (multi-sensors)		− sparse global coverage
					− affected by topography
	Papa et al. (2010)	2 sites			
	Tourian et al. (2017)	18 sites			
	Paris et al. (2016)	920 sites		Hydrodynamic model	
2. Discharge-width rating curve	Smith et al. (1995)	10 km river reach	Active microwave	*In-situ* river discharge	+ penetrates cloud and vegetation
	Smith et al. (1996)	3 river reaches (9–16 km)			− not readily automated
					− not suited to monitoring
	Smith and Pavelsky (2008)	316 km river reach	Visible/infrared optical		+ high temporal frequency
					+ near-global coverage
	Pavelsky (2014)	62 km river reach			− not readily automated
					− not suited to monitoring
					− affected by cloud and vegetation
3. Discharge-inundation rating curve	Papa et al. (2008)	3 basins	Passive microwave, active microwave and visible/infrared optical	*In-situ* river discharge	+ mitigates weaknesses of individual observation types
					− limited to large basins rather than specific river reaches
					− not readily automated
					− not suited to monitoring
4. C/M ratio	Brakenridge et al. (2007)	2 sites	Passive microwave	*In-situ* river discharge	+ readily automated
	Tarpanelli et al. (2013, 2017)	6 sites	Visible/infrared optical		+ suited to monitoring
					+ high temporal frequency
					+ near-global coverage
	Van Dijk et al. (2016)	5134 sites	Passive microwave or visible/infrared optical		+ does not require single, stable channel
	Hou et al. (2018)	4874 sites		Hydrological model	
	This study	371,953 sites	Visible/infrared optical		− affected by cloud and vegetation
5. Manning's equation	Bjerklie et al. (2005)	3 river reaches (9–16 km)	Active microwave	Topographic maps	+ constrained by hydraulic theory
					− highly parametrized for individual reaches
	Michailovsky et al. (2012)	4 sites	Altimetry	*In-situ* river depth and velocity	− not readily automated
	Sichangi et al. (2016)	14 sites	Altimetry and visible/infrared optical	*In-situ* river discharge	− not suited to monitoring
	Huang et al. (2018a, 2018b)	7 river reaches (10 km)			
6. AMHG	Gleason and Smith (2014)	3 river reaches (10–13 km)	Visible/infrared optical	Prior estimates of river velocity, depth or discharge	+ potential to combine multi-sensor strengths from future SWOT mission observations
7. MetroMan	Durand et al. (2014)	22.4 km river reach	Altimetry		
	Yoon et al. (2016)	2 river reaches (40–82 km)	Active microwave (simulated by hydrodynamic models)		− not readily automated
					− not suited to monitoring
8. MFG	Bonnema et al. (2016)	3 river reaches (64–187 km)			− requires single, stable channel
9. MFCR	Durand et al. (2016)	19 river reaches (11–223 km)			
10. GaMo					
11. BAM	Hagemann et al. (2017)				
	Feng et al. (2019)	11 river reaches (0.7–22.4 km)	Visible/infrared optical		

river depth or flow velocity data and an estimate of roughness coefficient are still required (Bjerklie et al., 2005; Huang et al., 2018b; Michailovsky et al., 2012; Sichangi et al., 2016). Therefore, all these methods rely on *in-situ* observations and are not applicable in ungauged rivers. River discharge estimation in ungauged rivers has been approached in several ways, including (i) the at-many-stations hydraulic geometry (AMHG) approach (Gleason and Smith, 2014; Gleason et al., 2014; Gleason and Wang, 2015); (ii) the GaMo algorithm (Durand et al., 2016; Garambois and Monnier, 2015); (iii) the Metropolis-Manning (MetroMan) algorithm (Durand et al., 2014; Yoon et al., 2016); (iv) the Mean Flow and Geomorphology (MFG) algorithm (Bonnema et al., 2016); (v) the MFCR and Ensemble Median Algorithm (Durand et al., 2016); and (vi) the Bayesian AMHG-Manning (BAM) algorithm (Feng et al., 2019; Hagemann et al., 2017). However, these methods are relatively complex in their application and still require prior information on velocity and depth or discharge. Satellite observations have also been used to improve river discharge forecasts through model calibration or assimilation (*e.g.*, Domeneghetti, 2016; Oubanas et al., 2018).

Our objective was to develop a simple and computationally efficient method to estimate discharge from satellite observations in near-real time, for both gauged and ungauged river reaches anywhere in the world. Brakenridge et al. (2007) and Tarpanelli et al. (2013) discovered that the ratio of the Advanced Microwave Scanning Radiometer (AMSR-E) passive microwave brightness temperature or Moderate Resolution Imaging Spectroradiometer (MODIS) near-infrared reflectance between a wet measurement grid cell and its nearby dry calibration grid cell (the calibration/measurement or C/M ratio) can represent river discharge variations in a river reach. The passive microwave C/M ratio has proven useful to train both empirical and model-based discharge estimation approaches (Brakenridge et al., 2012; Revilla-Romero et al., 2015). Van Dijk et al. (2016) used the same C/M approach with optical and passive microwave observations to construct satellite gauging reaches (SGRs) for gauged river reaches globally. Hou et al. (2018) expanded that approach to using modelled streamflow for ungauged reaches in the Amazon Basin with good results. Passive microwave and optical remote sensing each have their strengths, with the former much less affected by cloud or vegetation cover, whereas the higher spatial resolution of optical observations is sensitive to water extent changes in
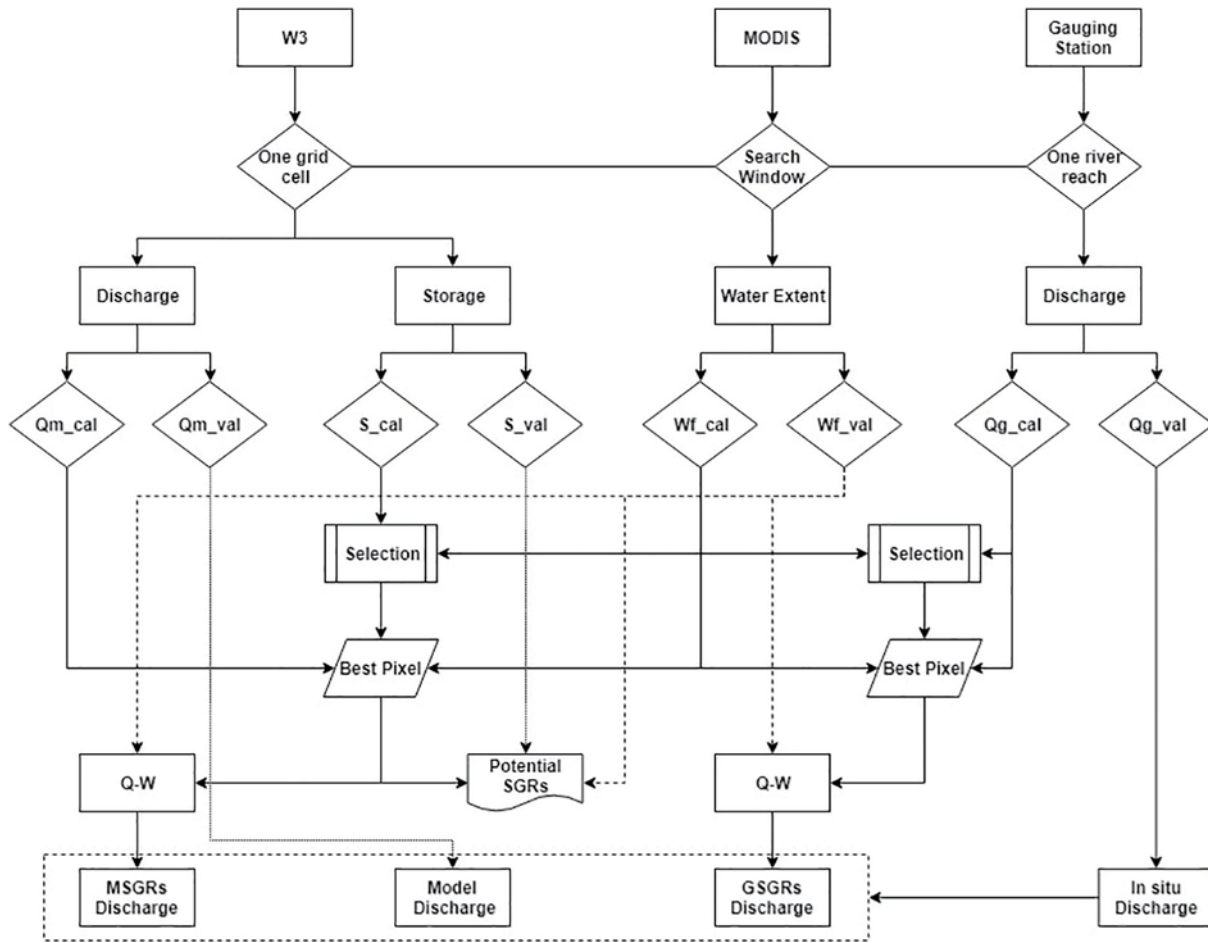
Fig. 1. Illustration of the workflow to construct gauge-based and model-based SGRs and to evaluate the performance of SGRs (Qm_cal, S_cal, Wf_cal, and Qg_cal: simulated discharge, simulated storage, MODIS-derived water extent, and *in-situ* discharge time series in the training periods; Qm_val, S_val, Wf_val, and Qg_val: simulated discharge, simulated storage, MODIS-derived water extent, and *in-situ* discharge time series in the validation periods; Q-W: the relationship between discharge and water extent; MSGRs: model-based SGRs; GSGRs: gauge-based SGRs).

Table 2
Training and validation periods for three-fold cross-validation.

Periods	I	II	III
Training period	2005–2014	2000–2004&2010–2014	2000–2009
Validation period	2000–2004	2005–2009	2010–2014

a larger number of river reaches.

Here, we extend the analysis of Hou et al. (2018) and assess the worldwide distribution of river reaches that can act as satellite gauging reaches (SGRs). We hypothesize (1) that model-based SGRs can achieve similar skill as gauge-based SGRs and (2) that the dominant factor that influences SGR performance is river morphology. To test these hypotheses, we constructed both model- and gauge-based SGRs globally and evaluated their river discharge predictions against *in-situ* discharge measurements. The influence of river morphology was analyzed by using high-resolution inundation frequency mapping. We aimed to answer the following questions:

(1) Where are river reaches (both gauged and ungauged) amenable to constructing SGRs globally?
(2) How does the performance of model and gauge-based SGRs compare?
(3) How does river morphology affect the performance of SGRs?
(4) Can the likelihood of constructing a successful SGR for a reach be predicted from globally available river morphology data?

2. Data and method

2.1. Data

2.1.1. Surface water extent time series

The Moderate Resolution Imaging Spectroradiometer (MODIS) sensor, aboard the NASA's Terra and Aqua satellites, has 36 spectral bands with varying moderate spatial resolution (250–1000 m) and high temporal resolution (1 or 2 days) for every location. Although MODIS provides daily observations, they are regularly affected by cloud contamination (Wilson and Jetz, 2016). MODIS 8-day or 16-day composited products can mitigate this issue to a considerable degree. We used estimates of surface water extent derived by Van Dijk et al. (2016), who used global shortwave infrared (SWIR) reflectance measurements by the MODIS satellite instruments that had been processed, temporally-composited and spatially-resampled to 8-day, global 0.05° × 0.05° grids of Nadir BRDF (Bidirectional Reflectance Distribution Function)-Adjusted Reflectance (NBAR) reflectance (product MCD43C4, Schaaf et al., 2002; Schaaf et al., 2011). The SWIR channel 7 (2105–2155 nm) was chosen because of the generally strong contrast between water and dry land in this wavelength. Surface water extent fraction (hereafter, water extent) for the period of 2000–2014 was estimated as:

$$w = \frac{\rho_M - \rho_{dry}}{\rho_{water} - \rho_{dry}}$$

(1)

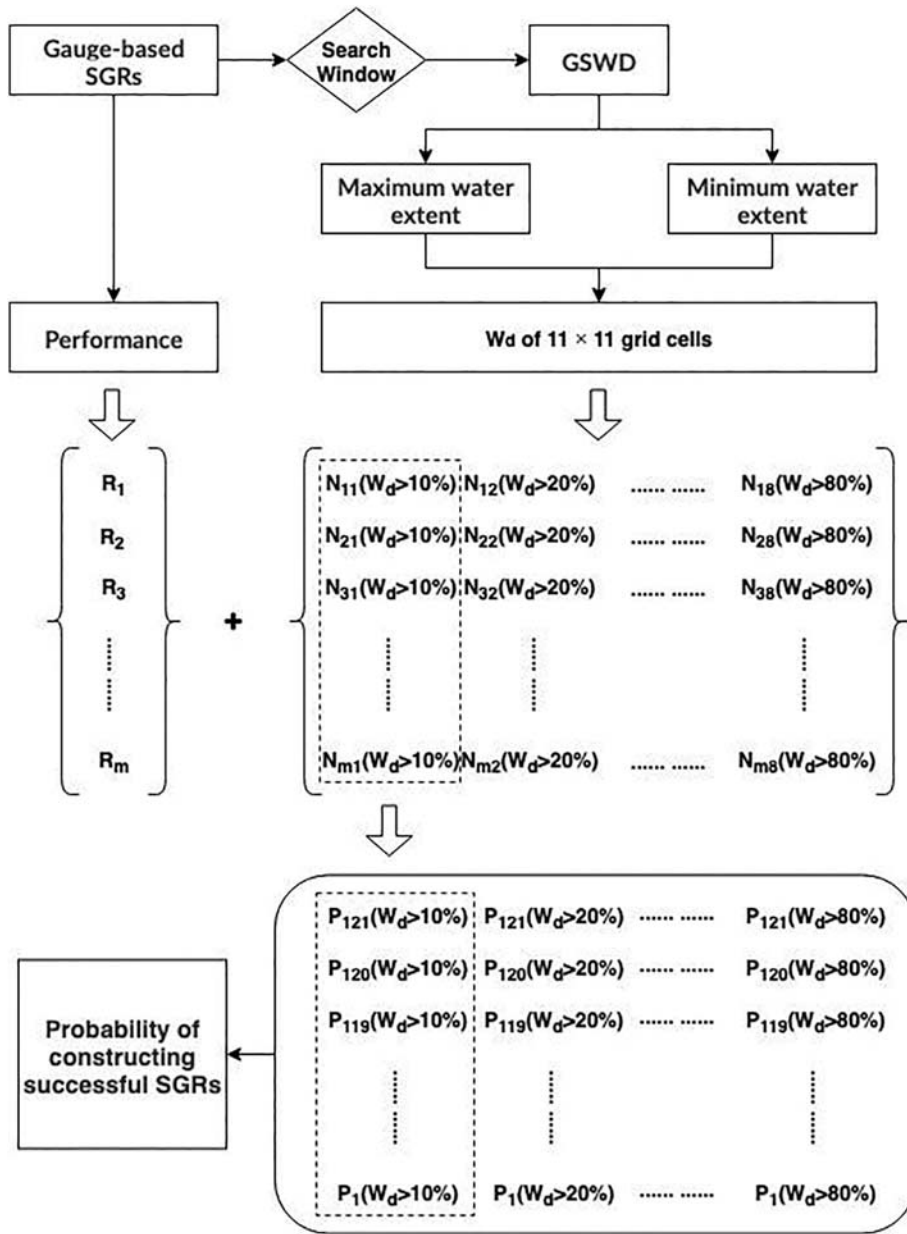where w is surface water extent fraction for each grid cell of each

Fig. 2. Illustration of the workflow to predict the probability of constructing a successful SGR based on water extent variations of each 0.05° grid cell in the 0.55° search window for all gauge-based SGRs (W_d: the temporal range of water extent as the difference between the maximum and minimum water extent for each grid cell; m: the number of gauge-based SGRs; R: the performance of gauge-based SGRs; N_{m1} ($W_d > 10\%$): the number (N) of grid cells in the search window with temporal water extent ranges > 10% (threshold values of 10–80% with 10% increments); P_1 ($W_d > 10\%$): the probability (P) of constructing a successful SGR when there are 1 (from 1 to 121) grid cell with temporal water extent ranges > 10% (threshold values of 10–80% with 10% increments) within the search window).

imagery, ρ_M is band 7 reflectance of the target cell *M*, ρ_{dry} is the fifth percentile highest reflectance in a 7 × 7 cell window around *M*, and ρ_{water} is the reflectance of surface water (assumed equal to 0.008; refer to Van Dijk et al., 2016 for further details).

2.1.2. Surface water occurrence

The Global Surface Water Dataset (GSWD) produced by the European Commission Joint Research Centre provides statistics on the extent and change of global surface water based on surface water mapping using 3 million images from the Landsat 5, 7, and 8 satellites during 1984–2015 (Pekel et al., 2016). Each pixel of this dataset was classified as water, land, and non-valid observation types, which was derived from Landsat 5–7 images using an expert system classifier that missed < 5% of water and produced < 1% of false water detections (Pekel et al., 2016). The global data provides information on surface water occurrence, occurrence change intensity, seasonality, recurrence, transitions, and maximum water extent, all at 30 m spatial resolution. The surface water occurrence data was used herein, which is expressed as the frequency with which surface water was detected in all valid observations. The GSWD dataset was only used as case study to analyze

the influence of river morphology on the performance of SGRs.

2.1.3. Modelled storage and discharge

The World-Wide Water (W3) model (version 2) is a 0.05° × 0.05° grid-based, one-dimensional water balance model that has a semi-distributed representation of the surface water, soil, groundwater stores. Full details about input climate data, vegetation, surface, soil and groundwater parameterisation data, river routing, calibration, and regionalisation can be found in Van Dijk et al. (2018). W3 is a global implementation of AWRA-L, developed initially by Van Dijk (2010) and currently used operationally by the Australian Bureau of Meteorology to provide daily landscape water balance information from 1911 onwards (Frost et al., 2018). Each model grid cell has three soil layers overlaying an unconfined groundwater store. The model considers the coupled water and energy balance as well as vegetation phenology. The input data and the performance of the W3 model are summarized in the Supplement. Global daily river storage and discharge during the period of 1980–2014 were simulated by the model and averaged to 8-day and monthly intervals, in line with the temporal resolution of remote sensing derived surface water extent.
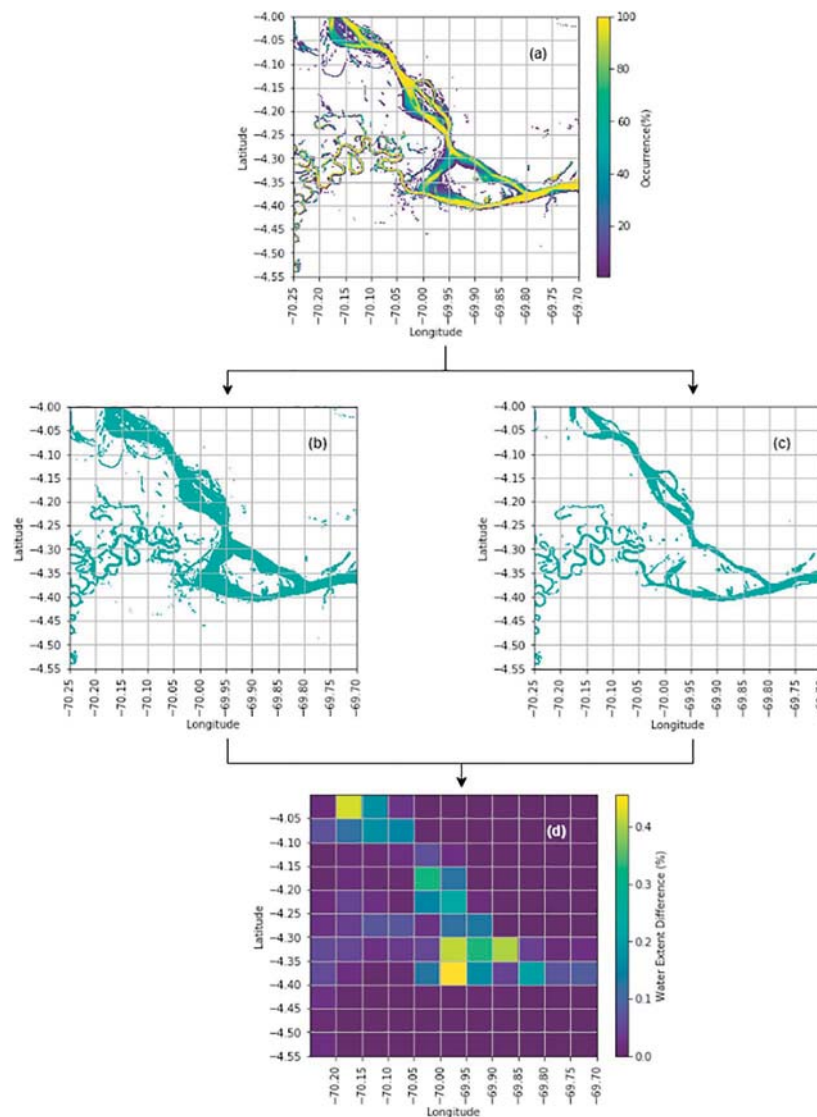
Fig. 3. The approach to calculate the temporal range of water extent (W_d) of 11×11 grid cells within the search window for each gauge-based SGR (a: surface water occurrence mapping of a search window; b: maximum water extent derived from a; c: minimum water extent derived from a; d: the calculated temporal range of water extent (W_d) for each grid cell within the search window based on the differences between a and b).

2.1.4. Observed discharge

Daily and monthly discharge observations were compiled from eight different national and international sources (Supplementary Table 1). Combined, 22,808 gauging records were available; 52% from North America, 17% from South America, 15% from Europe, 8% from Asia, 3% from Africa, 4% from Australia, and < 1% from Oceania. Nearly 700 of the records were for rivers with an annual mean discharge > 10,000 m^3/s, whereas > 12,000 were on rivers with mean discharge < 10 m^3/s. Data for a total of 9873 stations with at least 60 months (at least 20 months in each training and validation group for cross-validation method) of observations during 2000–2014 were selected here for use in the analysis.

2.2. Method

2.2.1. Global satellite-based river gauging

The availability of MODIS-derived water extent product, the W3 model simulation, and *in-situ* data limited our analysis to 2000–2014. SGRs were constructed empirically for every model grid cell globally, where there was a sufficiently strong correlation between modelled discharge and MODIS-derived surface water extent. Our approach was

the same as documented in Hou et al. (2018) (Fig. 1). Briefly, time series of surface water extent are derived from MODIS (see Section 2.1.1); the best-correlated MODIS pixel corresponding to each *in situ* or modelled discharge is selected; the relationship between discharge and selected water extent time series is established in the training period; and river discharge is then predicted based on the developed relationship using MODIS-derived water extent time series in the validation period. Therefore, the employed approach allows estimating river discharge from satellite observations.

A robust correlation between modelled channel storage and MODIS-derived water extent for a particular river reach was taken as an indication that an SGR might be possible. (There is a direct linear relationship between channel storage and discharge within the model structure, and hence the results would have been identical if modelled discharge had been used instead; but channel storage is conceptually more closely related to water extent.) Hou et al. (2018) empirically found that a search window of 0.55° × 0.55° (*i.e.* 11 × 11 = 121 MODIS grid cells) provided a good tradeoff for identifying the most suitable SGR grid cell for each river reach. The window was centered on the model grid cell that simulates river channel storage and discharge at the same 0.05° resolution. Model storage time series for the target grid
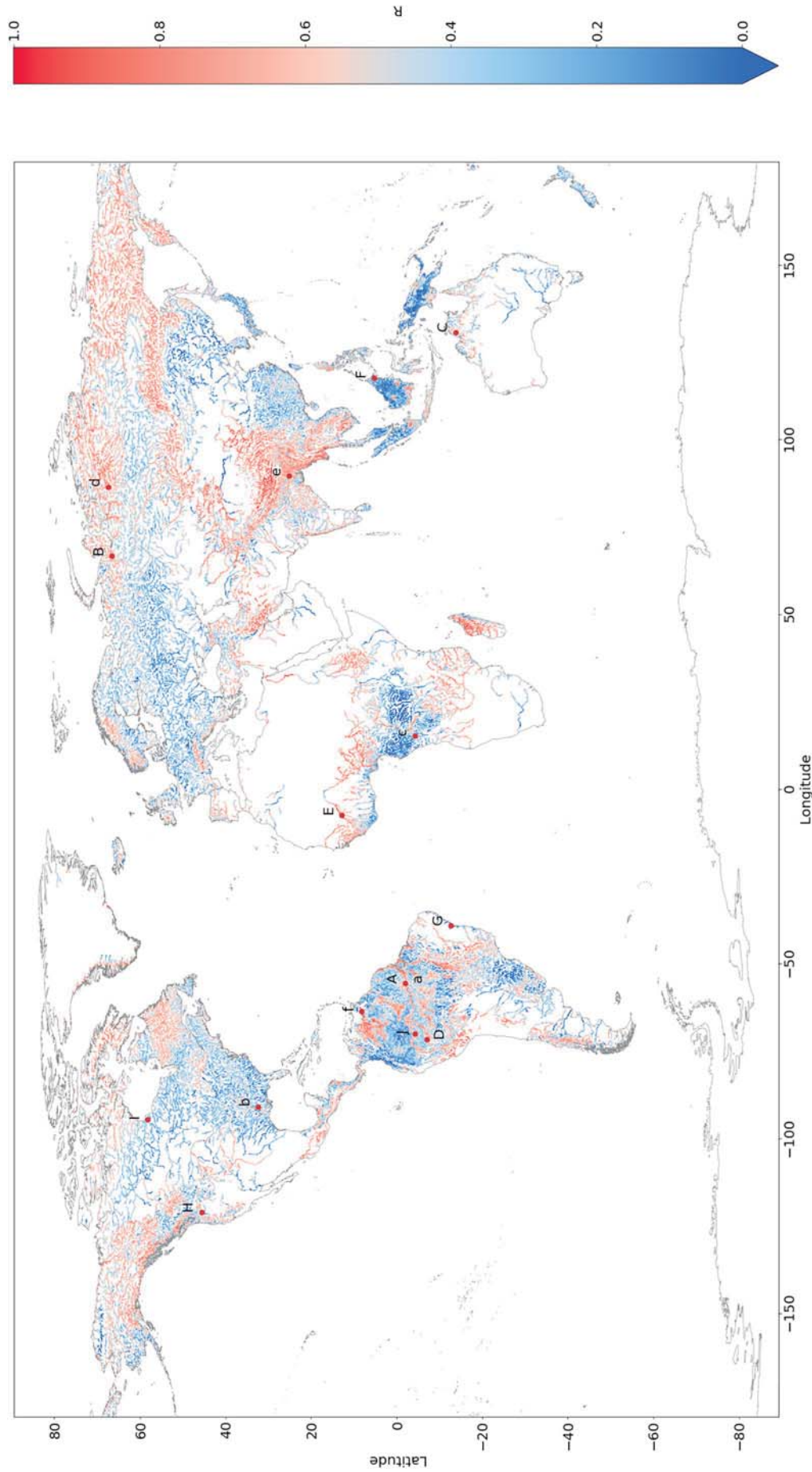
5

Fig. 4. Monthly correlations between MODIS-derived water extent and W3 model simulated river channel storage following the window search method. SGRs shown in subsequent figures are indicated by codes: A, D, J, a: Amazon; B: Ob; C: Daly; E: Niger; F: Sungai Malubuk; G: Paraguacu; H: Columbia; I: Churchill; b: Mississippi; c: Congo; d: Yenisey; e: Brahmaputra; f: Orinoco (uppercase letters: river morphology analysis; lower case letters: river discharge prediction capability analysis).
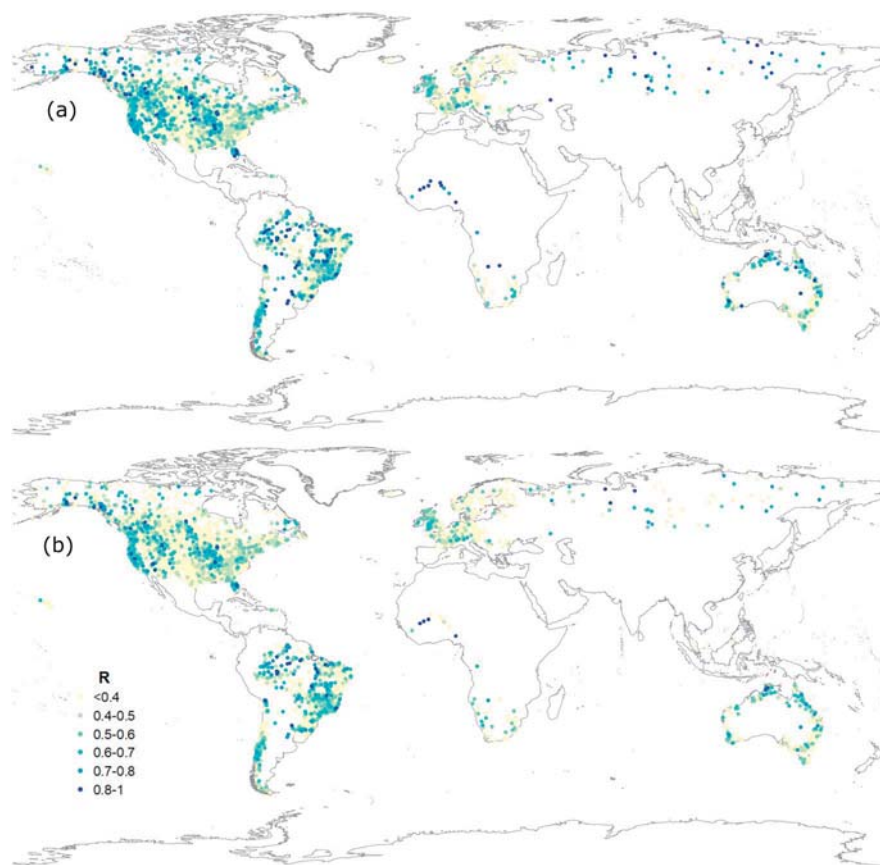
Fig. 5. The performance (monthly Pearson correlations between SGRs predictions and *in-situ* data) of (a) gauge-based and (b) model-based SGRs at gauged locations.
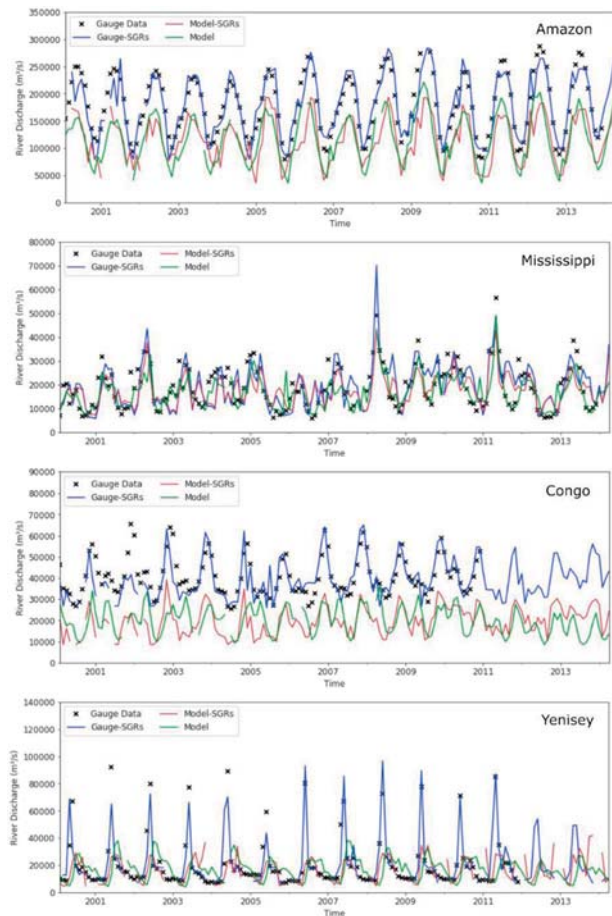
cell were compared with the 121 water extent time series for each cell within the search window. The greater of Spearman's rank correlation coefficient (ρ) and Pearson correlation (R) was interpreted as an indication of the likely monthly performance of the SGR. We evaluated SGR performance using temporal cross-validation (Table 2). The time series were split into three periods of five years each (2000–2004, 2005–2009, and 2010–2014). Any two of them were combined as training data and used to validate the remaining period for three rounds without repetitions. The MODIS remote sensing grid cell with the strongest correlation was selected using the training data while the performance was assessed for the validation period. This resulted in three experiments at each location. The mean result from the three experiments was used as the overall statistic to assess SGR performance.

To independently evaluate the model-based SGRs, we used them to predict river discharge for reaches where *in-situ* discharge data were available (Fig. 1). The same split-sample approach (Table 2) was followed, where model data was used to develop and train the SGR, and subsequently separate predictions for the three validation periods were combined and compared with observed discharge using Pearson correlation (*R*). River discharge estimation was carried out by cumulative distribution function (CDF) matching. In the training period, a rank-based look-up table is developed to rank all *in-situ* or modelled discharge and the selected MODIS grid water extent time series, and connect water extent to corresponding discharge based on their ranking. In the validation period, water extent estimates are ranked relative to the water extent observed during the training period and then matched to the corresponding discharge estimates. For comparison, SGRs based on *in-situ* records rather than model simulations were also constructed where possible (Fig. 1). In particular, the central MODIS grid cell of the search window for gauge-based SGRs is the grid cell that contains the gauge.

2.2.2. The influence of river morphology on satellite-based river gauging

The SGRs were constructed empirically, based on the correlation between the MODIS remote sensing time series for image grid cells within the search window and *in-situ* records or model simulations. We hypothesized that river morphology within the selected grid cell and more broadly within the search window are the primary determinant of SGR performance, specifically, the change in surface water extent (*i.e.* effective river width) in response to discharge changes. To test this, we extracted 30-m resolution surface water occurrence data for the 0.55° search window, and the selected 0.05° grid cell from the GSWD for each gauge-based SGR. For the search window, maximum surface water mapping was derived from the GSWD surface water occurrence data. Maximum surface water mapping was restricted to surface water detected at least once only in all cloud-free, 16-day temporal Landsat observations. The surface water grid cells in the mapping were segmented based on their connectivity and identified as river channel, floodplains, water bodies and off-channel storage segmentations according to their unique characteristics. The river channel segmentation was selected and river widths at 30 m intervals along the river channel were calculated after tracing a river vector using medial axis skeletonisation (the topological skeleton; Jain et al., 1995). The maximum and mean river widths were chosen to represent river channel characteristics. For the selected SGR grid cell, surface water extents at different recurrence frequencies from 0.5% to 80% were calculated based on the GSWD surface water occurrence data. These were normalised by maximum water extent to provide a dimensionless index of temporal surface water extent variability. Nine successful (R ≥ 0.4) and unsuccessful (R < 0.4) cases of SGRs were selected to illustrate river morphology conditions affecting the performance of SGRs, and analyzed and related to the calculated and mapped features.

To develop a methodology to predict the likely success of SGRs *a priori* based on globally available river morphology data, we calculated
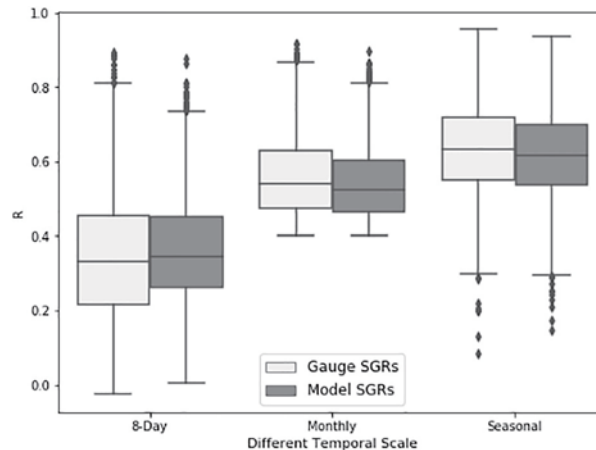
Fig. 6. River discharge predictions derived from the model-based (brown line) and gauge-based (blue line) SGRs and the model (green line) along with *in-situ* river discharge measurements (black crosses). (For interpretation of the references to colour in this figure legend, the reader is referred to the web version of this article.)

Fig. 7. The performance of 1705 accepted SGRs at different temporal scales (the 8-day and seasonal performance relates to SGRs constructed using monthly averaged data).
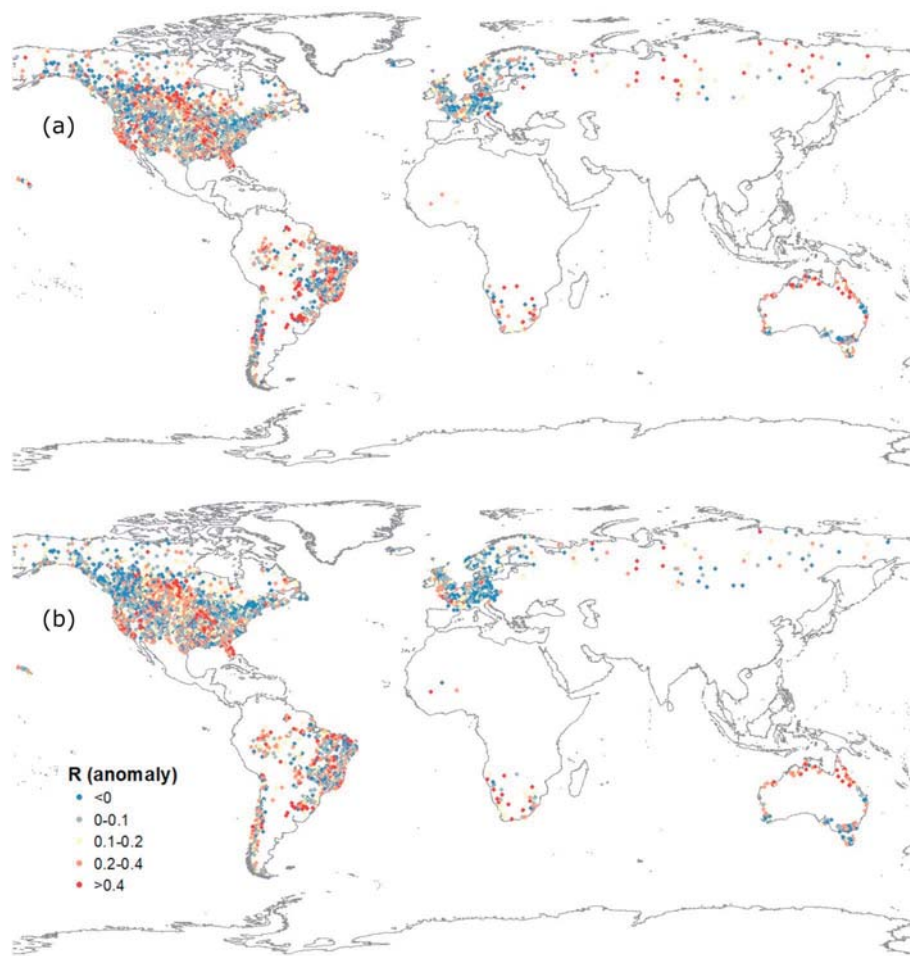
of SGRs demonstrating a Pearson correlation ≥ 0.4 to the total number ($N \geq 10$) of SGRs constructed. The success rate was calculated for each combination of a minimum number of grid cells exceeding the water extent range threshold.

3. Results and discussion

3.1. Global performance of satellite gauging reaches

Monthly correlations between MODIS-derived water extent and W3 model simulated river channel storage were calculated for 372 thousand grid cells containing river reaches with an annual mean discharge > 10 m³/s, having a combined length of *ca.* 1.86 million km (Fig. 4). A total of 62% of grid cells considered show a correlation coefficient ≥ 0.4. A total of 2% of cells with a combined river length of 36,530 km show correlation coefficients above 0.8. The strongest correlations occur along the main river reaches of South America and Africa and in northern high latitude regions, South Asia, and the Middle East.

The W3 model was calibrated uniformly against a large global set of headwater catchments (Van Dijk et al., 2016) rather than to individual gauge records, and therefore can show bias when evaluated for any particular river gauge. This model bias propagates into model-based SGRs, so model-based SGRs have limited capabilities to predict un-biased discharge depending on the quality of modelled discharge. Our objective was to develop a capability to infer temporal flow patterns in gauged and ungauged rivers alike, where necessary based on high-resolution estimated of discharge from a global hydrological model. In doing so, we expect the model to have systematic biases in regards to

descriptive statistics on surface water extent ranges for each 0.05° grid cell within the search window for all gauge-based SGRs (Fig. 2). Surface water occurrence mapping was again derived from the GSWD. We calculated the temporal range of water extent as the difference between the maximum and minimum water extent for each grid cell (Fig. 3). The number of grid cells with temporal water extent ranges greater than a threshold was calculated for threshold values of 0–80% with 10% increments for all gauging stations. For example, for a threshold range of 30%, the number of 0.05° grid cells within the 0.55° window around a gauging station with a water extent range of 30% or more was determined. The SGR success rate was defined as the ratio of the number

Table 3

The performance of model-based SGRs, gauge-based SGRs, and the model of Fig. 6.

Site	Type	2000–2004	2005–2009	2010–2014	2000–2014
Amazon	W3 model	0.94	0.92	0.94	0.93
	Model-based SGR	0.83	0.88	0.94	0.89
	Gauge-based SGR	0.91	0.93	0.94	0.92
Mississippi	W3 model	0.82	0.87	0.88	0.86
	Model-based SGR	0.50	0.69	0.71	0.64
	Gauge-based SGR	0.51	0.73	0.71	0.65
Congo	W3 model	0.6	0.57	0.8	0.58
	Model-based SGR	0.73	0.85	0.65	0.74
	Gauge-based SGR	0.69	0.85	0.93	0.74
Yenisey	W3 model	− 0.11	− 0.15	− 0.22	− 0.14
	Model-based SGR	0.39	0.50	0.28	0.41
	Gauge-based SGR	0.85	0.94	0.90	0.88

Fig. 8. The performance (monthly anomaly Pearson correlations between SGRs predictions and *in-situ* data) of (a) gauge-based and (b) model-based SGRs at gauged locations corresponding to Fig. 5.

true discharge, but these are fundamentally unknown in ungauged rivers. However, as long as the temporal pattern in model-simulated flows is sufficiently similar to true river hydrology, an SGR can still be constructed successfully, and will enable the detection of unusually high or low river discharge behavior (*i.e.* flood or drought conditions), if not necessarily absolute discharge volumes. For this reason, we did not use bias-influenced statistics such as Nash-Sutcliffe Efficiency, but instead chose measures of relative and ranking agreement, such as Pearson correlation and Spearman's rank correlation, in line with previous studies (*e.g.*, Hou et al., 2018; Van Dijk et al., 2016).

In contrast, the gauge-based SGRs are inherently free of bias. Clearly, the bias in the model and model-based SGRs can be addressed if independent gauging data are available, but this is counterfactual in ungauged rivers. Alternatively, the use of model ensembles has been shown capable of producing less biased discharge estimates (*e.g.*, Beck et al., 2017). To our knowledge, 0.05°-resolution global routed discharge time series are only available from the W3 model, but if such estimates become available from other models in future, then this could provide a promising opportunity to improve the SGR methodology developed here.

Optical remote sensing of water extent is affected by vegetation and by clouds and other forms of atmospheric contamination. The 8-day compositing used for MODIS products reduces such effects but also leads to temporal smoothing, which may affect the ability of SGRs to detect short-lived flood events. As an alternative, the daily Global Flood Detection System (GFDS) passive microwave remote sensing data (De Groeve et al., 2015) can also be used to construct SGRs (Hou et al., 2018). These observations are less affected by cloud and vegetation, but

do have other sources of error and are of coarser spatial resolution (0.1° × 0.09°), producing a smaller number of suitable SGRs sites globally (Van Dijk et al., 2016).

In our cross-validation framework, using data in different training and validation periods can result in different pixels being selected. As a result, SGRs trained during a dry period can be less successful in predicting river discharge during a wet period, and *vice versa*. To avoid such issues, the full period should be used for SGR construction and training in operational implementations.

3.2. Performance and uncertainties of satellite gauging reaches

Both model- and gauge-based SGRs performed well along many larger river reaches in South America, parts of middle and western North America, northern Australia, northern Russia, and the Niger River (Fig. 5). The gauge-based SGRs in northern Russia and the Niger River outperformed model-based SGRs. Poor results were obtained in the remainder of North America, eastern Brazil, southeastern Australia, Europe, South Africa, and Malaysia (Fig. 5). In total, 30% of gauge-based SGRs predicted river discharge with a Pearson correlation ≥ 0.4, slightly higher than that of model-based SGRs (25%). Of these, 322 gauge-based and 177 model-based SGRs produced Pearson correlations ≥ 0.7, mostly located in South America and northern Russia.

Monthly river discharge derived from the SGRs and the model was evaluated against *in-situ* records. Four typical examples representing the observed range of performance are shown in Fig. 6 and Table 3. The model accurately reproduced river discharge variations for the Amazon (Fig. 6, Table 3) and Mississippi rivers (Fig. 6, Table 3), but not the
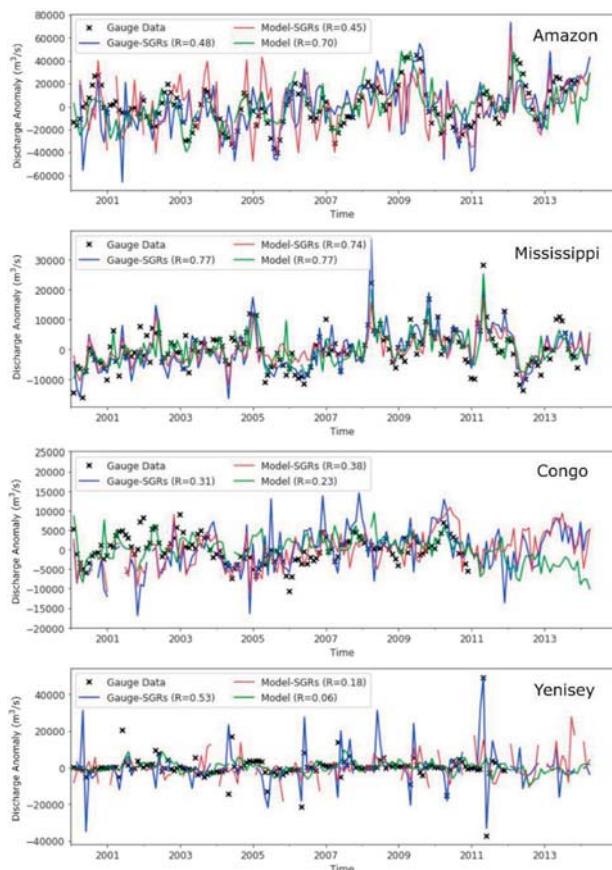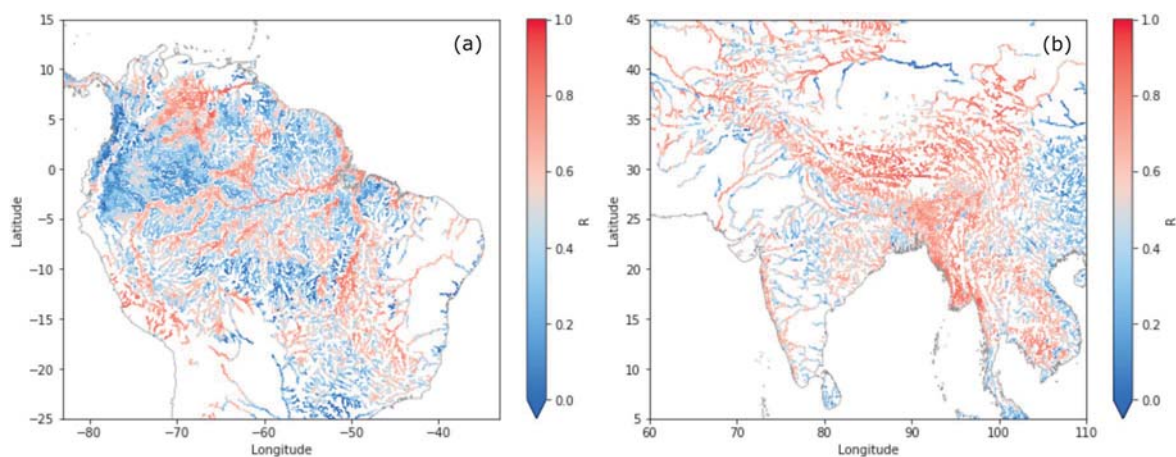
Fig. 9. River discharge anomaly predictions derived from the model-based (brown line) and gauge-based (blue line) SGRs and the model (green line) along with *in-situ* river discharge measurements (black crosses) corresponding to Fig. 6. (For interpretation of the references to colour in this figure legend, the reader is referred to the web version of this article.)

Yenisey River (Fig. 6, Table 3). Accordingly, the model-based SGR produced a relatively poor result for the Yenisey River (R = 0.41). By comparison, the gauge-based SGR showed a high Pearson correlation of 0.88 against *in-situ* data for the Yenisey River. The model under-estimated river discharges for the Congo River. Despite this, the model-based SGR still reproduced relative discharge variations with similar performance as the gauge-based SGR (R = 0.74 in both cases). Model- and gauge-based SGRs showed very similar performance for the Amazon River (R = 0.89–0.92) and the Mississippi River

(R = 0.64–0.65, Fig. 6, Table 3).

Our results showed that it is possible to construct SGRs from 0.05° MODIS optical remote sensing data for ~3000 gauged and > 200,000 ungauged river reaches. The SGRs can be used to monitor river dis-charge from MODIS observations at the global scale, particularly along the main rivers of South America and Africa, in northern high latitudes, and in South Asia and the Middle East (Fig. 5). SGRs sometimes show short discontinuities in river discharge estimation. For example, there is a one-month gap during the early 2002 in the Amazon River (Fig. 6). This is usually caused by cloud contamination, which is a drawback of using optical remote sensing observations. Model-based SGRs can have the same skill as gauge-based SGRs (Fig. 5), but this depends on the accuracy and reliability of the hydrological model. The performance of model-based SGRs was substantially worse than that of gauge-based SGRs for the rivers in northern Russia (Fig. 5). This appears to be mainly because the W3 model did not simulate river discharge dy-namics reliably, which we attribute to a comparatively poor perfor-mance in simulating snow hydrological processes, *e.g.* in the Yenisey River (Fig. 6, Table 3) (see also Beck et al., 2017). Errors in forcing data (*e.g.*, precipitation, radiation, temperature), suboptimal model para-meterisation, and/or model structural deficiencies can all affect the quality of model discharge estimates and can potentially lead to poorly constructed SGRs. For instance, neither the model nor the SGR based on it reproduced measured river discharge in the Congo River (Fig. 6, Table 3). Interestingly, the model-based SGRs did outperform the model itself in this case, and this occurred in some other cases as well (Fig. 6, Table 3). For example, the model-based SGRs for the Yenisey River were able to reproduce the reduction in river discharge during winter, where the model failed (Fig. 6, Table 3). Furthermore, the W3 model assumed a converging river flow network constructed on the basis of flow direction inferred from a 0.05° digital elevation model. This does not necessarily produce realistic discharge simulations in river systems that split into multiple distributaries over a width of > 5-km at high flow conditions, such as those sometimes found in low-relief arid re-gions (*e.g.* the Okavango delta and Australian Channel Country). The grid cell search window used may still allow an SGR to be constructed, but would correspond to the discharge in all distributaries combined. Such cases suggest that it is sometimes possible to improve model es-timates through assimilation of SGR discharge estimates, even if these are based on the model itself.

In total, there are 1705 potential SGRs for which there are daily gauging data with performance above 0.4 at monthly temporal scale. Of these, 35% still have Pearson correlations above 0.4 against 8-day gauging data (Fig. 7). The number of SGRs with performance above 0.7 decreases from 435 through 222 to 71 as time step is changed from seasonal, through monthly, to 8-day intervals (Fig. 7). The degrading performance at 8-day temporal scale is mainly due to the poor

Fig. 10. Promising regions for SGRs: (a) northern South America and (b) southern Asia.
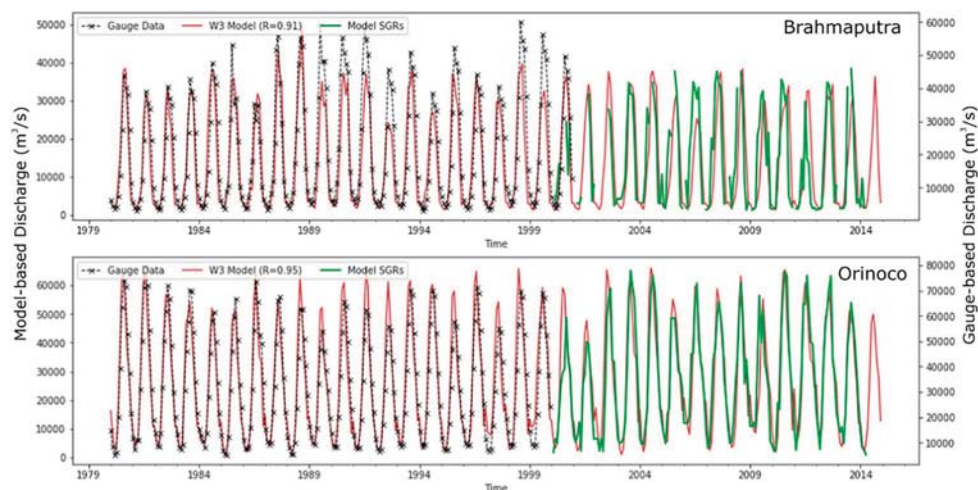
representation of the real 8-day dynamics by compositing of MODIS observations and the influence of cloud contamination on MODIS observations. These issues were reduced by using monthly or seasonal averaging of the imagery.

The presence of a strong seasonal discharge cycle with associated inundation enhances the chances of establishing a successful SGR. However, where this seasonal cycle is a large part of the total variance in water extent, the ability of the SGR to detect smaller deviations from the seasonal cycle may be limited. To assess this, we calculated Pearson correlations of seasonally-adjusted anomalies (*i.e.*, deviations from the average seasonal cycle) between gauged and SGR-estimated discharge for all potential SGRs (Fig. 8). Compared to Fig. 5, it is evident that most of SGRs have degraded performance for seasonally-adjusted anomalies. However, SGRs that have robust performance (R > 0.7) can still have reasonable capability to predict seasonal anomalies, with Pearson correlations > 0.4. To illustrate seasonally-adjusted anomaly prediction, we plot river discharge anomaly predictions derived from the model and SGRs against *in situ* anomaly observations, corresponding to Fig. 6 (Fig. 9). For successful cases, both the model and SGR are able to predict seasonal anomalies, with R > 0.7 in the Mississippi River, while the model outperforms SGRs in the Amazon River as SGRs overestimate peak flow and underestimate low flows (Fig. 9). For poor cases (despite well-performing gauge-based SGRs), the model fails to predict seasonal anomalies, which leads to the poor performance of model-based SGRs in the Congo River and Yenisey River (Fig. 9). However, the gauge-based SGRs in the Yenisey River can still track seasonal anomaly to some extent (R > 0.5). These results do not imply that the SGRs are redundant in highly seasonal rivers; as unusually-timed transitions between low and high flow conditions (*e.g.*, due to early or late spring snow melt or monsoon arrival) will still be correctly identified by the SGR, even if they may contribute little to the explained variance overall. In the context of a rapidly changing global climate system, this can provide an important monitoring capability.

Where possible, gauging stations are usually constructed along a single, narrow and stable channels without large floodplains. These aspects are directly at odds with the requirements for river gauging based on water extent, which is most amenable to multiple and broad channels with large floodplains. This difference probably leads to an underestimation of the potential of SGRs: there are no *in-situ* data in many reaches apparently suitable for SGRs, and hence we cannot evaluate their performance. For example, we found high correlations between water extent and modelled storage along the Brahmaputra and Orinoco Rivers (Fig. 10), but there were no *in-situ* data available after 2000 and hence we could not evaluate the model-based SGRs. An indirect validation is possible to some extent, however. There were strong correlations between *in-situ* discharge measurements and modelled

discharge before 2000 (Fig. 11). This suggests that the W3 model was able to reproduce measured river discharges. In turn, the strong correlation between discharge from the model and the model-based SGRs suggest that the latter have good discharge prediction skill (Fig. 11).

3.3. The importance of river morphology for satellite gauging reach development

River morphology and SGR performance were compared for a large number of SGRs. Common river morphology conditions that enable a successful SGR are illustrated in Figs. 12 and 13. The reaches of the lower Amazon River (R = 0.92) and Ob River (R = 0.93) have very wide channels with maximum widths of approximately 4.5 km and 7.0 km, respectively, with broad floodplains and multiple stable channels (Fig. 12, Table 4). The automatically selected SGR grid cell was located on the ephemerally-inundated floodplain for the Amazon River and over braided channels for the Ob River, with water extent ranges of 70% and 30%, respectively. The Niger River reach (Fig. 12, Table 4) had a mean width of 609 m and no obvious floodplain or stable permanent channel. The selected SGR grid cell included the channel with a water extent range of nearly 80%. The river channels of the upper Amazon River and the Daly River were quite narrow with mean widths of 218 m and 67 m, respectively (Fig. 12, Table 4). The Daly River shows a less tortuous channel with several large but infrequently-flooded floodplains. The upper Amazon River shows strongly meandering channels with oxbow lakes, some of which may be disconnected (alternatively, tree cover may have prevented detection of connecting flood events). The selected SGR grid cell for the Daly River covers a part of the floodplain, whereas that for the upper Amazon River includes several off-channel meander lakes, with water extent ranges of almost 100% and 70%, respectively (Fig. 12). Common for all reaches is that the MODIS-derived water extent time series are temporally correlated with *in-situ* discharge measurements, with Pearson correlations of 0.72–0.93, although there is some noise in the MODIS signal for the Daly and upper Amazon rivers (Fig. 13).

Earlier studies have shown that river width, floodplain, flood potential, land cover type, climate, hydraulic structure and local topography can all affect the effectiveness of remote sensing-based river discharge estimation (Kim and Sharma, 2019; Revilla-Romero et al., 2014). However, dynamic river morphology factors such as river width and floodplain inundation might be expected to have a more direct influence. They also formed the basis for the hydraulic geometry theory relating river width to discharge (Leopold and Maddock, 1953). We analyzed the impact of river morphology measures derived from high spatial resolution Landsat-derived surface water occurrence dataset (GSWD) on the performance of gauge-based MODIS SGRs. We identified
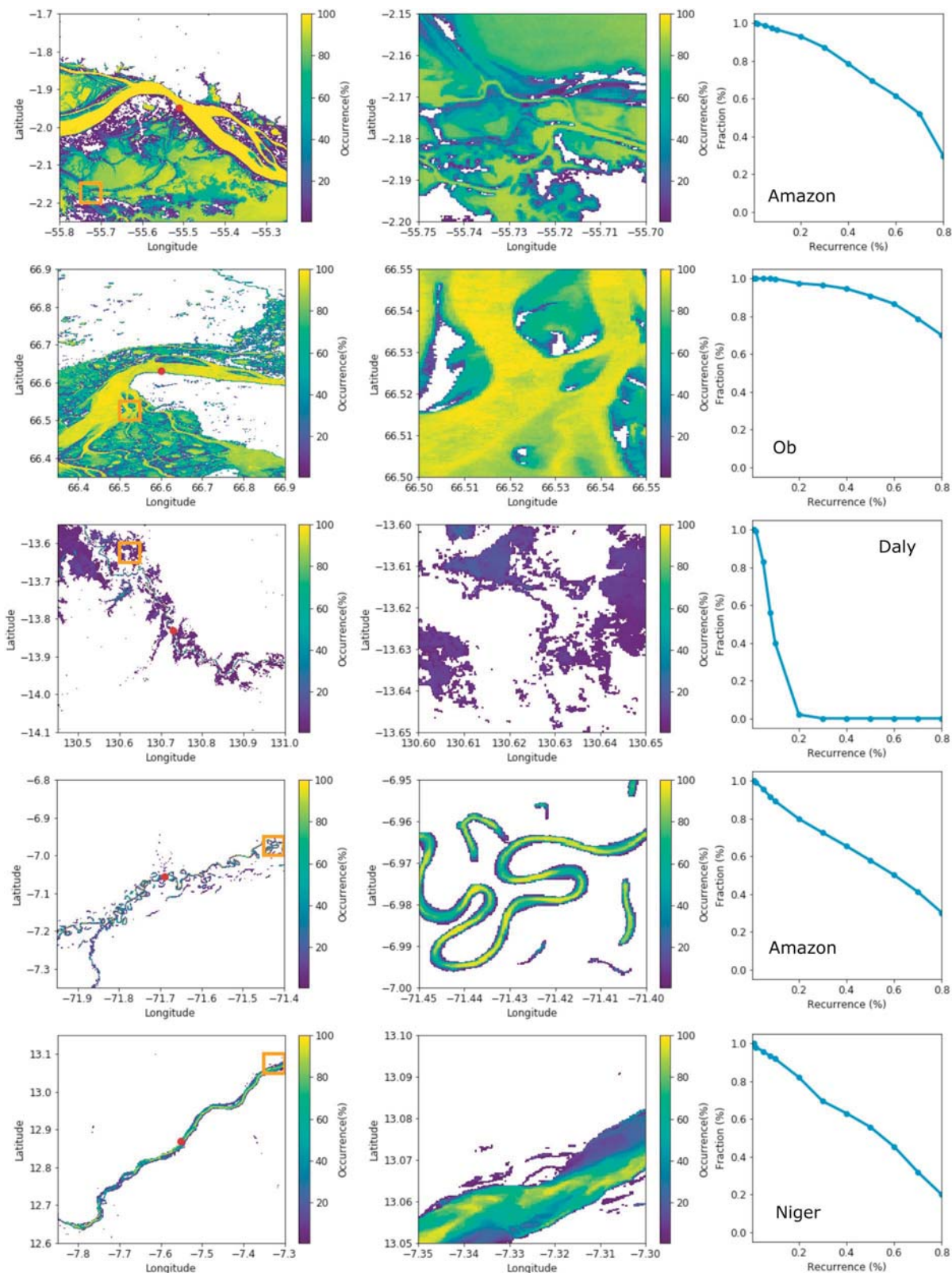
Fig. 12. Illustrative river morphology conditions that contribute to a successful SGR: (left) water extent occurrence from the GSWD within the search window with the selected SGR highlighted in orange, (middle) water extent occurrence from the GSWD for the selected SGR grid cell, and (right) SGR grid cell water extent at different temporal recurrence frequencies.

typical river morphology conditions that are amenable to successful SGRs. Wide reaches with strong temporal variations in water extent are beneficial. These can occur if the river channel itself is wide, or if there is an extensive floodplain or multiple braided channels that connect to the river reaches during high flow conditions. If the river channel is narrow, a large number of meandering channels can be beneficial. By contrast, narrow incised river channels without a large floodplain prevent the establishment of SGRs (Fig. 14). For narrow river channels
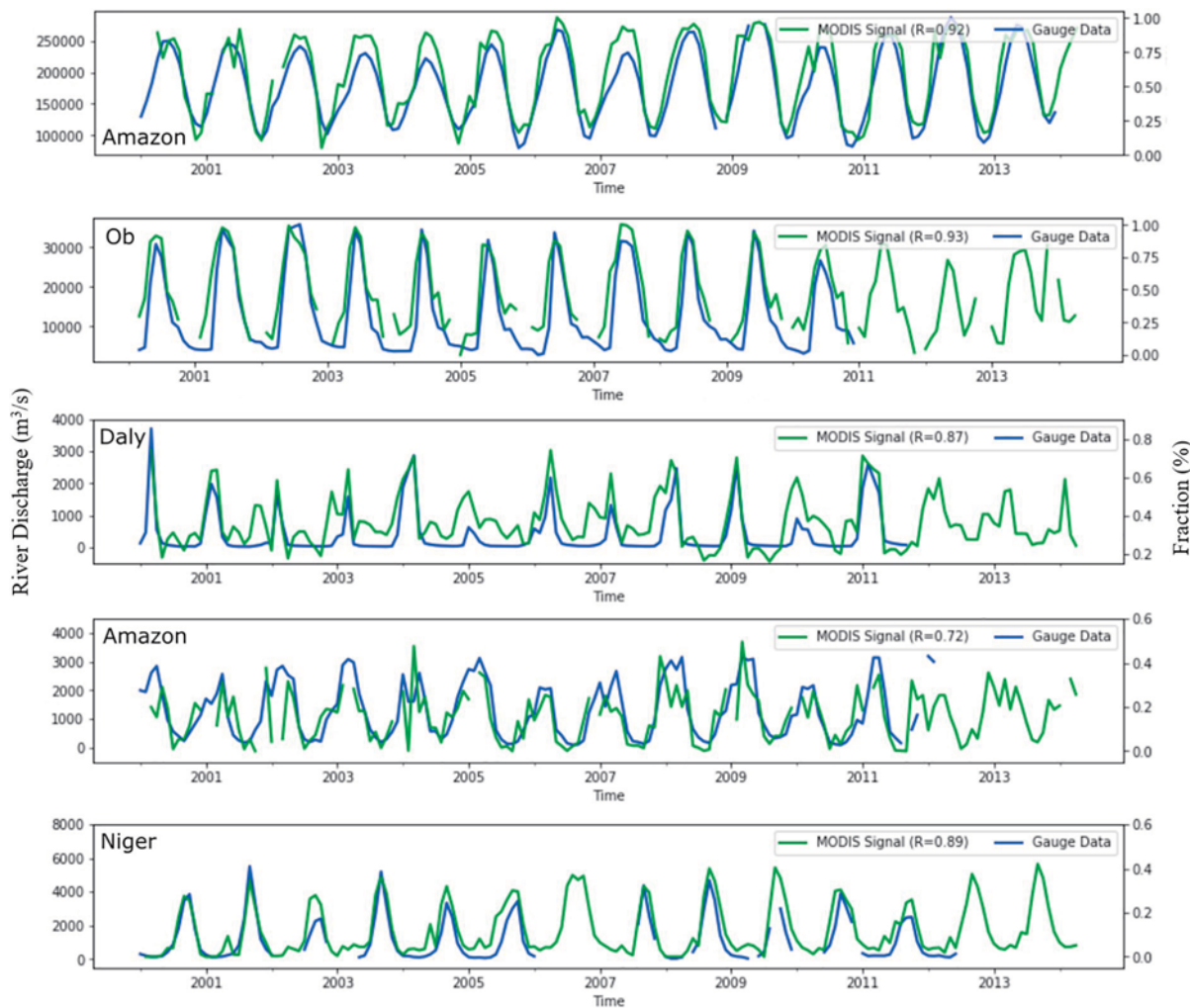
Fig. 13. MODIS-derived water extent time series of the selected SGR grid cell (units on right axis) compared against *in-situ* river discharge measurements (units on left axis).

Table 4
The river channel width and the performance of SGRs for the river reaches shown in Figs. 6, 12 and 14.

Index	River name	Latitude (°)	Longitude (°)	R	Maximum width (m)	Mean width (m)
A, a	lower Amazon	−1.95	−55.51	0.92	4450	1782
B	Ob	66.63	66.60	0.93	6957	1769
C	Daly	−13.83	130.73	0.87	158	67
D	upper Amazon	−7.06	−71.69	0.72	532	218
E	Niger	12.87	−7.55	0.89	1484	609
F	Malubuk	5.30	117.59	0.09	320	86
G	Paraguacu	−12.60	−38.98	0.03	3731	956
H	Columbia	45.61	−121.17	0.17	1346	527
I	Churchill	58.12	−94.62	0.21	1110	415
b	Mississippi	32.31	−90.91	0.65	1664	870
c	Congo	−4.30	15.30	0.74	5538	1495
d	Yenisey	67.43	86.48	0.88	8739	3105

with narrow floodplains, SGRs tend to select the grid cell that covers the floodplains, but this often does not respond to the full range of river discharge (Fig. 14). When there are many not or poorly connected water bodies around the river reach, the selected grid cell will still tend to cover these, but in those cases, the correlation between water extent and river discharge may be poor and affected by hysteresis (Fig. 14). Reservoir dams or other types of hydraulic infrastructures can cause a

disconnection in hydrological conditions upstream and downstream, and also prevent a successful SGR (Fig. 14).

3.4. Predicting the potential for constructing a satellite gauging reach

The probability of constructing a successful SGR (R ≥ 0.4) was calculated across the *in-situ* data set, considering a different aggregate number of grid cells within the search window with water extent ranges above different thresholds (Fig. 15). For a given extent range threshold, the number of SGRs decreases as the number of cell with water extent above the threshold increases, as more and more stations will not have that many grid cells exceed the extent range threshold. Probabilities are not shown where the number of stations was less than N = 10. For each threshold, the probability of constructing a successful SGR increases as the number of grid cells with a water extent range above the threshold increases. Furthermore, with greater extent range thresholds, the number of grid cells required to construct a successful SGR decreases.

The minimum conditions of developing a successful SGR in terms of a certain probability can be inferred based on a given number of 0.05° grid cells in the 0.55° × 0.55° search window with a water extent range exceeding a given threshold fraction from the statistical results in Fig. 15. For example, to achieve > 30% probability of constructing a successful SGR, at least 3 grid cells with water extent variations of 1% (0.25 km^2) or 1 grid cell with changes of 2% (0.5 km^2) should exist; if targeting > 60% probability, 1 grid cell with water area dynamics of 60% (15 km^2) or 30 grid cells with variations of 8% (2 km^2) should
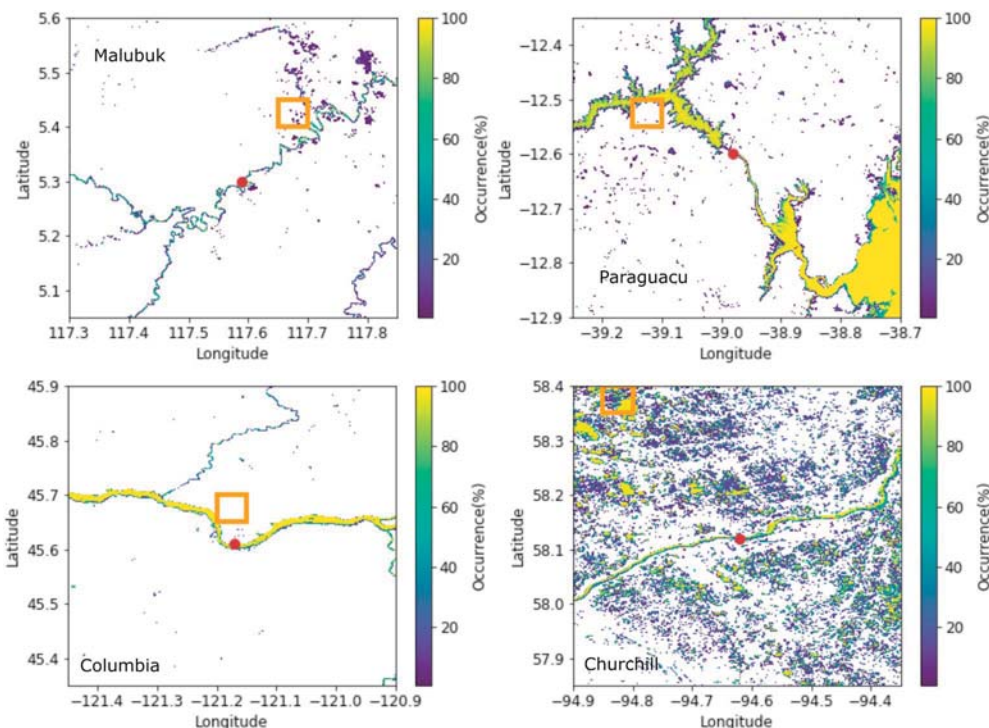
Fig. 14. Illustrative river morphological conditions preventing a successful SGR.
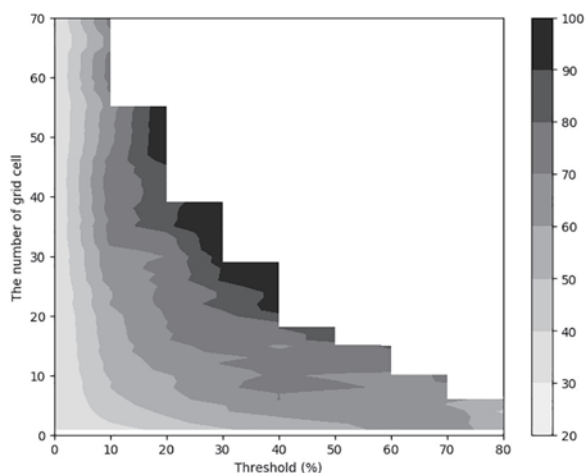

Fig. 15. Empirically calculated probability of constructing a successful SGR for a given number of 0.05° grid cells in the 0.55° × 0.55° search window with a water extent range exceeding a given threshold fraction.
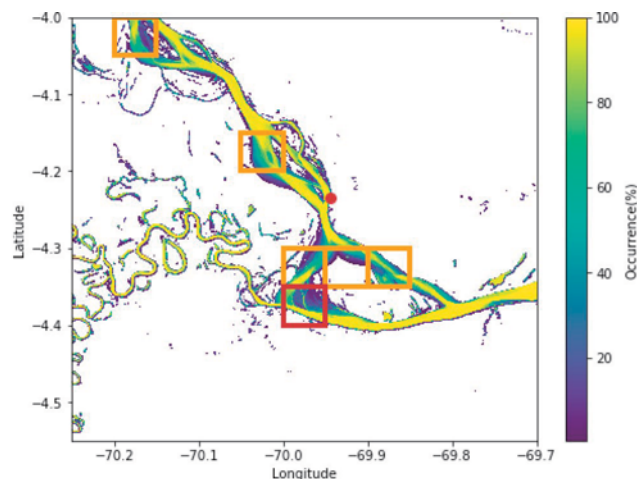

Fig. 16. The river morphology condition in the midstream of the Amazon River (brown square: the best-correlated grid cell; orange grids: the other grid cells with large water extent ranges). (For interpretation of the references to colour in this figure legend, the reader is referred to the web version of this article.)

exist.

A larger number of grid cells with a large temporal water extent range indicated a higher probability of constructing a successful SGR (Fig. 15). This does not mean that grid cells can be selected without needing to consider their correlation with *in-situ* or model-based discharge estimates. For a middle reach of the Amazon River, we compared the correlation with *in-situ* measurement for water extent time series over the statistically-selected grid cell (*i.e.* the 'best grid cell'), with those over the grid cells with the greatest water extent range ('combination grid cells'), and those that cover the entire river reach ('reach grid cells') (Figs. 16 and 17). The results showed that the best grid cell does indeed perform better (R = 0.81) than the combination grid cells (R = 0.69) and reach grid cells (R = 0.65), respectively. Nonetheless, a combination of grid cells that have large water extent ranges or different levels of water extent changes may still prove a

suitable approach to develop SGRs without correlation-based grid cell selection.

3.5. Further opportunities to improve satellite-based river gauging

Constructing empirical rating curves between *in-situ* discharge and a satellite-observed hydraulic variable has been the most widely used method to derive river discharge from remote sensing (*e.g.*, Kouraev et al., 2004; Papa et al., 2008; Smith et al., 1995). Deriving discharge-height rating curves is currently limited to a small fraction of rivers globally because radar altimeters have sparse spatial coverage and are affected by surrounding topography, although the combination of multiple radar altimeters can help to produce long-term records and near-real time monitoring capability (*e.g.* Topex/Poseidon
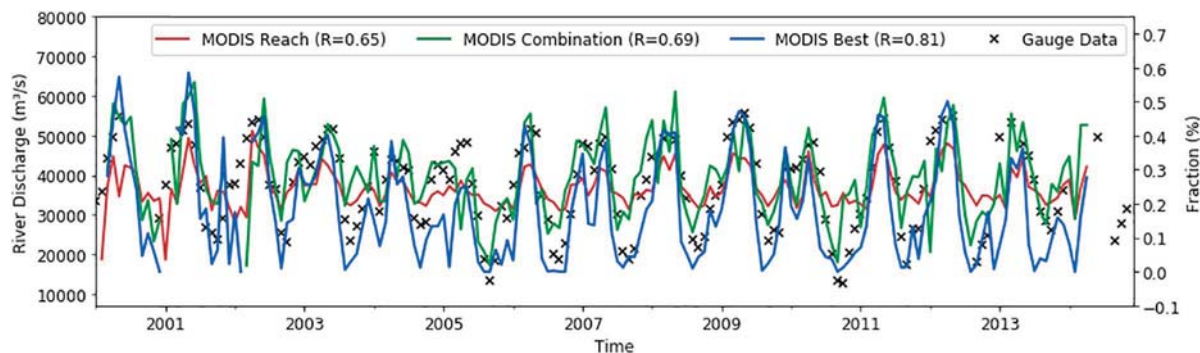
Fig. 17. The performance of the selected best-correlated grid cell (blue line), grid cells covering all river reaches (brown line), and the combination of grid cells that have large water extent range (green line) (units on right axis) evaluated against *in-situ* discharge data (black crosses) (units on left axis). (For interpretation of the references to colour in this figure legend, the reader is referred to the web version of this article.)

(1992–2002), ENVISAT (2002–2010), Jason-2 and 3 (2008–current)). Optical remote sensing (*e.g.,* MODIS (2000–current)) enables discharge-width rating curves to estimate discharge, but is affected by cloud and vegetation cover (*e.g.,* Smith and Pavelsky, 2008). This can be mitigated using synthetic aperture radar (*e.g.,* Smith et al., 1995) but these in turn have conventionally be limited by a low revisit frequency. Papa et al. (2008) employed passive and active microwave along with visible and infrared optical remote sensing to estimate discharge based on discharge-inundation rating curves, but their method is restricted to the entirety of large basins. Satellite-derived water elevation, slope and width can be used together to estimate discharge based on Manning's equation (*e.g.,* Bjerklie et al., 2005), but this approach requires ancillary *in-situ* data, and is highly parametrized and specific to individual river reaches (Biancamaria et al., 2016). Gleason and Smith (2014) proposed the AMHG algorithm, which provides the potential to estimate river discharge from multi-temporal Landsat-derived width observations. However, the AMHG method requires a single river channel with modest width variations. The Surface Water and Ocean Topography (SWOT) satellite mission is planned to launch in 2021, and its ability to measure river width, elevation, and slope simultaneously provide an alternative opportunity to estimate river discharge without station data (Pavelsky et al., 2014). Approaches have been developed to optimally combine these observations (*e.g.,* MetroMan, Durand et al., 2014; Yoon et al., 2016; MFG, Bonnema et al., 2016; MFCR, Durand et al., 2016; GaMo, Durand et al., 2016; Garambois and Monnier, 2015; BAM, Feng et al., 2019; Hagemann et al., 2017). However, all the approaches mentioned are designed for river discharge estimation at scale of larger (*e.g.,* > 1 km) river reaches.

In contrast, the empirical C/M ratio approach (Brakenridge et al., 2007; Li et al., 2019; Tarpanelli et al., 2017; Tarpanelli et al., 2013) can be used to estimate river discharge at local scale using either passive microwave or optical remote sensing. The SGR methodology developed further here based on previous studies (Hou et al., 2018; Van Dijk et al., 2016) is readily applicable to a very large number of river reaches at both gauged and ungauged sites through the automated procedure developed here, and suited to near-real time application. It is suited to monitor discharge in single, multiple, braided and shifting channels, provided that water extent changes in response to discharge. We demonstrated that SGRs can be used to infer river discharge at global scale, especially in sparsely gauged basins in South America, Africa and Asia. We analyzed how river morphology affects the performance of SGRs, and identified reasons why some SGRs work and others do not. Overall, we found that wide channels and broad floodplains generally provide the best conditions for SGRs, in direct contrast with conditions suitable for *in situ* gauging. A new approach was introduced to predict the potential for constructing a successful SGR in any river reach, based on high-resolution inundation summary data available globally. In addition, we developed a theoretical insight into the basis for the successful MODIS window search grid cell selection method, rather than

the selection of multiple grid cells along the entire river reach or those with the greatest water extent range.

River morphology determines where SGRs can be established. However, a major limitation here was the relatively coarse resolution of MODIS. Higher spatial and temporal resolution remote sensing would enhance opportunities for tracking more rapid changes in discharge and detecting river reaches with small surface water extent changes. The recent launch of ESA's Sentinel 1, 2 and 3 missions provide a promising prospect for water extent monitoring with high spatial detail (10–60 m) as well as higher observation frequency and hence provide excellent new opportunities for satellite-based river gauging, particularly if they can be combined in a single, consistent time series. In the short term, the recently published daily 500-m resolution surface water change database for 2001–2006 of Ji et al. (2018) offers good prospects. Moreover, a hydromorphological dataset, including river width dynamics, flow regime and river gradient, produced by Hou et al. (2019) will help better determine potential locations for satellite-based river gauging.

4. Conclusion

We developed model- and gauge-based SGRs using 0.05° MODIS optical remote sensing at both gauged and ungauged river reaches globally. The model-based SGRs achieved a river discharge prediction skill that was often similar to gauge-based SGRs. Our results showed promising opportunities to develop SGRs in South America, Africa, and Asia, where the network of gauging stations is generally sparse. River size and morphology are the main factors determining the performance of SGRs. Wide channels with strong temporal variations in inundation provide the best conditions to construct a successful SGR. Relatively wide channels, broad floodplains, multiple braided channels, or a large number of meandering or anastomosing channels also contribute towards successful SGRs. The probability of constructing a successful SGR could be predicted based on readily available high-resolution inundation data and can thus be predicted for any river reach. Higher spatial and temporal resolution remote sensing will further increase the number of river reaches for which satellite-based discharge gauging will become possible.

Author contribution statement

Jiawei Hou: Conceptualization, Methodology, Validation, Formal analysis, Investigation, Data curation, Writing - Original draft, Visualization. **Albert I.J.M. van Dijk**: Conceptualization, Writing - Review & editing, Supervision. **Hylke E. Beck**: Data curation, Writing - Review & editing.

Declaration of competing interest

Acknowledgements

Appendix A. Supplementary data

Supplementary data to this article can be found online at https://doi.org/10.1016/j.rse.2019.111629.

References

Alsdorf, D.E., Rodriguez, E., Lettenmaier, D.P., 2007. Measuring surface water from space. Rev. Geophys. 45.

Beck, H.E., van Dijk, A.I., de Roo, A., Dutra, E., Fink, G., Orth, R., Schellekens, J., 2017. Global evaluation of runoff from 10 state-of-the-art hydrological models. Hydrol. Earth Syst. Sci. 21, 2881.

Biancamaria, S., Hossain, F., Lettenmaier, D.P., 2011. Forecasting transboundary river water elevations from space. Geophys. Res. Lett. 38.

Biancamaria, S., Lettenmaier, D.P., Pavelsky, T.M., 2016. The SWOT mission and its capabilities for land hydrology. Remote Sens. Water Resour. 117–147 (Springer).

Birkinshaw, S.J., O'donnell, G.M., Moore, P., Kilsby, C.G., Fowler, H.J., Berry, P.A.M., 2010. Using satellite altimetry data to augment flow estimation techniques on the Mekong River. Hydrol. Process. 24, 3811–3825.

Bjerklie, D.M., Dingman, S.L., Vorosmarty, C.J., Bolster, C.H., Congalton, R.G., 2003. Evaluating the potential for measuring river discharge from space. J. Hydrol. 278, 17–38.

Bjerklie, D.M., Moller, D., Smith, L.C., Dingman, S.L., 2005. Estimating discharge in rivers using remotely sensed hydraulic information. J. Hydrol. 309, 191–209.

Bonnema, M.G., Sikder, S., Hossain, F., Durand, M., Gleason, C.J., Bjerklie, D.M., 2016. Benchmarking wide swath altimetry-based river discharge estimation algorithms for the Ganges river system. Water Resour. Res. 52, 2439–2461.

Brakenridge, G.R., Nghiem, S.V., Anderson, E., Mic, R., 2007. Orbital microwave measurement of river discharge and ice status. Water Resour. Res. 43.

Brakenridge, G.R., Cohen, S., Kettner, A.J., De Groeve, T., Nghiem, S.V., Syvitski, J.P.M., Fekete, B.M., 2012. Calibration of satellite measurements of river discharge using a global hydrology model. J. Hydrol. 475, 123–136.

Coe, M.T., Birkett, C.M., 2004. Calculation of river discharge and prediction of lake height from satellite radar altimetry: example for the Lake Chad basin. Water Resour. Res. 40.

Davids, J.C., Rutten, M.M., Pandey, A., Devkota, N., van Oyen, W.D., Prajapati, R., van de Giesen, N., 2019. Citizen science flow – an assessment of simple streamflow measurement methods. Hydrol. Earth Syst. Sci. 23, 1045–1065.

De Groeve, T., Brakenridge, G.R., Paris, S., 2015. Global flood detection system data product specifications. In: JRC Technical Report, . http://www.gdacs.org/flooddetection/Download/Technical_Note_GFDS_Data_Products_v1.pdf.

Domeneghetti, A., 2016. On the use of SRTM and altimetry data for flood modeling in data-sparse regions. Water Resour. Res. 52, 2901–2918.

Durand, M., Neal, J., Rodríguez, E., Andreadis, K.M., Smith, L.C., Yoon, Y., 2014. Estimating reach-averaged discharge for the River Severn from measurements of river water surface elevation and slope. J. Hydrol. 511, 92–104.

Durand, M., Gleason, C.J., Garambois, P.A., Bjerklie, D.M., Smith, L.C., Roux, H., Rodriguez, E., Bates, P.D., Pavelsky, T.M., Monnier, J., Chen, X., Di Baldassarre, G., Fiset, J.M., Flipo, N., Frasson, R.P., Fulton, J., Goutal, N., Hossain, F., Humphries, E., Minear, J.T., Mukolwe, M.M., Neal, J.C., Ricci, S., Sanders, B.F., Schumann, G., Schubert, J.E., Vilmin, L., 2016. An intercomparison of remote sensing river discharge estimation algorithms from measurements of river height, width, and slope. Water Resour. Res. 52, 4527–4549.

Fay, M., Alberto Andres, L., Fox, C., Narloch, U., Straub, S., Slawson, M., 2017. Rethinking Infrastructure in Latin America and the Caribbean: Spending Better to Achieve More. The World Bank.

Feng, D., Gleason, C.J., Yang, X., Pavelsky, T.M., 2019. Comparing discharge estimates made via the BAM algorithm in high-order Arctic rivers derived solely from optical CubeSat, Landsat, and Sentinel-2 data. Water Resour. Res. 55, 7753–7771.

Frost, A.J., Ramchurn, A., Smith, A., 2018. The Australian Landscape Water Balance model (AWRA-L v6). Technical description of the Australian Water Resources

Assessment Landscape model version 6. Bureau of Meteorology http://www.bom.gov.au/water/landscape/assets/static/publications/AWRALv6_Model_Description_Report.pdf.

Garambois, P.-A., Monnier, J., 2015. Inference of effective river properties from remotely sensed observations of water surface. Adv. Water Resour. 79, 103–120.

García, L.E., Rodríguez, D.J., Wijnen, M., Pakulski, I., 2016. Earth Observation for Water Resources Management: Current Use and Future Opportunities for the Water Sector. World Bank Group, Washington, DC.

Gleason, C.J., Smith, L.C., 2014. Toward global mapping of river discharge using satellite images and at-many-stations hydraulic geometry. Proc. Natl. Acad. Sci. 111, 4788–4791.

Gleason, C.J., Wang, J., 2015. Theoretical basis for at-many-stations hydraulic geometry. Geophys. Res. Lett. 42, 7107–7114.

Gleason, C.J., Smith, L.C., Lee, J., 2014. Retrieval of river discharge solely from satellite imagery and at-many-stations hydraulic geometry: sensitivity to river form and optimization parameters. Water Resour. Res. 50, 9604–9619.

Hagemann, M., Gleason, C., Durand, M., 2017. BAM: Bayesian AMHG-Manning inference of discharge using remotely sensed stream width, slope, and height. Water Resour. Res. 53, 9692–9707.

Hannah, D.M., Demuth, S., van Lanen, H.A.J., Looser, U., Prudhomme, C., Rees, G., Stahl, K., Tallaksen, L.M., 2011. Large-scale river flow archives: importance, current status and future needs. Hydrol. Process. 25, 1191–1200.

Hou, J., Van Dijk, A.I.J.M., Renzullo, L.J., Vertessy, R.A., 2018. Using modelled discharge to develop satellite-based river gauging: a case study for the Amazon Basin. Hydrol. Earth Syst. Sci. 22, 6435–6448.

Hou, J., Van Dijk, A.I.J.M., Renzullo, L.J., Vertessy, R.A., Mueller, N., 2019. Hydromorphological attributes for all Australian river reaches derived from Landsat dynamic inundation remote sensing. Earth Syst. Sci. Data 11, 1003–1015.

Huang, Q., Long, D., Du, M., Zeng, C., Li, X., Hou, A., Hong, Y., 2018a. An improved approach to monitoring Brahmaputra River water levels using retracked altimetry data. Remote Sens. Environ. 211, 112–128.

Huang, Q., Long, D., Du, M., Zeng, C., Qiao, G., Li, X., Hou, A., Hong, Y., 2018b. Discharge estimation in high-mountain regions with improved methods using multisource remote sensing: a case study of the Upper Brahmaputra River. Remote Sens. Environ. 219, 115–134.

Jain, R., Kasturi, R., Schunck, B.G., 1995. Machine Vision. McGraw-Hill, New York.

Ji, L., Gong, P., Wang, J., Shi, J., Zhu, Z., 2018. Construction of the 500-m resolution daily global surface water change database (2001–2016). Water Resour. Res. 54, 10,270–210,292.

Kim, S., Sharma, A., 2019. The role of floodplain topography in deriving basin discharge using passive microwave remote sensing. Water Resour. Res. 55, 1707–1716.

Kouraev, A.V., Zakharova, E.A., Samain, O., Mognard, N.M., Cazenave, A., 2004. Ob'river discharge from TOPEX/Poseidon satellite altimetry (1992–2002). Remote Sens. Environ. 93, 238–245.

Leopold, L.B., Maddock, T., 1953. The Hydraulic Geometry of Stream Channels and Some Physiographic Implications. U.S. Government Printing Office, Washington, D.C.

Li, H., Li, H., Wang, J., Hao, X., 2019. Extending the ability of near-infrared images to monitor small river discharge on the northeastern Tibetan Plateau. Water Resour. Res. 55.

Michailovsky, C.I., McEnnis, S., Berry, P.A.M., Smith, R., Bauer-Gottwein, P., 2012. River monitoring from satellite radar altimetry in the Zambezi River basin. Hydrol. Earth Syst. Sci. 16, 2181–2192.

Oubanas, H., Gejadze, I., Malaterre, P.O., Durand, M., Wei, R., Frasson, R.P.M., Domeneghetti, A., 2018. Discharge estimation in ungauged basins through variational data assimilation: the potential of the SWOT mission. Water Resour. Res. 54, 2405–2423.

Papa, F., Prigent, C., Rossow, W., 2008. Monitoring flood and discharge variations in the large Siberian rivers from a multi-satellite technique. Surv. Geophys. 29, 297–317.

Papa, F., Durand, F., Rossow, W.B., Rahman, A., Bala, S.K., 2010. Satellite altimeter-derived monthly discharge of the Ganga-Brahmaputra River and its seasonal to interannual variations from 1993 to 2008. J. Geophys. Res. Oceans 115.

Paris, A., Dias de Paiva, R., Santos da Silva, J., Medeiros Moreira, D., Calmant, S., Garambois, P.A., Collischonn, W., Bonnet, M.P., Seyler, F., 2016. Stage-discharge rating curves based on satellite altimetry and modeled discharge in the Amazon basin. Water Resour. Res. 52, 3787–3814.

Pavelsky, T.M., 2014. Using width-based rating curves from spatially discontinuous satellite imagery to monitor river discharge. Hydrol. Process. 28, 3035–3040.

Pavelsky, T.M., Durand, M.T., Andreadis, K.M., Beighley, R.E., Paiva, R.C., Allen, G.H., Miller, Z.F., 2014. Assessing the potential global extent of SWOT river discharge observations. J. Hydrol. 519, 1516–1525.

Pekel, J.-F., Cottam, A., Gorelick, N., Belward, A.S., 2016. High-resolution mapping of global surface water and its long-term changes. Nature 540, 418–422.

Revilla-Romero, B., Thielen, J., Salamon, P., De Groeve, T., Brakenridge, G.R., 2014. Evaluation of the satellite-based Global Flood Detection System for measuring river discharge: influence of local factors. Hydrol. Earth Syst. Sci. 18, 4467–4484.

Revilla-Romero, B., Beck, H.E., Burek, P., Salamon, P., de Roo, A., Thielen, J., 2015. Filling the gaps: calibrating a rainfall-runoff model using satellite-derived surface water extent. Remote Sens. Environ. 171, 118–131.

Schaaf, C.B., Gao, F., Strahler, A.H., Lucht, W., Li, X., Tsang, T., Strugnell, N.C., Zhang, X., Jin, Y., Muller, J.-P., Lewis, P., Barnsley, M., Hobson, P., Disney, M., Roberts, G., Dunderdale, M., Doll, C., d'Entremont, R.P., Hu, B., Liang, S., Privette, J.L., Roy, D., 2002. First operational BRDF, albedo nadir reflectance products from MODIS. Remote Sens. Environ. 83, 135–148.

Schaaf, C.B., Liu, J., Gao, F., Strahler, A.H., 2011. MODIS albedo and reflectance anisotropy products from Aqua and Terra. In: Land Remote Sensing and Global Environmental Change: NASA's Earth Observing System and the Science of ASTER

and MODIS. 11. pp. 549–561.

Sheffield, J., Wood, E.F., Pan, M., Beck, H., Coccia, G., Serrat-Capdevila, A., Verbist, K., 2018. Satellite remote sensing for water resources management: potential for supporting sustainable development in data-poor regions. Water Resour. Res. 54, 9724–9758.

Sichangi, A.W., Wang, L., Yang, K., Chen, D., Wang, Z., Li, X., Zhou, J., Liu, W., Kuria, D., 2016. Estimating continental river basin discharges using multiple remote sensing data sets. Remote Sens. Environ. 179, 36–53.

Smith, L.C., 1997. Satellite remote sensing of river inundation area, stage, and discharge: a review. Hydrol. Process. 11, 1427–1439.

Smith, L.C., Pavelsky, T.M., 2008. Estimation of river discharge, propagation speed, and hydraulic geometry from space: Lena River, Siberia. Water Resour. Res. 44.

Smith, L.C., Isacks, B.L., Forster, R.R., Bloom, A.L., Preuss, I., 1995. Estimation of discharge from braided glacial rivers using ERS 1 synthetic aperture radar: first results. Water Resour. Res. 31, 1325–1329.

Smith, L.C., Isacks, B.L., Bloom, A.L., Murray, A.B., 1996. Estimation of discharge from three braided rivers using synthetic aperture radar satellite imagery: potential application to ungaged basins. Water Resour. Res. 32, 2021–2034.

Tarpanelli, A., Brocca, L., Lacava, T., Melone, F., Moramarco, T., Faruolo, M., Pergola, N., Tramutoli, V., 2013. Toward the estimation of river discharge variations using MODIS data in ungauged basins. Remote Sens. Environ. 136, 47–55.

Tarpanelli, A., Amarnath, G., Brocca, L., Massari, C., Moramarco, T., 2017. Discharge estimation and forecasting by MODIS and altimetry data in Niger-Benue River.

Remote Sens. Environ. 195, 96–106.

Tourian, M.J., Sneeuw, N., Bárdossy, A., 2013. A quantile function approach to discharge estimation from satellite altimetry (ENVISAT). Water Resour. Res. 49, 4174–4186.

Tourian, M., Schwatke, C., Sneeuw, N., 2017. River discharge estimation at daily resolution from satellite altimetry over an entire river basin. J. Hydrol. 546, 230–247.

Van Dijk, A.I.J.M., 2010. The Australian Water Resources Assessment System. Technical Report 3. Landscape Model (version 0.5) Technical Description. In: CSIRO. Water for a Healthy Country National Research Flagship. http://www.clw.csiro.au/publications/waterforahealthycountry/2010/wfhc-aus-water-resources-assessment-system.pdf..

Van Dijk, A.I.J.M., Brakenridge, G.R., Kettner, A.J., Beck, H.E., De Groeve, T., Schellekens, J., 2016. River gauging at global scale using optical and passive microwave remote sensing. Water Resour. Res. 52, 6404–6418.

Van Dijk, A.I.J.M., Schellekens, J., Yebra, M., Beck, H.E., Renzullo, L.J., Weerts, A., Donchyts, G., 2018. Global 5 km resolution estimates of secondary evaporation including irrigation through satellite data assimilation. Hydrol. Earth Syst. Sci. 22, 4959–4980.

Wilson, A.M., Jetz, W., 2016. Remotely sensed high-resolution global cloud dynamics for predicting ecosystem and biodiversity distributions. PLoS Biol. 14, e1002415.

Yoon, Y., Garambois, P.A., Paiva, R.C., Durand, M., Roux, H., Beighley, E., 2016. Improved error estimates of a discharge algorithm for remotely sensed river measurements: test cases on Sacramento and Garonne Rivers. Water Resour. Res. 52, 278–294.

Chapter 4: Hydromorphological attributes for all Australian river reaches derived from Landsat dynamic inundation remote sensing

River width data is indispensable in hydraulic and hydrologic models, to help improve river routing and better estimate river discharge. This chapter develops an approach to produce hydromorphological attributes, including spatial and temporal river width, flow regime and river gradient for all of 1.4 million Australian river reaches and proposes a parameter that can be used to classify reaches by the degree to which flow regime tends towards permanent, frequent, intermittent, or ephemeral. The study also highlights river features over the Australian continent and discusses the relationships between river width and contributing catchment area, river discharge, and reach gradient. The content of this chapter was published in the journal Earth System Science Data as follows:

Hou, J., Van Dijk, A.I.J.M., Renzullo, L.J., Vertessy, R.A., and Mueller, N., 2019. Hydromorphological attributes for all Australian river reaches derived from Landsat dynamic inundation remote sensing, Earth System Science Data, 11, https://doi.org/10.5194/essd-11-1003-2019.

Earth System
Science
Data
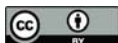
Hydromorphological attributes for all Australian river reaches derived from Landsat dynamic inundation remote sensing

Jiawei Hou[1], **Albert I. J. M. van Dijk**[1], **Luigi J. Renzullo**[1], **Robert A. Vertessy**[1,2], **and Norman Mueller**[3]

[1]Fenner School of Environment and Society,
Australian National University, Canberra, Australian Capital Territory, Australia
[2]School of Engineering, University of Melbourne, Melbourne, Victoria, Australia
[3]Geoscience Australia, GPO Box 378, Canberra, Australian Capital Territory, Australia

Correspondence: Jiawei Hou (jiawei.hou@anu.edu.au)

Abstract. Hydromorphological attributes such as flow width, water extent, and gradient play an important role in river hydrological, biogeochemical, and ecological processes and can help to predict river conveyance capacity, discharge, and flow routing. While there are some river width datasets at global or regional scales, they do not consider temporal variation in river width and do not cover all Australian rivers. We combined detailed mapping of 1.4 million river reaches across the Australian continent with inundation frequency mapping from 27 years of Landsat observations. From these, the average flow width at different recurrence frequencies was calculated for all reaches, having a combined length of 3.3 million km. A parameter γ was proposed to describe the shape of the frequency–width relationship and can be used to classify reaches by the degree to which flow regime tends towards permanent, frequent, intermittent, or ephemeral. Conventional scaling rules relating river width to gradient and contributing catchment area and discharge were investigated, demonstrating that such rules capture relatively little of the real-world variability. Uncertainties mainly occur in multi-channel reaches and reaches with unconnected water bodies. The calculated reach attributes are easily combined with the river vector data in a GIS, which should be useful for research and practical applications such as water resource management, aquatic habitat enhancement, and river engineering and management. The dataset is available at https://doi.org/10.25914/5c637a7449353 (Hou et al., 2019).

1 Introduction

Temporal and spatial information on river morphology is fundamental for understanding CO_2 and nutrient exchange, aquatic habitat distribution and migration, fishery management, transportation, flooding hazards, and hydrologic and hydrodynamic models (Miller et al., 2014). Combining detailed data on river morphology with hydrological modelling, our understanding of the flow and storage of water across spatio-temporal scales can be improved further (Van Schaik et al., 2019). River morphology is mainly controlled by eight variables: width, gradient, depth, velocity, discharge, roughness, sediment size, and sediment load (Leopold et al., 1964).

In the platform dimension, river patterns have been categorized as either single or anabranching channels. Laterally, active channels and inactive channels can be further classified as straight, sinuous, meandering, and braided forms (Nanson and Knighton, 1996). For a deeper understanding of river morphology, Rosgen (1994) established a river classification inventory system using delineation criteria or ranges in different levels including the number of channels, entrenchment, width–depth ratio, sinuosity, gradient, and channel material. Importantly, the interaction between river channel and floodplain results in different river morphology. For instance, the width of a channel changes in response to formation and destruction of the floodplain, which subsequently alters bar

patterns as bar pattern is dominated by width–depth ratio (Kleinhans and Van den Berg, 2011).

Among the variables affecting river morphology, river width is an essential parameter to calculate river discharge, assess river conveyance capacity, and improve river routing in models (Yamazaki et al., 2014). River width at overbank flow level plays a significant role in delineating inundated area, which affects water vapour fluxes and groundwater recharge (Dadson et al., 2010; Pedinotti et al., 2012; Doble et al., 2014). From flood inundation simulation with one-dimensional finite difference solutions of the St. Venant equations to two-dimensional finite element and finite difference models, the need for data on river morphology increases from field survey measurements to continuous digital elevation models. Using a low-resolution digital elevation model (DEM), details of flow channel features and connectivity cannot be provided. Thus, river characteristics are not always represented well in coarse-resolution grids used in large-scale river routing models (Yamazaki et al., 2011). Although a high-resolution DEM can mitigate this issue, there is an associated increase in computational cost and sufficient computing resources are not always available. One way to deal with this problem is to construct a simpler model structure (Bates and De Roo, 2000). Another way is to parameterize sub-grid-scale topography of river channels and floodplains in modelling (Neal et al., 2012; Yamazaki et al., 2011). For example, Coe et al. (2008) considered sub-grid-scale floodplain morphology (i.e. fractional flooding of grid cells), which resulted in significant improvement in the simulations of seasonal and inter-annual flooding.

The lack of detailed data on river characteristics often means that river width is either ignored or left as a parameter for calibration, which may increase model uncertainty and decrease accuracy (Andreadis et al., 2013). River width may be set to a constant value without consideration of spatial and temporal variations (Biancamaria et al., 2009). Alternatively, river width may be estimated by empirical functions of drainage area (Coe et al., 2008; Paiva et al., 2013) or river discharge (Decharme et al., 2008; Getirana et al., 2012, 2013; Andreadis et al., 2013). However, river width estimates from empirical functions cannot provide accurate representations of river reach morphology, as relationships between river width and discharge or drainage area are known to vary in different geomorphological and climate conditions (Yamazaki et al., 2014). If river width is overestimated in hydrological modelling, it may result in both overestimation of river channel storage and underestimation of water storage on the floodplain and vice versa (O'Loughlin et al., 2013). This will in turn cause errors in the timing and location of flood wave and floodplain inundation predictions.

The development of a more accurate and explicit river width dataset has been approached in several ways. Pavelsky and Smith (2008) developed a software tool, RivWidth, to automatically extract river width along a river course, combining one channel mask distinguishing water pixels from non-

water pixels and another river mask describing areas within the river boundary or outside it. Miller et al. (2014) and Allen and Pavelsky (2015, 2018) successfully applied this pioneering approach to map river width at mean discharge for the Mississippi River basin, North American rivers, and the whole world, respectively. However, laborious manual inspection and corrections are needed in pre-processing of the water masks, which prohibit its automated application over large scales. For example, undetected channels in water masks have to be drawn manually in order to make the river network fully connected (Neal et al., 2012). To address this issue, Yamazaki et al. (2014) applied an automated algorithm to produce a global river width database for large rivers, GWD-LR, using flow direction maps and water masks. Isikdogan et al. (2017) also developed an automated analysis and mapping engine, RivMap, which is able to delineate rivers and estimate river width, and used it to generate a river width dataset for North America. However, none of these regional and global datasets considers temporal variability of river width or river width beyond overbank flow conditions.

Our aim was to develop a method for estimating temporal and spatial river width dynamics and use these to find summary parameters to represent river morphology characteristics that could support a classification of river type over the Australian continent. River width dynamics at different recurrence frequencies were estimated from 27-year time series of 25 m resolution surface water extent maps from Landsat remote sensing (Mueller et al., 2016) and a detailed Geographic Information System (GIS) database containing all 1 410 404 river segments and 1 474 271 sub-catchments mapped across Australia (Bureau of Meteorology, 2012a). The width estimates were compared with the global river width dataset (Allen and Pavelsky, 2018) at average flow conditions in 218 river regions of Australia. We analysed the relationships between river width and discharge, drainage area, and gradient, and calculated the coefficient and exponent of a hydraulic geometry equation for Australia. The river morphology parameters were intended to provide a description of temporal river width dynamics relating to the dominant flow regime (permanent, frequent, intermittent, or ephemeral). We demonstrate the usefulness of our dataset by showing the longitudinal profile of hydromorphological attributes for the main river channel of the Murray River and other complex river systems in a dry, low-relief environment.

2 Data and method

2.1 Data

2.1.1 River and sub-catchment segments

The Australian Hydrological Geospatial Fabric (Geofabric) is a digital database of spatial surface and groundwater features based on a GIS platform that relates important hydrologic features such as catchments, rivers, lakes, and aquifers
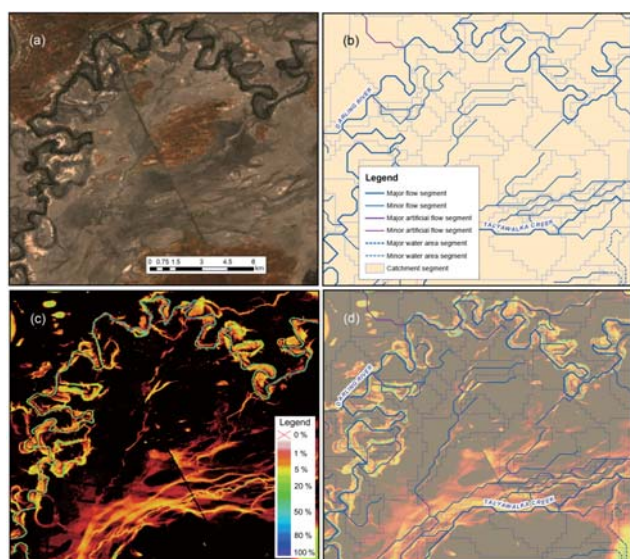
Figure 1. Illustration of the data used in the investigations: **(a)** true colour median-value composite of Landsat-8 data for a 15.7 km × 15.3 km area centered on 31.62° S and 143.42° N; **(b)** river segments and corresponding sub-catchment area from the Geofabric Surface Network; **(c)** WOfS water summary showing the percentage of times surface water was observed; and **(d)** overlay of the Geofabric onto WOfS (i.e. **b** and **c**).

(Bureau of Meteorology, 2012a). The Geofabric Surface Network provides a consistent hydrological surface stream network which was derived using the 9 s ANUDEM raster streams product (Bureau of Meteorology, 2012b). The surface network has six attributes, namely network stream, upstream network connectivity, downstream network connectivity, network node, water body, and catchment area. Any information associated with the surface network can be easily connected to features in other Geofabric products, including surface cartography, surface catchment, groundwater cartography, and hydrological reporting catchments and regions, for further applications. The network stream is divided into major rivers and minor rivers, and major rivers generally represent the main watercourses across Australia (Fig. 1a and b). These rivers are further classified as flow segments (natural rivers), water area segments (rivers passing through a water body), and artificial segments (to keep the stream network connected). The catchment refers to a sub-catchment corresponding to each river segment. The network stream and catchment features are the main data we used to extract information from surface water extent observations (Fig. 1d).

2.1.2 Surface water extent observations

Water Observations from Space (WOfS) is a publicly accessible 25 m resolution gridded dataset providing surface water persistence and recurrence information for the Australian continent (Mueller et al., 2016). This historical flood infor-

mation product was developed using a decision tree method on a combination of normalized difference indices and corrected spectral band values from approximately 184 500 Landsat images (Mueller et al., 2016). The Landsat images used to produce WOfS were the Australian archives of Landsat-5 and Landsat-7 data, which were derived from raw data using the USGS Landsat Product Generation System with a spatial resolution of 0.00025° (approximately 25 m pixel size) and cover 27 years from 1987 to 2014 (Mueller et al., 2016). Here we used the water summary product from WOfS, which provides the recurrence frequency of surface water occurring as a percentage of the number of times the surface was clearly observed for each grid cell. For example, a frequency of 5 % means surface water extent was detected on average once in 20 clear-sky Landsat acquisitions for that given pixel (Fig. 1c). The WOfS product reflects inundation extent for rivers at both in-channel and overflow levels, but cannot relate inundated area to its associated river regime directly (Fig. 1a and c). However, this can be achieved by the network stream and catchment features from the Geofabric (Fig. 1d).

2.2 Method

2.2.1 River widths at different recurrence frequencies

We used Geofabric sub-catchment boundaries to divide the WOfS water summary map into 1 474 271 segments (Fig. 1d). Of these, there is a total of 1 379 224 sub-catchments that have river segments. The strong agreement between Geofabric water courses and WOfS surface water was demonstrated by Mueller et al. (2016). The sub-catchment polygon is used to select the area and extract information from the inundation frequency raster for its corresponding river polyline. We calculated inundation extent at different recurrence frequencies (Table 1) in each of these sub-catchments. This step required considerable computational power, and so we used a high-performance computer. Next, we estimated corresponding effective width for each sub-catchment by dividing inundation extent at different recurrence frequencies by the geodesic length of the river segment calculated from the Geofabric using Vincenty's inverse method (Vincenty, 1975). In addition, DEM information was extracted from the 1 s DEM, an elevation data product developed by Geoscience Australia using the Shuttle Radar Topography Mission (SRTM) data (Gallant et al., 2011), for the upstream and downstream end points of each river segment. River gradient was calculated by dividing the elevation difference between upstream and downstream points by river length for each river segment. Finally, we obtained estimated spatial and temporal river widths, and river gradients for 1 379 224 river reaches across the Australian continent.

We compared our spatial and temporal river width data to the Global River Widths from Landsat (GRWL) dataset (Allen and Pavelsky, 2018) over Australia. Allen and Pavel-

www.earth-syst-sci-data.net/11/1003/2019/

Earth Syst. Sci. Data, 11, 1003–1015, 2019

Table 1. The categories of recurrence frequency for which calculations were performed.

Frequency	Description	Frequency	Description
0 %	Water not detected	5 %	Water detected 5 times in 100 observations
0.1 %	Water detected 1 time in 1000 observations	8 %	Water detected 8 times in 100 observations
0.2 %	Water detected 2 times in 1000 observations	10 %	Water detected 10 times in 100 observations
0.3 %	Water detected 3 times in 1000 observations	20 %	Water detected 20 times in 100 observations
0.4 %	Water detected 4 times in 1000 observations	50 %	Water detected 50 times in 100 observations
0.5 %	Water detected 5 times in 1000 observations	80 %	Water detected 80 times in 100 observations
0.8 %	Water detected 8 times in 1000 observations	90 %	Water detected 90 times in 100 observations
1 %	Water detected 1 time in 100 observations	95 %	Water detected 95 times in 100 observations
2 %	Water detected 2 times in 100 observations	100 %	Water detected always

sky (2018) produced estimates of global river width at approximately mean discharge, which is related to the month that rivers are most likely to be at the mean discharge value from the nearest gauging station for each Landsat tile. However, it is less likely to represent the average conditions of ungauged river reaches as the distance from the nearest gauging station increases; most river reaches around the world are ungauged. Additionally, mean discharge does not correspond to any particular recurrence frequency. Thus, to facilitate comparison between the two sets of results, we calculated Spearman correlations between our river width estimates at a frequency of 50 % and GRWL river widths separately for the 218 river regions in Australia. High correlations mean our river width data reflect the same relative width variations along the river channel from upstream to downstream for a river region as the global river width dataset.

In addition, upstream cumulative mean runoff of each river segment was calculated based on the Australian Water Resources Assessment (AWRA) landscape hydrology model (Van Dijk, 2010), which is used by the Australian Bureau of Meteorology to operationally estimate daily water balance components across Australia at a spatial resolution of $0.05° \times 0.05°$ (Frost et al., 2018). We analysed the relationship between river width and upstream cumulative runoff or upstream drainage area and also the correspondence between river width and gradient for Australia. Furthermore, we established hydraulic geometry power-law relationships that relate river width to upstream cumulative runoff or upstream drainage area as follows:

$$w = aQ^b, \tag{1}$$

$$w = cA^d, \tag{2}$$

where w is river width (m), Q is cumulative upstream runoff (m^3 s^{-1}), and A is upstream drainage area (km^2). Coefficients a and c and exponents b and d were fitted and compared to the results from published studies.

2.2.2 River morphology characteristics

The pixels in WOfS do not have equal numbers of clear observations, mainly due to overlapping Landsat scenes, with minor influence of cloud and shadow frequency. The number of clear observations in the overlapping scene areas could be more than twice that in most of the rest areas. The estimated river width is supposed to increase much more sharply in the overlapping areas than the rest areas as recurrence changes towards very low ranges, even for the same river reach, as a larger number of clear observations provide more chances to catch the extreme conditions. As a result, the surface water extent map shows oblique strips across the Australian continent for very low recurrence frequencies. To standardize the width and analyse width dynamics of rivers across Australia as a whole, a more homogeneous mapping was desirable. To avoid these artefacts, we generated river width maps by varying recurrence frequency from low to high until the majority of artefacts disappeared. We regarded the resulting lowest-frequency river width map without artefacts as representing the maximum river width. Next, we standardized river widths at different recurrence frequencies by dividing them by maximum river width, producing a width fraction representing the ratio of river width at different recurrence frequencies to maximum width.

$$F_i = W_i / W_{\max}, \tag{3}$$

where F_i is width fraction at the ith frequency (Table 1), W_i is river width (m) at the ith frequency, and $W_{\max}$ is the maximum river width (m). The relationship between width fraction and its corresponding frequency was generally well-described by a Weibull distribution, and therefore we used the Weibull inverse survival function (NIST/SEMATECH e-Handbook of Statistical Methods, 2018) to fit the relationship for each river reach as follows:

$$F_i = (-\ln(R))^{1/\gamma}, \tag{4}$$

where R is the width fraction corresponding frequency i and γ is a parameter. We used differential evolutions (Storn and Price, 1997) to estimate the parameter for each river reach. The parameter γ reflects different curve shapes for relationships between width fraction and frequency (Fig. 2) and was used to characterize river morphology for 1 379 224 river reaches across the continent. The larger γ is, the more time
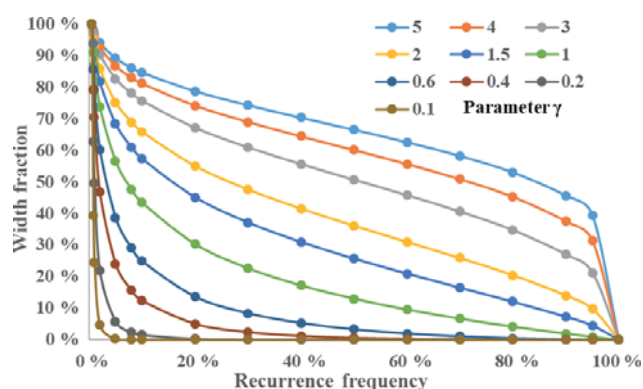
Figure 2. Different river width distributions for different values of the gamma parameter.

the river width is close to maximum width, and the closer to 0, the more time the river width is close to minimum width. The characteristic curves for rivers of invariable width show a horizontal line, which leads to infinitely large estimates of γ. We empirically limited γ between 0 and 5, which was suitable for the large majority of rivers in Australia.

After γ was estimated for each river reach, we classified river reaches into 10 categories according to their corresponding γ values (Table 2). We selected median values of width fraction at certain recurrence frequencies (Table 1), respectively, for each category, and used Eq. (4) to fit the relationship between width fraction and its corresponding frequency for estimating γ values. Lastly, we used Eq. (4) and estimated γ values to predict width fraction for each category, and compared them with observed width fractions. The standard differences were calculated for each category to evaluate their biases by the equation as follows:

$$\mathrm{SD} = \sqrt{\frac{\sum(\mathbf{O} - \mathbf{M})^2}{n}}, \tag{5}$$

where $\mathbf{O}$ is the observation matrix, $\mathbf{M}$ is the estimate matrix, n is the number of elements, and SD is the standard difference. This process was intended to test whether the parameter γ represented recurrence–width relationships for different river reaches well.

3 Results

3.1 Reach width–frequency distribution

Temporal observation frequency artefacts largely disappeared at 0.5 % frequency. Hence, we selected river width at this frequency as the maximum river width (Fig. 3a). We chose inundation at 80 % frequency to represent minimum river extent (Fig. 3b). Large differences existed between maximum and minimum widths (Fig. 3). Although there are many river reaches across Australia, most of them

are ephemeral. Most of the (semi-)permanent rivers are located along the northern and eastern coasts. There are many ephemeral river reaches with very broad maximum widths in the tributary catchments of the Murray–Darling Basin and in the interior Lake Eyre catchment, as well as along the Gulf of Carpentaria. River reaches flowing through a large water body, e.g. reservoir or lake, also have very large calculated widths. We did not exclude these river reaches, because they keep the river network connected and because such reaches are identified in the Geofabric mapping and hence can be selected as required. Some regions showed no meaningful river network (Fig. 3a). Most of these regions are arid catchments with a sandy alluvial substrate. Presumably, this leads to an infiltration capacity that is sufficient to prevent significant surface runoff accumulation, whereas several of the catchments also contain recent dune systems that have interrupted a pre-existing drainage network (Fig. 3a).

We divided river reaches into three categories based on their maximum width: small (< 25 m), medium (25–250 m), and large (> 250 m). It is noted that small rivers will not be narrower than 25 m along their entire width; a non-zero width is calculated because some of the 25 m pixels along the reach were mapped as inundated at 0.5 % maximum extent. Therefore, we only list summary statistics here for medium and large rivers (Table 3). The total length of reaches in different maximum and minimum width classes is listed in Table 3, showing the same distribution pattern regardless of whether segments flowing through water bodies are included or excluded. The total length decreases as maximum and minimum river width increases from 25 m up to more than 10 km. The total reach length in different width ranges and at different recurrence frequencies (Fig. 4) decreases by a factor of 21 as frequency increases from 0.5 % to 80 %. The majority of river reaches are 25–250 m broad irrespective of frequency range (Fig. 4).

We compared river width at different recurrence frequencies with river gradient for all river reaches, as well as with upstream drainage area and cumulative runoff. For comparison with drainage area and runoff, we included only major rivers because the contribution of upstream flow to minor rivers can be uncertain, for example for anabranches and distributaries. Upstream drainage area and total runoff best predicted maximum reach width, with Pearson correlations of 0.52 and 0.43, respectively, while gradient showed the expected negative relationship with maximum river width (Fig. 5). Reflecting the most common method of river width estimation, we fitted Eq. (1) to our data. We excluded river widths with small upstream cumulative runoff ($< 10^{4.5}$ m^3 or 0.37 m^3 s^{-1}) due to the influence of their sparse distribution on the overall relationship. This resulted in a relationship with a coefficient $a = 13.17$ and exponent $b = 0.49$. We found that reach gradient affects a significantly, with decreasing width as gradient increases, but it did not appear to affect b, except perhaps for the highest gradient class (> 0.01, Fig. 6).

www.earth-syst-sci-data.net/11/1003/2019/

Earth Syst. Sci. Data, 11, 1003–1015, 2019

Table 2. Ten categories of river reaches based on γ values.

Flow regime	Ephemeral			Intermittent			Frequent			Permanent
γ	0–0.05	0.05–0.1	0.1–0.2	0.2–0.4	0.4–0.6	0.6–0.8	0.8–1	1–1.5	1.5–3	3–5

Table 3. The length percentages in different width ranges of maximum (a) and minimum (b) river widths for Australia (all river segments include flow segments and segments flowing through water bodies).

River	Length (all river segments)		Length (flow segments)	
Width Range (m)	Maximum Width ($R = 0.5\%$)	Minimum Width ($R = 80\%$)	Maximum Width ($R = 0.5\%$)	Minimum Width ($R = 80\%$)
25–50	22.56 %	28.59 %	25.69 %	35.46 %
50–100	20.95 %	25.67 %	22.84 %	31.69 %
100–250	24.86 %	24.16 %	25.99 %	23.91 %
250–500	14.79 %	10.11 %	14.22 %	5.95 %
500–1000	9.46 %	6.51 %	7.56 %	1.90 %
1000–2500	5.56 %	3.86 %	3.16 %	1.00 %
2500–5000	1.31 %	0.88 %	0.41 %	0.08 %
5000–10000	0.39 %	0.20 %	0.09 %	0.01 %
> 10 000	0.14 %	0.02 %	0.03 %	0.00 %
Total (m)	5.84×10^8	2.80×10^7	4.12×10^8	1.66×10^7

River width at 50 % frequency (i.e. median width) was compared with river widths considered representative of "average" flows contained in the GRWL. Among the 218 Australian river regions, only 111 regions had any inundated river channel under "average" conditions in the GRWL river width dataset, whereas all 218 river regions contained detected rivers in our analysis results. The Spearman rank correlation between median river width and river widths from the global dataset exceeded 0.6 for 68 % (75) of 111 river regions and exceeded 0.4 for 86 % (95) of them, suggesting that the two datasets show reasonably similar relative width variations (Fig. 7).

3.2 River hydromorphology classification

The parameter γ represents the degree to which rivers tend towards permanent or ephemeral flow regimes. Most rivers, particularly the larger rivers along the coast, flow through estuaries or other (quasi) permanent water bodies, and hence are classified as permanent or frequent ($\gamma > 0.8$, Fig. 8). Calculating the combined length of medium and large river reaches in different γ ranges (Fig. 9) shows that the majority fall within $\gamma = 0.1$–0.6, indicating that the dominant flow regime for Australian rivers is ephemeral or intermittent.

The average frequency–width data and fitted curves for different γ classes are shown in Fig. 10. The standard differences between observed and fitted width fractions range from 0.0075 to 0.0725 (Table 4). Relative width was overestimated for frequencies between 20 % and 50 % for γ 0.6–1.5 and for frequencies between 5 % and 20 % for γ 0.2–0.8. De-

spite these biases, the curves generally capture the relationship between width fraction and frequency well.

3.3 Qualitative evaluation

A longitudinal profile of river width, gradient, and flow regime parameter γ for the main channel of the Murray River (Fig. 11) illustrates several features in the data. Strong width variations between 0.5 % and 80 % frequency can occur, indicating that the river channel contains water for most of the time (> 50 % frequency) but contained within a relatively narrow channel. River width increases significantly between 5 %–8 % and 1 %–2 % frequency, which coincides with the threshold for overbank flows. The greatest widths are in reaches flowing through large water bodies, such as Lake Hume (C; storage reservoir), Yarrawonga Weir (D; impoundment), Lake Alexandrina (K; the terminal lake system), and other wetlands (H and I). Where river flows are confined, widths do not change much (e.g. G; Mildura). Where flow splits into multiple channels before converging again, minimum channel width reduces (e.g. E and F), whereas maximum width increases, corresponding to a broader floodplain. Between A and B, river reaches have water for 5 %–8 % of the time in our data, but not in the GRWL dataset (Allen and Pavelsky, 2018) (Fig. 11b). The GRWL widths under "average" conditions are contained within the distribution in our data, but for rather widely varying frequencies. A narrowing relative difference between the 0.5 % and 80 % frequency widths corresponds to higher γ values and vice versa (Fig. 11b). This shows that the river morphology parame-
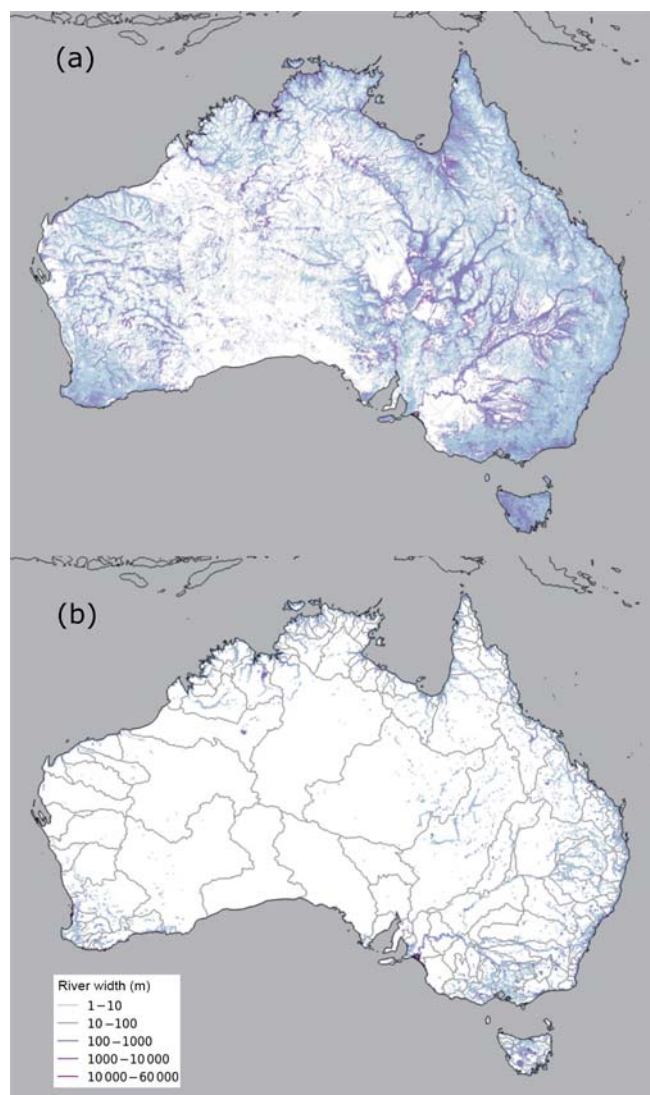
Figure 3. Maximum **(a)** and minimum **(b)** river width across Australia; 218 river regions delineated in grey in **(b)**.
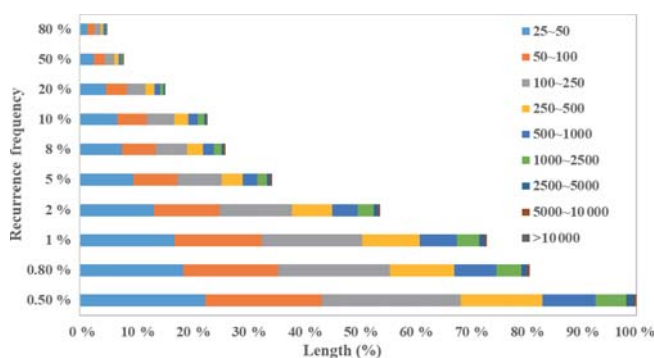
Figure 4. The length percentages in different width ranges at different recurrence frequencies for Australia.

ter γ can capture the river flow regime. In line with Fig. 5c, river width increases as gradient decreases from upstream to downstream overall (Fig. 11b and c).

Figure 12 illustrates some of the data characteristics and challenges in complex river systems common in Australia's dry and low-relief environments. During floods, all river channels are inundated and rivers are broad (Fig. 12a). Only the main Darling River channel contains water frequently (Fig. 12b), but is still very narrow during low flows (Fig. 12c). All reaches have an ephemeral or intermittent flow regime (Fig. 12f) with $\gamma < 0.8$, with the southern Talyawalka Creek showing a more ephemeral regime than the Darling River.

4 Discussion

The Geofabric contains nearly 1.4 million river segments across the Australian continent and provides valuable information on river path, length, and contributing sub-catchment area. We were able to assign summary metrics derived from spatial and temporal surface water extent information contained in the satellite-derived WOfS to the river reaches and calculate river widths at different recurrence frequencies. The Geofabric Surface Network had a total length of 3.3 million km. Compared to HydroSHEDS (Lehner et al., 2008), probably the most commonly used global hydrological dataset, the Geofabric delineates a finer-resolution stream network and describes the natural variation in drainage density and complex distributary and anabranching drainage patterns better (Stein et al., 2014). Nonetheless, the 9 s DEM resolution is still insufficient to delineate all floodplains and river flow paths accurately. A new version of the Geofabric at 1 s resolution has been produced for part of Australia, and once available nationally could be used to improve derived river characteristics. Similarly, the WOfS data will continue to receive updates.

Errors in the calculated river characteristics also derive from uncertainties in WOfS inundation mapping. Narrow rivers, small water bodies, and wetlands with vegetation cover may be missed in mapping, and conversely topographical shadows in steep terrain or in high-rise cityscapes can be misclassified as water. Noise in very clear water can also result in misclassification (Mueller et al., 2016). There are also data gaps in WOfS and occasional linear artefacts caused by the Scan-Line-Corrector-Off (SLC-Off) problem in Landsat-7 (Mueller et al., 2016). Nevertheless, the overall accuracy of the water classifier used in WOfS was 97 %, which gives confidence in our derived metrics.

Our dataset has some advantages over existing datasets such as GRWL. Firstly, it provides spatial and temporal information on river dynamics at both in-channel and overbank flows. Secondly, if one river reach has multiple channels, we calculated river width for each channel rather than considering them a single channel. Thirdly, our data provide more
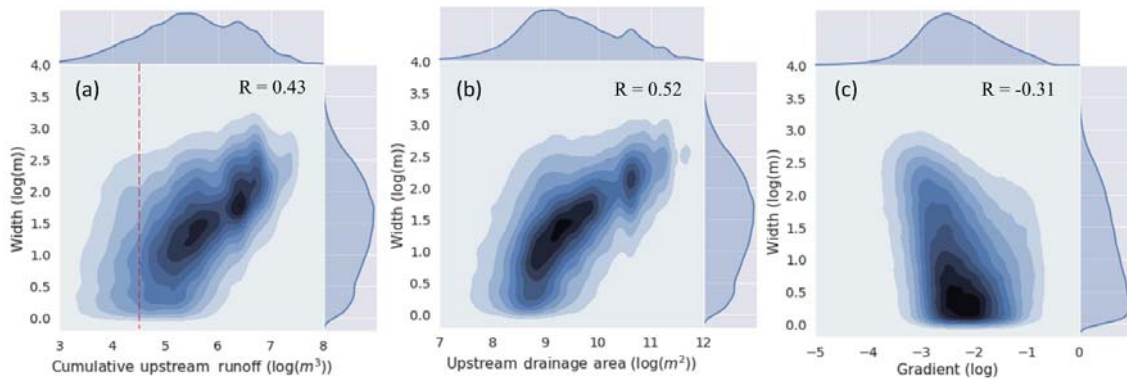
Figure 5. The relationships between maximum river width and cumulative upstream runoff **(a)**, upstream drainage area **(b)**, and river gradient **(c)** (the colour coding is related to data counts with the highest in dark blue and lowest in light blue, which corresponds to the histogram on the axes; red dash line: the threshold (data below this threshold are excluded due to the influence of their sparse distribution on the overall relationship when we fitted Eq. 1 to our data)).

Table 4. Validation of curves fitting for different river morphology categories.

γ interval	0–0.05	0.05–0.1	0.1–0.2	0.2–0.4	0.4–0.6	0.6–0.8	0.8–1	1–1.5	1.5–3	3–5
Percentage	6.18 %	11.68 %	18.64 %	28.93 %	13.39 %	5.82 %	3.49 %	5.12 %	4.35 %	0.98 %
Coefficient γ	0.04	0.07	0.15	0.30	0.51	0.73	0.94	1.32	2.31	4.07
Standard difference	0.0075	0.0104	0.0202	0.0446	0.0725	0.0489	0.0344	0.0337	0.0407	0.0206
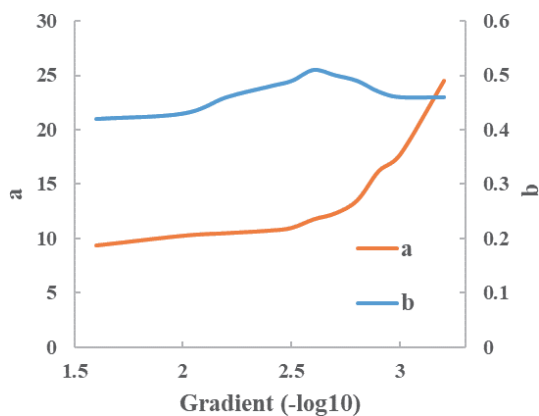
Figure 6. The coefficients a and exponents b of the power scaling relationship predicting maximum river width from upstream cumulative runoff (Eq. 1) calculated for different reach gradients.
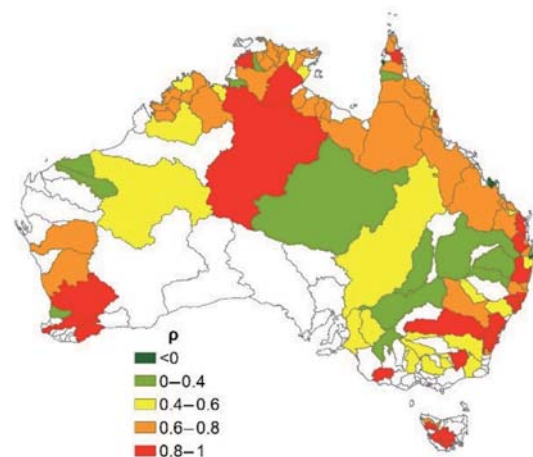

Figure 7. The Spearman rank correlations between our dataset and the GRWL dataset in 111 river regions across Australia.

detailed information due to the finer river network contained in the Geofabric. Finally, our product can readily be related to any hydrological feature in the Geofabric for further application.

The relationship between river width and contributing catchment area, cumulative runoff, and reach gradient can be compared to literature values. The positive relationships of discharge–width and catchment area–width, and negative relationship of width–gradient have also been demonstrated by Frasson et al. (2019). Empirically relating drainage area

to river width (i.e. Eq. 2), Coe et al. (2008) obtained a coefficient $c = 0.42$ and exponent $d = 0.59$, whereas Paiva et al. (2013) found c of 0.35–3.75 and d of 0.36–0.63 for different river basins (Table 5). We found intermediate values of $c = 0.91$ and $d = 0.43$. A more common way to estimate river width is from mean annual discharge (i.e. Eq. 1). Decharme et al. (2008), Getirana et al. (2012, 2013), and Andreadis et al. (2013) all assumed an exponent $b = 0.5$, as suggested by Leopold and Maddock (1953) and Leopold et

(a)

(b)

Parameter γ
— 0–0.2
— 0.2–0.8
— 0.8–3
— 3–5
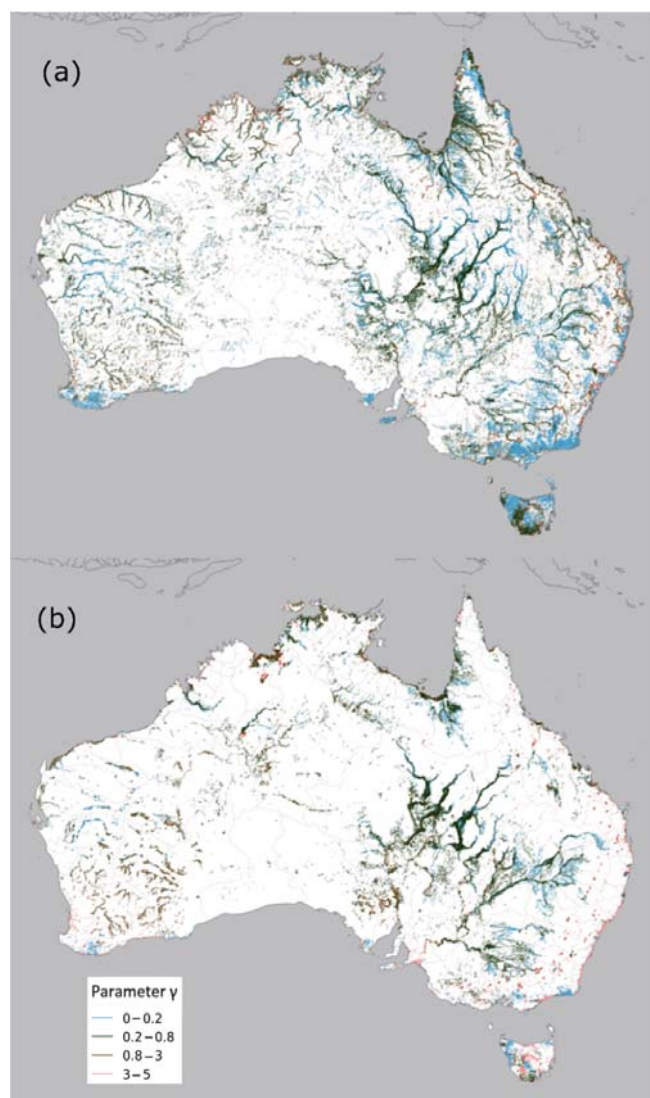
Figure 8. River morphology classification γ parameter values for medium (**a**) and large (**b**) rivers for Australia.
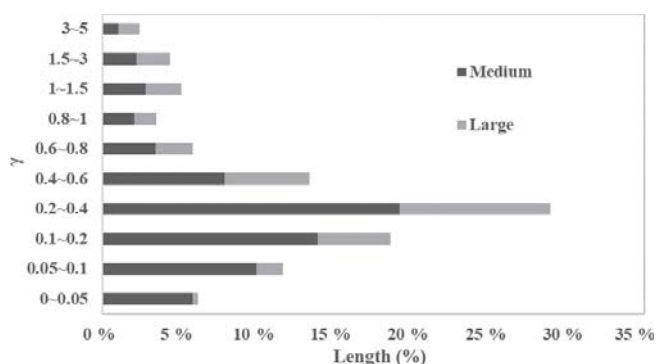
Figure 9. The length percentages of medium and large rivers for different γ value ranges across Australia.
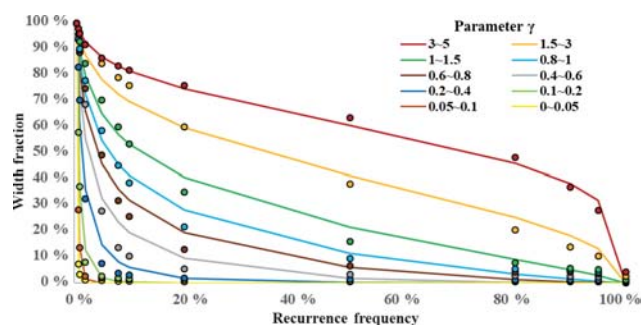
Figure 10. Curve characteristics for different river morphology categories (line: prediction; dot: observation).

al. (1964) (Table 5). We found very similar values for the exponent. By contrast, the value of the coefficient a varies widely between studies (Table 5). Getirana et al. (2012, 2013) used a high value of $a = 18$ for the Amazon basin, whereas Andreadis et al. (2013) used $a = 7.2$ for their global application. We estimated $a = 13.1$ for all Australian reaches combined, but also found evidence that a correlates with the river reach gradient (Fig. 6), which may help explain differences between previous studies.

Although the empirical scaling functions discussed here can be used to estimate river width based on drainage area or modelled runoff with modest skill, there are also clear limitations. Firstly, they are not able to estimate river widths at different recurrence frequencies. Secondly, individual river reach with the same upstream drainage area or cumulative runoff can have widely different river widths. For example, as mentioned, we found evidence that a reach with a more gentle gradient can be expected to be wider in comparison (Fig. 6), consistent with the Manning equation. Thirdly, scaling equations cannot be applied to multi-channel rivers. Therefore, rather than empirical functions, the river width–frequency relationships derived here should help to improve the description of river morphology in hydrological modelling.

Some uncertainties are inherent to the approach followed here and would benefit from further research. Firstly, we calculated river width based on inundation extent within the entire designated sub-catchment boundary for each river reach. Although this excluded most unrelated water bodies and other river channels, the water mapping may still include unconnected water bodies, such as off-channel storages. This would cause overestimation of river width. However, for analysing width dynamics, normally unconnected water bodies remaining in the sub-catchment can be assumed to be part of the river channel conceptually, because they generally merge with channels at low recurrence frequencies (i.e. high flows) and separate at high recurrence frequencies (i.e. low flows). If these nearby water bodies are removed, it could fail to detect the maximum river width; if they are retained at high flows and removed at low flows, there would be abrupt

www.earth-syst-sci-data.net/11/1003/2019/

Earth Syst. Sci. Data, 11, 1003–1015, 2019

Table 5. Comparison of coefficients and exponents for Eqs. (1) and (2) between different studies.

Research	Equation	a	b	c	d	Scale
Coe et al. (2008)	$w = cA^d$	–	–	0.42	0.59	Amazon
Paiva et al. (2013)	$w = cA^d$	–	–	0.35–3.75	0.36–0.63	Amazon
Decharme et al. (2008)	$w = \max(25, aQ^b)$	$a = (10^{-4}Q_{m,\text{mouth}} + 6)^{*1}$	0.5	–	–	South America
Getirana et al. (2012, 2013)	$w = \max(10, aQ^b)$	18	0.5	–	–	Amazon
Andreadis et al. (2013)[*2]	$w = aQ^b$	7.2	0.5 ± 0.02	–	–	Globe
This study	$w = aQ^b$; $w = cA^d$	13.17	0.49	0.91	0.43	Australia

[1] Suggested by Arora and Boer (1999) ($Q_{m,\text{mouth}}$ is the mean annual discharge at the mouth of the river). [2] Based on the regression relation developed by Moody and Troutman (2002).
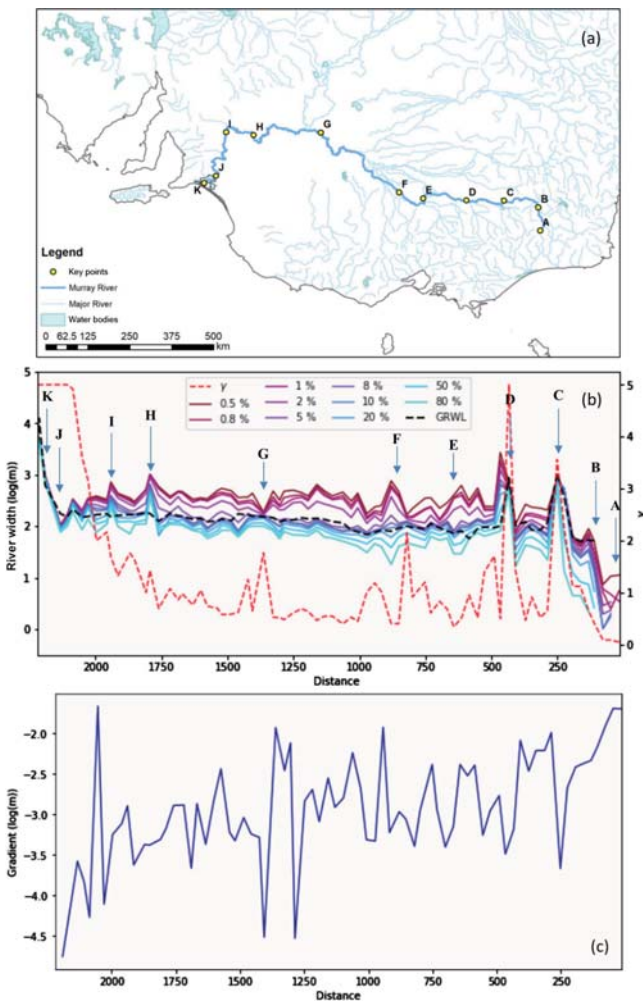
Figure 11. Longitudinal profile of the Murray River showing **(a)** location of river and selected locations; **(b)** profile of width at different frequencies and river morphology parameter γ; and **(c)** profile of river gradient. Values are averaged for 30 km sections along the river channel. Letters indicate (A) source according to our data; (B) source according to GRWL data (Allen and Pavelsky, 2018); (C) Lake Hume; (D) Yarrawonga Weir; (E–F) anabranching locations; (G) Mildura; (H–I) Lower Murray wetlands; and (J–K) Lake Alexandrina.

changes in river width. Secondly, although the data provide detailed information on the width of individual channels in anabranching river systems, the multiple channels will often merge into a single channel during overbank flow events. Our data do not reflect this merging and separating of channels at different flow levels, and it is challenging to find a way to conceptually address this in the Geofabric framework.

Besides, there are some uncertainties from input variables, including DEM, runoff, and length. The SRTM-derived 1 s (approximately 30 m) DEM has a root mean square (rms) error of 3.868 m, and its uncertainties include residual stripes, broad-scale stripes, steps in elevation, large offsets along the edge of the valley floor, noise due to the nature of the radar acquisition and processing, incomplete removal of vegetation offsets and urban and built infrastructure, and vegetation height overestimated (Gallant et al., 2011). However, the majority of rivers flow on flat plains without vegetation cover, and urban and built infrastructure and river gradients were only produced for the main river reaches, presumably with wider channels, which reduce the influence from uncertainties and limitations of DEM. Uncertainties from input data, parameterization, and conceptual structure in the model could affect runoff estimates, although the AWRA-L model has a strong documented pedigree in runoff estimation in comparisons with gauge data (e.g. Van Dijk and Warren, 2010; Frost et al., 2018). The raster–vector conversion anomalies to produce the Geofabric lead to overestimation of the segment length, which to some extent may counterbalance the overestimation of river width.

Looking beyond Australia, the method proposed here is applicable in any region of the world where high-resolution inundation time series mapping is feasible, and where good-quality DEM-derived river path, length, and sub-catchment area data are available. Thus, it would seem feasible to use a similar methodology to that employed here to develop a global river hydromorphology dataset using global inundation time series Landsat mapping produced by Donchyts et al. (2016), Pekel et al. (2016), or Jones (2019), for example.

5 Data availability

The river hydromorphology data are available at https://doi.org/10.25914/5c637a7449353 (Hou et al.,
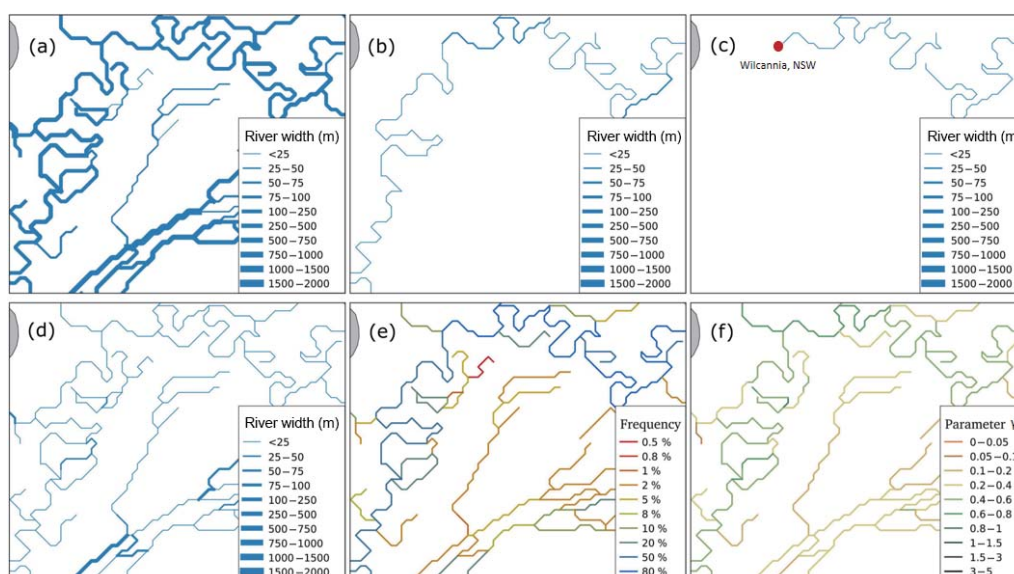
Figure 12. Illustration of data characteristics for an area including the Darling River and adjoining Talyawalka Creek near Wilcannia (NSW) (15.7 by 15.3 km centred on 31.62° S, 143.42° E). Shown are **(a)** maximum river width (0.5 % frequency); **(b)** median width (50 %); **(c)** minimum river width (80 %); **(d)** least detected river width and **(e)** corresponding frequency; and **(f)** hydromorphology parameter γ.

2019) and also can be downloaded directly from http://wald.anu.edu.au/data/ (last access: 20 May 2019; ANU Centre for Water and Landscape Dynamics, 2019). The data are in ASCII format, which can be directly joined to the Geofabric products, including surface cartography, surface catchments, surface network, groundwater cartography, and hydrological reporting catchments and regions. The Geofabric Surface Network can be accessed from http://www.bom.gov.au/water/geofabric/ (last access: 20 May 2019; Bureau of Meteorology, 2012b). The instruction for using these data can be found in the "readme" file. The data may be converted to any format (e.g. shapefile or raster) and combined with other Geofabric data, such as river name, length, feature type (nature, artificial, or water area flow segment), hierarchy (major or minor rivers), flow direction, and upstream drainage area.

6 Conclusions

We developed a river hydromorphology dataset for Australia by combining surface water recurrence information from the WOfS Landsat-derived dynamic water mapping product and GIS-based hydrological features from the Australian Geofabric. Our data provide river widths at different recurrence frequencies for 5.84×10^8 m river reaches across the Australian continent. A river morphology parameter γ is proposed to describe the shape of the width–frequency curve and can be interpreted as the degree to which rivers tend towards permanent, frequent, intermittent, or ephemeral. The majority of medium and large rivers in Australia have widths between 25 and 250 m and show an ephemeral or intermit-

tent flow regime. The data show correlation between maximum river width and cumulative upstream runoff, upstream drainage area, and gradient, in line with previously published results. The hydromorphological dataset developed contains river width dynamics, flow regime, and river gradient information for all Australian river reaches. The data provide new opportunities to analyse floodplain–river interactions at different scales and analyse the influence of climate, hydrology, vegetation, and terrain on river morphology. Such an understanding can help to predict future changes in landscape evolution in response to e.g. climate change. The dataset developed here may also be useful in providing fundamental information for understanding hydrological, biogeochemical, and ecological processes in floodplain–river systems; describing river width features in hydrological modelling; estimating river depth and discharge; assessing river conveyance capacity; identifying flooding-prone areas, and determining potential locations for satellite-based river gauging (Hou et al., 2018).

Author contributions. JH and AIJMVD conceived the idea. AIJMVD, LJR, RAV, and NM guided the study. JH carried out the research and wrote the manuscript with contributions from all the co-authors.

References

Allen, G. H. and Pavelsky, T. M.: Patterns of river width and surface area revealed by the satellite-derived North American river width data set, Geophys. Res. Lett., 42, 395–402, https://doi.org/10.1002/2014GL062764, 2015.

Allen, G. H. and Pavelsky, T. M.: Global extent of rivers and streams, Science, 361, 585–588, https://doi.org/10.1126/science.aat0636, 2018.

Andreadis, K. M., Schumann, G. J. P., and Pavelsky, T.: A simple global river bankfull width and depth database, Water Resour. Res., 49, 7164–7168, https://doi.org/10.1002/wrcr.20440, 2013.

ANU Centre for Water and Landscape Dynamics, available at: http://wald.anu.edu.au/, last access: 20 May 2019.

Arora, V. K. and Boer, G. J.: A variable velocity flow routing algorithm for GCMs, J. Geophys. Res.-Atmos., 104, 30965–30979, https://doi.org/10.1029/1999JD900905, 1999.

Bates, P. D. and De Roo, A. P. J.: A simple raster-based model for flood inundation simulation, J. Hydrol., 236, 54–77, https://doi.org/10.1016/S0022-1694(00)00278-X, 2000.

Biancamaria, S., Bates, P. D., Boone, A., and Mognard, N. M.: Large-scale coupled hydrologic and hydraulic modelling of the Ob river in Siberia, J. Hydrol., 379, 136–150, https://doi.org/10.1016/j.jhydrol.2009.09.054, 2009.

Bureau of Meteorology: Australian Hydrological Geospatial Fabric (Geofabric) Product Guide, available at: http://www.bom.gov.au/water/geofabric/documents/v2_1/ahgf_productguide_V2_1_release.pdf (last access: 20 May 2019), 2012a.

Bureau of Meteorology: Australian Hydrological Geospatial Fabric (Geofabric) Data Product Specification, available at: http://www.bom.gov.au/water/geofabric/documents/v2_1/ahgf_

dps_surface_network_V2_1_release.pdf (last access: 20 May 2019), 2012b.

Coe, M. T., Costa, M. H., and Howard, E. A.: Simulating the surface waters of the Amazon River basin: impacts of new river geomorphic and flow parameterizations, Hydrol. Process., 22, 2542–2553, https://doi.org/10.1002/hyp.6850, 2008.

Dadson, S. J., Ashpole, I., Harris, P., Davies, H. N., Clark, D. B., Blyth, E., and Taylor, C. M.: Wetland inundation dynamics in a model of land surface climate: Evaluation in the Niger inland delta region, J. Geophys. Res.-Atmos., 115, D23114, https://doi.org/10.1029/2010JD014474, 2010.

Decharme, B., Douville, H., Prigent, C., Papa, F., and Aires, F.: A new river flooding scheme for global climate applications: Offline evaluation over South America, J. Geophys. Res.-Atmos., 113, D11110, https://doi.org/10.1029/2007JD009376, 2008.

Doble, R., Crosbie, R., Peeters, L., Joehnk, K., and Ticehurst, C.: Modelling overbank flood recharge at a continental scale, Hydrol. Earth Syst. Sci., 18, 1273–1288, https://doi.org/10.5194/hess-18-1273-2014, 2014.

Donchyts, G., Baart, F., Winsemius, H., Gorelick, N., Kwadijk, J., and Van De Giesen, N.: Earth's surface water change over the past 30 years, Nat. Clim. Change, 6, 810–813, https://doi.org/10.1038/nclimate3111, 2016.

Frasson, R. P. D. M., Pavelsky, T. M., Fonstad, M. A., Durand, M. T., Allen, G. H., Schumann, G., Lion, C., Beighley, R. E., and Yang, X.: Global relationships betwee river width, slope, catchment area, meander wavelength, sinuosity, and discharge, Geophys. Res. Lett., 46, 3252–3262, https://doi.org/10.1029/2019GL082027, 2019.

Frost, A. J., Ramchurn, A., and Smith, A.: The Australian Landscape Water Balance model (AWRA-L v6), Technical Description of the Australian Water Resources Assessment Landscape model version 6, Bureau of Meteorology Technical Report, available at: http://www.bom.gov.au/water/landscape/assets/static/publications/AWRALv6_Model_Description_Report.pdf (last access: 20 May 2019), 2018.

Gallant, J. C., Dowling, T. I., Read, A. M., Wilson, N., Tickle, P., and Inskeep, C.: 1 second SRTM Derived Digital Elevation Models User Guide, Geoscience Australia, available at: https://d28rz98at9flks.cloudfront.net/72759/1secSRTM_Derived_DEMs_UserGuide_v1.0.4.pdf (last access: 20 May 2019), 2011.

Getirana, A. C. V., Boone, A., Yamazaki, D., Decharme, B., Papa, F., and Mognard, N.: The hydrological modeling and analysis platform (HyMAP): Evaluation in the Amazon basin, J. Hydrometeorol., 13, 1641–1665, https://doi.org/10.1175/JHM-D-12-021.1, 2012.

Getirana, A. C. V., Boone, A., Yamazaki, D., and Mognard, N.: Automatic parameterization of a flow routing scheme driven by radar altimetry data: Evaluation in the Amazon basin, Water Resour. Res., 49, 614–629, https://doi.org/10.1002/wrcr.20077, 2013.

Hou, J., Van Dijk, A. I. J. M., Renzullo, L. J., and Vertessy, R. A.: Using modelled discharge to develop satellite-based river gauging: a case study for the Amazon Basin, Hydrol. Earth Syst. Sci., 22, 6435–6448, https://doi.org/10.5194/hess-22-6435-2018, 2018.

Hou, J., Van Dijk, A. I. J. M., Renzullo, L. J., Vertessy, R. A., and Mueller, N.: Hydromorphological attributes for all Australian

river reaches, Dataset, https://doi.org/10.25914/5c637a7449353, 2019.

Isikdogan, F., Bovik, A., and Passalacqua, P.: RivaMap: An automated river analysis and mapping engine, Remote Sens. Environ., 202, 88–97, https://doi.org/10.1016/j.rse.2017.03.044, 2017.

Jones, J. W.: Improved Automated Detection of Subpixel-Scale Inundation – Revised Dynamic Surface Water Extent (DSWE) Partial Surface Water Tests, Remote Sens., 11, 374, https://doi.org/10.3390/rs11040374, 2019.

Kleinhans, M. G. and Van Den Berg, J. H.: River channel and bar patterns explained and predicted by an empirical and a physics-based method, Earth Surf. Process. Landf., 36, 721–738, https://doi.org/10.1002/esp.2090, 2011.

Lehner, B., Verdin, K., and Jarvis, A.: New global hydrography derived from spaceborne elevation data, Eos, Trans. Am. Geophys. Union, 89, 93–94, https://doi.org/10.1029/2008EO100001, 2008.

Leopold, L. B. and Maddock, T.: The hydraulic geometry of stream channels and some physiographic implications, U.S. Government Printing Office, Washington, D.C., 1953.

Leopold, L. B., Wolman, M. G., and Miller, J. P.: Fluvial processes in geomorphology, W.H. Freeman and Company, San Francisco, 1964.

Miller, Z. F., Pavelsky, T. M., and Allen, G. H.: Quantifying river form variations in the Mississippi Basin using remotely sensed imagery, Hydrol. Earth Syst. Sci., 18, 4883–4895, https://doi.org/10.5194/hess-18-4883-2014, 2014.

Moody, J. A. and Troutman, B. M.: Characterization of the spatial variability of channel morphology, Earth Surf. Process. Landf., 27, 1251–1266, https://doi.org/10.1002/esp.403, 2002.

Mueller, N., Lewis, A., Roberts, D., Ring, S., Melrose, R., Sixsmith, J., Lymburner, L., McIntyre, A., Tan, P., Curnow, S., and Ip, A.: Water observations from space: Mapping surface water from 25 years of Landsat imagery across Australia, Remote Sens. Environ., 174, 341–352, https://doi.org/10.1016/j.rse.2015.11.003, 2016.

Nanson, G. C. and Knighton, A. D.: Anabranching rivers: their cause, character and classification, Earth Surf. Process. Landf., 21, 217–239, https://doi.org/10.1002/(SICI)1096-9837(199603)21:3<217::AID-ESP611>3.0.CO;2-U, 1996.

Neal, J., Schumann, G., and Bates, P.: A subgrid channel model for simulating river hydraulics and floodplain inundation over large and data sparse areas, Water Resour. Res., 48, W11506, https://doi.org/10.1029/2012WR012514, 2012.

NIST/SEMATECH e-handbook of statistical methods, available at: http://www.itl.nist.gov/div898/handbook (last access: 20 May 2019), 2018.

O'Loughlin, F., Trigg, M. A., Schumann, G. J. P., and Bates, P. D.: Hydraulic characterization of the middle reach of the Congo River, Water Resour. Res., 49, 5059–5070, https://doi.org/10.1002/wrcr.20398, 2013.

Paiva, R. C. D., Buarque, D. C., Collischonn, W., Bonnet, M. P., Frappart, F., Calmant, S., and Mendes, C. A. B.: Large-scale hydrologic and hydrodynamic modeling of the Amazon River basin, Water Resour. Res., 49, 1226–1243, https://doi.org/10.1002/wrcr.20067, 2013.

Pavelsky, T. M. and Smith, L. C.: RivWidth: A software tool for the calculation of river widths from remotely

sensed imagery, IEEE Geosci. Remote Sens. Lett., 5, 70–73, https://doi.org/10.1109/LGRS.2007.908305, 2008.

Pedinotti, V., Boone, A., Decharme, B., Crétaux, J. F., Mognard, N., Panthou, G., Papa, F., and Tanimoun, B. A.: Evaluation of the ISBA-TRIP continental hydrologic system over the Niger basin using in situ and satellite derived datasets, Hydrol. Earth Syst. Sci., 16, 1745–1773, https://doi.org/10.5194/hess-16-1745-2012, 2012.

Pekel, J.-F., Cottam, A., Gorelick, N., and Belward, A. S.: High-resolution mapping of global surface water and its long-term changes, Nature, 540, 418–422, https://doi.org/10.1038/nature20584, 2016.

Rosgen, D. L.: A classification of natural rivers, Catena, 22, 169–199, https://doi.org/10.1016/0341-8162(94)90001-9, 1994.

Stein, J. L., Hutchinson, M. F., and Stein, J. A.: A new stream and nested catchment framework for Australia, Hydrol. Earth Syst. Sci., 18, 1917–1933, https://doi.org/10.5194/hess-18-1917-2014, 2014.

Storn, R. and Price, K.: Differential evolution–a simple and efficient heuristic for global optimization over continuous spaces, J. Global Optim., 11, 341–359, https://doi.org/10.1023/A:1008202821328, 1997.

Van Dijk, A. I. J. M.: Australian Water Resources Assessment System. Technical Report 3. Landscape Model (version 0.5) Technical Description. CSIRO: Water for a Healthy Country. National Research Flagship, available at: http://www.clw.csiro.au/publications/waterforahealthycountry/2010/wfhc-aus-water-resources-assessment-system.pdf (last access: 20 May 2019), 2010.

Van Dijk, A. I. J. M. and Warren, G.: The Australian Water Resources Assessment System. Technical Report 4, Landscape Model (version 0.5) Evaluation Against Observations, CSIRO: Water for a Healthy Country National Research Flagship, available at: http://www.clw.csiro.au/publications/waterforahealthycountry/2010/wfhc-awras-evaluation-against-observations.pdf (last access: 20 May 2019), 2010.

Van Schaik, L., Hohenbrink, T., Jackisch, C., Laudon, H., Pfister, L., Hassler, S. K., Renner, M., and Gelfan, A. (Eds.): Linking landscape organisation and hydrological functioning: from hypotheses and observations to concepts, models and understanding, special issue jointly organized between Hydrology and Earth System Sciences and Earth System Science Data, https://www.earth-syst-sci-data.net/special_issue13_985.html, 2019.

Vincenty, T.: Direct and inverse solutions of geodesics on the ellipsoid with application of nested equations, Surv. Rev., 23, 88–93, https://doi.org/10.1179/sre.1975.23.176.88, 1975.

Yamazaki, D., Kanae, S., Kim, H., and Oki, T.: A physically based description of floodplain inundation dynamics in a global river routing model, Water Resour. Res., 47, W04501, https://doi.org/10.1029/2010WR009726, 2011.

Yamazaki, D., O'Loughlin, F., Trigg, M. A., Miller, Z. F., Pavelsky, T. M., and Bates, P. D.: Development of the global width database for large rivers, Water Resour. Res., 50, 3467–3480, https://doi.org/10.1002/2013WR014664, 2014.

Chapter 5: Changes in precipitation a greater threat to global water reservoir security than increased water use

Around two thirds of the world's rivers longer than 1,000 km^2 are no longer free-flowing over their entire length due to the construction of reservoir dams. This chapter documents research to reconstruct global reservoir storage and examines storage trends, changes in reservoir resilience and vulnerability over the past three decades. It also analyses how multi-decadal changes in precipitation, streamflow, evaporation, and human activity affected global reservoir water security. The content of this chapter was under review as follows:

Hou, J., Van Dijk, A.I.J.M., Beck, H.E., Renzullo, L.J., and Wada, Y., 2020. Changes in precipitation a greater threat to global water reservoir security than increased water use, under review.

Changes in precipitation a greater threat to global water reservoir security than increased water use

Jiawei Hou[1*], Albert I.J.M. van Dijk[1], Hylke E. Beck[2], Luigi J. Renzullo[1], Yoshihide Wada[3]

Affiliations:

[1]Fenner School of Environment and Society, Australian National University, Australia.

[2] Department of Civil and Environmental Engineering, Princeton University, United States of America.

[3] International Institute for Applied Systems Analysis, Laxenburg, Austria.

*Correspondence to: jiawei.hou@anu.edu.au.

Abstract: Recent water crises have raised concerns about the impact of population growth and climate change on reservoir water storage security worldwide. So far, a global assessment has not been undertaken, because reservoir measurements are generally not publicly available. Here, we use satellite observations to reconstruct monthly storage for the majority of large reservoirs worldwide between 1984 and 2015. We relate reservoir storage to water security and resilience and analyze their response to precipitation, streamflow and evaporation. We find reservoir security has diminished substantially for 23% of reservoirs over the three decades but increased for 21%. The greatest declines were in dry basins in southeastern Australia (-29%), central Chile (-13%), southwestern USA (-10%) and eastern Brazil (-9%). The greatest gains occurred in the Nile Basin (+67%), Mediterranean basins (+31%) and southern Africa (+22%). The observed reservoir changes were explained by changes in precipitation and river inflows, emphasizing the importance of multi-decadal precipitation changes for reservoir water security, rather than changes in net evaporation or dam water releases.

Main Text: Globally the number of large reservoirs – dams impounding more than 3 million m^3 [1] – reached 57,985 in 2020 with a combined capacity of more than 10,000 km^3 [2]. Reservoirs now provide 30–40% of global irrigation water requirements, 17% of electricity generated, and various other services, including domestic and industrial water supply, recreation, fisheries, and flood and pollution control [3,4]. With projected population increases, demand for water and electricity are also expected to increase substantially [5,6]. Meeting this demand by constructing new reservoirs has become challenging due to a shortage of suitable construction sites and

remaining 'underdeveloped' water resources, as well as increased recognition of the profound impacts that impoundments have on the local population and riverine ecosystem [7-9].

Adding to the challenge, evidence is emerging that existing reservoirs in some regions are becoming less secure. Recent water supply failures or near-failures have occurred in the US Colorado River Basin since 2000 [10], southeast Australia between 2002–2009 [11], Barcelona, Spain, in 2007–2008 [12], Sao Paolo, Brazil, in 2014–2015 [13] and Cape Town, South Africa, in 2015–2017 [14]. However, it is unclear if these events are part of a global climate trend or due to local supply or demand changes. The underlying causes are also not necessarily the same in each case: reservoir storage dynamics are the net result of river inflows, net evaporation (i.e., evaporation minus direct precipitation onto the reservoir) and dam water releases downstream. A change in the balance between these three terms leads to a change in storage level. There are also interactions. The physical connection between precipitation, streamflow generation and atmospheric moisture demand creates positive feedbacks in storage volume changes: e.g., assuming the entire water supply system experiences comparable dry conditions, inflows will decrease while net evaporation and downstream demand for water releases for consumptive use will increase. To mitigate this feedback, reservoir operation rules will typically aim to reduce dam releases in response to lowering storage levels. Only a detailed analysis of the water balance of an individual reservoir can conclusively separate the contributions of these three processes to a change in water security. However, in practice, a loss of reservoir water security in the presence of a decrease in upstream or downstream river flows within the river system indicates that reduced precipitation conditions are the most likely cause, whereas the absence of such a precipitation and streamflow decrease, or even an increase, points towards less prudent reservoir operation, possibly in response to increased demand. Therefore, knowledge of temporal trends in reservoir storage and river flow can be combined to interpret whether trends in reservoir water security are widespread globally, and if so, whether they are likely to be due to changing climate conditions or due to other factors. For the majority of large reservoirs, operators keep records of releases and estimated storage volume, inflows and net evaporation. Unfortunately, these data are typically not publicly available, for a variety of commercial, logistical, political and security reasons. Probably mainly because of this, so far there has been no attempt at a global assessment and attribution of trends in water reservoir security.

We used satellite observations between 1984 and 2015 to reconstruct storage dynamics for 6,743 reservoirs representing the majority of combined reservoir storage capacity worldwide, and calculated trends in reservoir storage, resilience, and vulnerability (See Materials and Methods). The three measures were correlated (Fig. S6 and S7) and therefore we only report on trends in mean storage. Overall, there was a positive trend in combined global reservoir storage of +3.1 km^3 y^{-1}, but this was almost entirely explained by positive trends for the two largest reservoirs in

the world, Lake Kariba (+0.8 km^3 y^{-1}) on the Zambezi River and Lake Aswan (+1.9 km^3 y^{-1}) on the Nile River (Fig. S8).

Globally, 1,034 reservoirs showed decreasing trends at p<0.05 and 948 reservoirs increasing trends (Fig. 1). Basins losing or gaining more than 5% of their combined storage over the three decades could be found on every continent (Fig. 2c). There was no apparent relationship between primary reservoir purpose (i.e., irrigation, hydroelectric power generation, domestic water supply) and overall trend, arguably a first tentative indication that climatological influences dominate changes in release management.
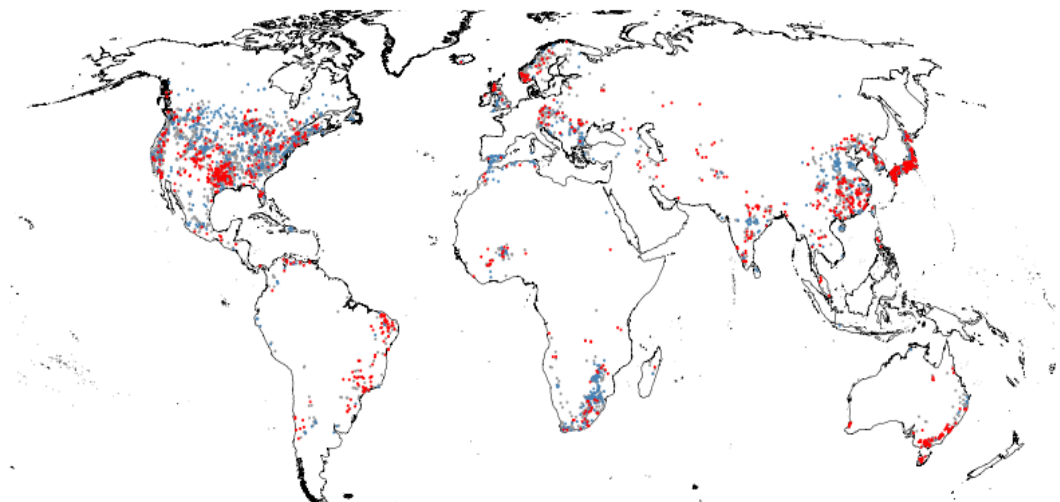
Fig. 1. Storage trends (1984-2015) for individual reservoirs globally (*p*<0.05; increasing: blue; no change: grey; decreasing: red).

Trends in human-made reservoirs found here are consistent with trends reported in a previous study for 200 natural lakes across North America, Europe, Asia and Africa during 1992–2019 [15]. Additionally, total terrestrial water storage (i.e., the sum of groundwater, soil water and surface water) derived from GRACE satellite gravimetry for the shorter period 2002-2016 showed decreases in endorheic basins in Central Eurasia and the southwestern USA and increases in Southern Africa consistent with our storage changes [16].

We summed storage for individual reservoirs to calculate combined storage in 134 river basins worldwide. Among these, 26 (19%) showed a significant decreasing and 39 (29%) a significant increasing trend in reservoir storage (Fig. 2c). For the majority of these 65 basins, trends were of the same sign for storage, runoff and precipitation, suggesting that precipitation changes are ultimately the most likely explanation for observed trends (Fig. 2a and b, Fig. S9 and Fig. S10). We also found that changes in net evaporation account for well below 10% of the overall trends in storage for each of those 65 basins (Fig. S11). Opposite precipitation (or runoff) and storage trends were found for 12 out of 134 basins, with six decreasing and six increasing storage trends. Most of these could be explained by spatial variation within the respective basins

(Fig. S13). In summary, we did not find evidence for widespread reductions in reservoir water security due to increased releases.
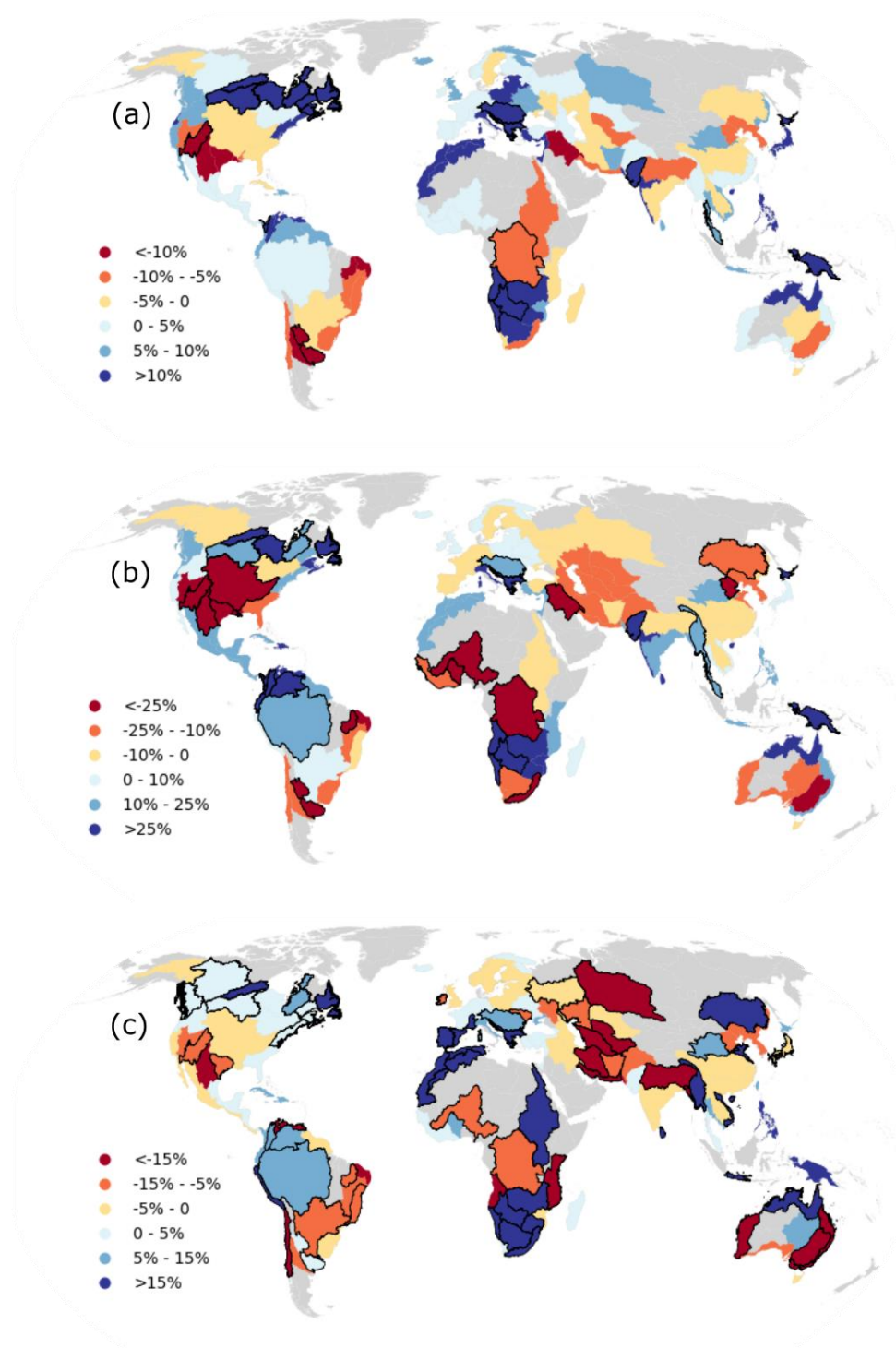
Fig. 2. Linear trends in annual, basin-average (a) precipitation, (b) simulated streamflow and (c) reservoir storage between 1984–2015 (grey shade: no reservoir data; black outlines: trend significant at $p<0.05$).

The greatest storage gains occurred in the Nile Basin (+67%), western Mediterranean (+31%) and southern Africa (+22%), and were attributed to very high inflows during 1996-2008, 2008-2010 and 1996-2000, respectively (Fig. S14). Substantial decreases were found for arid to sub-humid basins in southeastern Australia (-29%), southwestern USA (-10%), Brazil (-9%) and central Chile (-13%) (Fig. 3). Both simulated and observed river discharge data show similar trends and explain the observed storage declines (Fig. 2b and Fig. S12). During Australia's Millennium Drought (2001-2009) [11], river flows in the Murray-Darling Basin fell to about half that for 1984–1999 (Fig. 3a), causing a halving of combined storage, but recovering due to high inflows during 2009-2011. In the southwestern USA, three distinct dry periods occurred (Fig. 3b). Sharp decreases in river flow after 2011 in eastern Brazil and after 2006 in central Chile led to the lowest reservoir storage levels, with combined losses of almost 18% in 2015 in Brazil and 24% in 2013 in Chile (Fig. 3c and d). Reservoirs in basins with reduced storage also predominantly showed reduced resilience (i.e., they fell to low capacity more often) and increased vulnerability (i.e., they endured larger deficits; Figs S6 and S7).
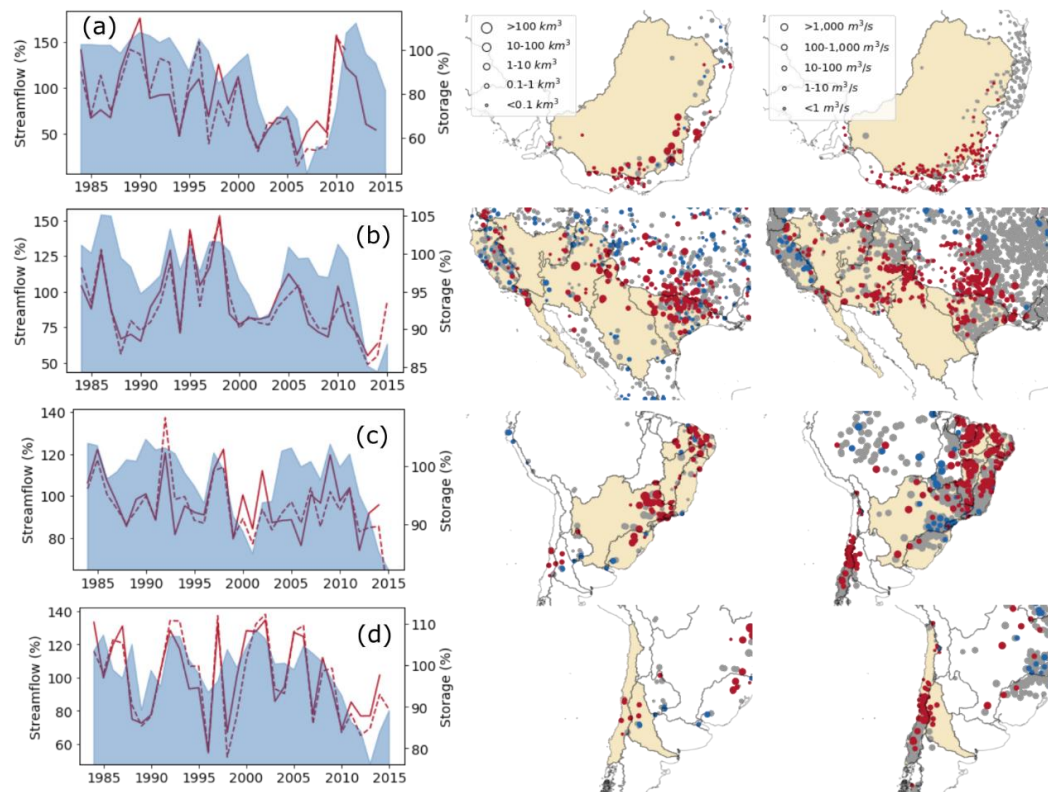
Fig. 3. Time series (left column) of annual combined storage (blue shaded) along with simulated (solid) and observed (dashed line) streamflow, indexed to the reference period 1984–1999, and trends in storage (middle column) and observed streamflow (right column) during 1984–2015 ($p<0.05$; increasing: blue; no change: grey; declining: red). Shown are (top row) southeastern Australia, (second row) southwestern USA, (third row) Brazil, and (bottom row) central Chile.

Overall, we found that reservoir storage changed significantly in nearly half of all basins worldwide between 1984–2015, with increases and decreases similarly common and mostly explained by corresponding precipitation and runoff changes. Increases appeared slightly more common in cooler regions and decreases more common in drier regions (Fig. 1). We did not find evidence that changes in water releases or net evaporation contributed meaningfully to global trends. Changes in reservoir water security appear to be predominantly determined by periods of low inflow in response to low precipitation. Future changes in precipitation variability are among the most uncertain predictions by climate models [17]. Therefore, a prudent approach to reservoir water management appears the only available means to avoid water supply failure for individual river systems.

Methods Summary

Monthly reservoir storage for 1984-2015 for individual reservoirs was estimated using satellite-derived surface water height and extent. The 'Global Reservoirs and Lakes Monitor' (G-REALM) water surface height product was produced by the US Department of Agriculture's Foreign Agricultural Service based on altimetry observations from the Topex/Poseidon (1992-2002), Jason-1 (2002-2008), Jason-2 (2008-2016), and the Jason-3 (2016-present) mission. The surface water extent product [18] was derived by post-processing of the Landsat satellite-derived Global Surface Water Dataset [19]. For reservoirs with water extent data only, storage was estimated from surrounding topography [20]. The accuracy of the storage estimates was quantified using publicly available observed storage volume estimates for several reservoirs in the US, Australia and Egypt. Trends in annual mean storage volume, reservoir vulnerability and resilience were all calculated and found to be correlated (Figs S6 and S7). To assess factors driving storage trends we used precipitation and net evaporation from merged station, satellite and forecast data [21] and streamflow from a multi-model ensemble [22] as well as observed at ca. 8,000 gauging stations (see Material and Methods). Combined reservoir storage, precipitation, streamflow and net evaporation were also calculated for each river basin [23]. The Mann-Kendall test ($p < 0.05$) was used to test the significance of linear trends.

References:

1. The International Commission on Large Dams. (2020). *https://www.icold-cigb.org/GB/world_register/general_synthesis.asp*.

2. B. F. Chao, Y. Wu, Y. Li, Impact of artificial reservoir water impoundment on global sea level. *Science* **320**, 212-214 (2008).

3. S. Yoshikawa, J. Cho, H. G. Yamada, N. Hanasaki, S. Kanae, An assessment of global net irrigation water requirements from various water supply sources to sustain irrigation: rivers and reservoirs (1960–2050). *Hydrology and Earth System Sciences* **18**, 4289-4310 (2014).

4.   REN21, Renewables 2016. Global Status Report. REN21. https://www.ren21.net/gsr-2016/ (2016).

5.   E. Crist, C. Mora, R. Engelman, The interaction of human population, food production, and biodiversity protection. *Science* **356**, 260-264 (2017).

6.   C. Zarfl, A. E. Lumsdon, J. Berlekamp, L. Tydecks, K. Tockner, A global boom in hydropower dam construction. *Aquatic Sciences* **77**, 161-170 (2015).

7.   B. Lehner *et al.*, High-resolution mapping of the world's reservoirs and dams for sustainable river-flow management. *Frontiers in Ecology and the Environment* **9**, 494-502 (2011).

8.   C. Nilsson, C. A. Reidy, M. Dynesius, C. Revenga, Fragmentation and flow regulation of the world's large river systems. *Science* **308**, 405-408 (2005).

9.   G. Grill *et al.*, An index-based framework for assessing patterns and trends in river fragmentation and flow regulation by global dams at multiple scales. *Environmental Research Letters* **10**, 015001 (2015).

10.   B. Udall, J. Overpeck, The twenty-first century Colorado River hot drought and implications for the future. *Water Resources Research* **53**, 2404-2418 (2017).

11.   A. I. J. M. Van Dijk *et al.*, The Millennium Drought in southeast Australia (2001–2009): Natural and human causes and implications for water resources, ecosystems, economy, and society. *Water Resources Research* **49**, 1040-1057 (2013).

12.   H. March, L. Domenech, D. Saurí, Water conservation campaigns and citizen perceptions: the drought of 2007–2008 in the Metropolitan Area of Barcelona. *Natural Hazards* **65**, 1951-1966 (2013).

13.   H. Escobar, Drought triggers alarms in Brazil's biggest metropolis. *Science* **347**, 812-812 (2015).

14.   P. M. Sousa, R. C. Blamey, C. J. Reason, A. M. Ramos, R. M. Trigo, The 'Day Zero' Cape Town drought and the poleward migration of moisture corridors. *Environmental Research Letters* **13**, 124025 (2018).

15.   B. M. Kraemer, A. Seimon, R. Adrian, P. B. McIntyre, Worldwide lake level trends and responses to background climate variation. *Hydrology and Earth System Sciences* **24**, 2593-2608 (2020).

16.   J. Wang *et al.*, Recent global decline in endorheic basin water storages. *Nature Geoscience* **11**, 926-932 (2018).

17. K. E. Trenberth *et al.*, Global warming and changes in drought. *Nature Climate Change* **4**, 17-22 (2014).

18. G. Zhao, H. Gao, Automatic correction of contaminated images for assessment of reservoir surface area dynamics. *Geophysical Research Letters* 45, 6092-6099 (2018).

19. J.-F. Pekel, A. Cottam, N. Gorelick, A. S. Belward, High-resolution mapping of global surface water and its long-term changes. *Nature* 540, 418-422 (2016).

20. M. L. Messager, B. Lehner, G. Grill, I. Nedeva, O. Schmitt, Estimating the volume and age of water stored in global lakes using a geo-statistical approach. *Nature Communications* 7, 13603 (2016).

21. H. E. Beck et al., MSWEP: 3-hourly 0.25 global gridded precipitation (1979-2015) by merging gauge, satellite, and reanalysis data. *Hydrology and Earth System Sciences* 21, 589 (2017).

22. J. Schellekens et al., A global water resources ensemble of hydrological models: The eartH2Observe Tier-1 dataset. *Earth System Science Data* 9, 389-413 (2017).

23. B. Lehner, G. Grill, Global river hydrography and network routing: baseline data and new approaches to study the world's large river systems. *Hydrological Processes* 27, 2171-2186 (2013).

Chapter 6: Summary and outlook

6.1 Conclusions

Traditionally, methods to estimate river discharge from remote sensing-derived river width, elevation, or inundation need to be trained using discharge observed in-situ first. This approach can be only applied where there are gauging stations. To address this issue, this research proposed that, for ungauged river reaches, sufficiently reliable hydrological models such as the W3 model (Van Dijk et al., 2016) can be used to train remote sensing based river discharge methods instead. A simple automated statistical method, based on so-called satellite gauging reaches (SGRs) was developed to link remote sensing measurements efficiently and effectively to in situ discharge at gauged sites, as well as modelled discharge at ungauged sites. The method was able to retrieve historical time series, fill the gap of observed data, and provide near real-time information at global scale. The approach was shown suitable to both optical (MODIS) and passive microwave remote sensing (GFDS). The advantage of GFDS was that passive microwave is less affected by dense vegetation and cloud than optical remote sensing. However, the overall performance of MODIS-derived SGRs was better than that of GFDS-derived SGRs probably mainly because MODIS has a higher spatial resolution.

The MODIS 8-day composite (MCD43C4) alleviates cloud contamination issues to a considerable degree and was used globally following the developed approach. Suitable SGRs could be constructed over river reaches with a combined length of ca. 1.15 million km at global scale, especially in South America, Africa, South Asia, the Middle East, and northern high latitude regions. Model-based SGRs performed with similar skill as gauged-based SGRs. The performance of SGRs can be explained by river morphology. Wide channels with strong temporal inundation variations, broad floodplains, relatively wide channels, multiple braided channels, or a large number of meandering or anastomosing channels provide the best conditions to construct an SGR. A method was proposed to assess whether SGRs can be constructed in a selected river reach based on high-resolution inundation summary data.

River morphology is not only an essential factor that affects the performance of SGRs to predict river discharge, but itself also can be used to improve river routing in models to estimate river discharge. Hydromorphological attributes, including spatial and temporal river width, flow regime and river gradient were derived from Landsat imagery for 1.4 million Australian river reaches. A parameter, gamma, was proposed to describe river reaches by the degree to which flow regime tends towards permanent, frequent, intermittent, or ephemeral. The dataset indicates the majority of rivers over the Australian continent ranges between 25 (noting that the spatial resolution of Landsat-derived observations was limited to 25 m) to 250 m width, irrespective of dynamic characteristics, and the dominant flow regime is ephemeral or intermittent. The relationships between river width and contributing catchment area, river discharge, and reach gradient were investigated. The coefficients for conventional scaling rules were found to be

related to river reach gradient. This helps to explain why previous studies do not report identical coefficients for the empirical scaling functions. With a high-resolution inundation time series mapping, such as the Landsat-derived global surface water dataset (GSWD) (Pekel et al. 2016), the method proposed here can be readily applicable in any region worldwide where good-quality DEM-derived river sub-catchment area, length, and path data are available.

Monthly reservoir storage dynamics were estimated using Landsat-derived surface water extents and surface water heights derived from various altimetry missions including Topex/Poseidon (1992-2002), Jason-1 (2002-2008), Jason-2 (2008-2016) and Jason-3 (2016-present). A large number of reservoirs have no altimetry data, and for these storages dynamics were estimated using a geo-statistical approach based on surface water area and the surrounding average slope. Storage dynamics for 6,743 reservoirs worldwide between 1984-2015 were reconstructed. The results indicated that storages in some regions, particularly in southeastern Australia, central Chile, the USA, and eastern Brazil, have declined, accompanied by reduced reservoir resilience and increased vulnerability. Storage gains mainly occurred in the Nile Basin, Mediterranean basins and southern Africa. Based on a comprehensive analysis of streamflow from a multi-model ensemble and as observed at ca. 8,000 gauging stations, precipitation from a combination of station, satellite and forecast data, and open water evaporation estimates, we concluded that the change in global water reservoir security is induced by multi-decadal precipitation changes affecting river flow into storages, rather than by changes in net evaporation or dam release patterns. This suggests that prudent reservoir water management should be considered to avoid future functional failure, particularly during periods of low inflow and precipitation.

6.2 Future perspectives

This research presents new approaches for measuring spatial and temporal river discharge, river morphology, and reservoir storage from space. The main limitation in the methods is the insufficient spatial and temporal resolution of remote sensing. MODIS has a relatively coarse spatial resolution (250-500 m), and fails to detect many small rivers and reservoirs. Although Landsat has a higher spatial resolution of c. 30 m, its temporal resolution is as long as 16 days, which renders it unable to track rapid changes. The main benefits of using these two types of optical remote sensing are that Landsat can retrieve inland water bodies measurements going back decades while MODIS can provide near real-time information. On the other hand, these optical sensors are subjected to cloud contamination. Although synthetic aperture radar (SAR) instrument can complement this drawback of optical sensors, it needs complex image processing, which prevents its implementation in an operational framework or its automated application at large scale.

The more recent launch of ESA's Sentinel missions, especially Sentinel 2, provide promising opportunities for water extent monitoring with higher spatial and temporal resolution. The

Sentinel 2 mission is composed of two satellites, Sentinel 2A launched in 2015 and Sentinel 2B launched in 2017, continuing the missions of the Landsat and the SPOT series of satellites. The Sentinel 2 multispectral Instrument (MSI) has 13 spectral bands: four bands (Band 2/3/4/8, visible and near-infrared bands) at 10 meters spatial resolution, six bands (Band 5/6/7/8a/11/12, red-edge and shortwave-infrared bands) at 20 meters spatial resolution, and three bands (Band 1/9/10, atmospheric correction bands) at 60 meters spatial resolution. Sentinel 2 covers all continental land surface areas between latitudes 56° south and 84° north with 10 days per cycle by one satellite, or 5 days per cycle by two satellites, at the equator. At present, Sentinel 2 has limited application to river discharge estimation as there is little gauging data available after 2015 that can be used to train Sentinel-based method. As a new satellite mission, Sentinel 2 is also not able to provide long-term dynamics in surface water bodies. However, it is likely to provide such pragmatic applications after one or two decades of measurement.

The NASA Surface Water and Ocean Topography (SWOT) is another promising satellite mission that offers opportunities to observe surface water extent and height at the same time. It is scheduled for launch in 2021 and should serve a nominal 3 years for science data collection with an orbit repeat period of 21 days. It should also provide 1-day repeat observations of the Earth for 6 months. The Ka-band radar interferometer onboard SWOT will distinguish water from land surfaces based on the differences in the magnitude of the returned microwave power to the ground. The accuracy of SWOT reservoir height measurements is expected to within 10 cm for water bodies greater than 1 km^2 and within 25 cm for those with a surface area of 0.0625 - 1 km^2 (Biancamaria et al., 2016). The projected error of SWOT reservoir surface extent observations is expected to be within 15 % of the total area (Solander et al., 2016). Solander et al. (2016) suggest that temporal errors could be <5% for reservoir with a water surface area less than 10 km^2 and <0.1% for those with a surface area greater than 100 km^2. In addition, the orbit of SWOT may cover more than half of global floods (Frasson et al., 2019). Unfortunately, the lifespan of SWOT is too short to observe long-term changes in global water availability. In terms of hydrology and climate science, a decades-long satellite mission would be needed to observe water level and extent simultaneously at global scale with a daily repeat orbit and high spatial resolution (e.g. 10 m).

This research produced river discharge data for the period 2000-2014 and reservoir storage data for 1984-2015 at global scale. The methods developed here can be further applied to produce near real-time information. This could enable a global near real-time river, lakes, and reservoirs monitoring system to regularly provide information on the historical and current status of water availability globally. The prototype operating framework of such system (prototyped as the ANU Water Monitor: http://anuwald.science/water) is described in Appendix 5. Briefly, historical river discharge and lake and reservoir water storage are estimated by following approaches proposed in this thesis. The discharge-extent and storage-elevation relationships are stored on the National Computational Infrastructure (NCI) and new imagery from MODIS (MCD43C4 version 6) is

automatically acquired from the NASA Land Processes Distributed Active Archive Center (LP DAAC) Distribution Server at the USGS Earth Resources Observation and Science (EROS) Center. Updated surface water elevations are parsed from United States Department of Agriculture Foreign Agricultural Service web server. Near real-time discharge and storage can then be calculated based on the corresponding relationships with the new surface water extent derived from the updated MODIS image and the new altimetry data, respectively. These dynamics information is displayed online through a web application using NCI web services.

Development of this system is planned to continue. The current version includes historical and near real-time data for global rivers, lakes, and reservoirs. The lake storage data were developed based on the same method as for reservoirs. A difference is that it uses other water extent data sources, i.e. the MODIS 500-m resolution daily global surface water change database produced by Ji et al. (2018) and BLUEDOT Water Observatory data (https://www.blue-dot-observatory.com/aboutwaterobservatory) derived from Sentinel-2. However, cloud contamination in the first product has not been solved to an acceptable level for practical applications and there is no available data after 2016. Although the second product can provide updated water extent data, it has not been validated and for individual water bodies the boundaries are not consistent. Thus, it would be necessary to design a new, automated approach to retrieve historical data and produce near real-time information with cloud contamination mitigated to a greater degree and with high temporal resolution (e.g. daily). Based on the enhanced water extent dataset, lake and reservoir storage estimates could then be further improved and even global wetland storage be produced.

As this research found, multi-decadal precipitation change has posed a threat to global reservoir water security. Whether these precipitation and streamflow changes also alter lake and wetland storage remains to be addressed in future research. Combining global river morphology and reservoir storage data, we can address how man-made reservoirs have influenced downstream ecosystems (e.g. through changes in inundation and vegetation coverage) and the degree to which flood-control dams have been able to mitigate flooding events downstream (e.g. the changes in frequency and magnitude of flooding inundation in urban and rural areas). River width dynamics and gradients for all Australian rivers can be applied in Australian hydrological models (e.g. AWRA-L) (Frost et al., 2018, Van Dijk, 2010) to improve river routing for better predication of river discharge. Based on our approach, a global river morphology dynamics dataset could be produced in future, and could find a wide range of applications in hydrology, biogeochemistry, and ecology. River morphology time series data can provide more useful insights than the statistical recurrence frequency measurement developed in this study. A challenge is to produce monthly or annual hydromorphological data, as a large fraction of Landsat imagery are contaminated by clouds and the low (16-day) temporal resolution further amplifies this issue. Water extent-derived SGRs are applicable to river reaches with variable width or broad floodplains. Altimetry derived SGRs could complement the river discharge prediction abilities of

water extent-derived SGRs as the relationship between discharge and elevation should be robust in stable river channels.

Although SGRs were proven to be a useful approach to predict river discharge, gauging stations remain ideal to provide precise measurements for calibrating hydrological models and training remote sensing based methods. In practical applications, gauge-based SGRs can be used to fit in situ measurement gaps, for example, when gauging stations were damaged, out of order, or upgraded, and retrieve historical data before gauging stations were constructed. Meanwhile, model-based SGRs can extend information from gauged sites. Satellite observations are practical for lake and reservoir storage estimation considering their large size in terms of water extent, but in situ water level and depth data are a prerequisite for calibrating altimetry data to estimate water depth in order to reconstruct absolute storage. All these considerations emphasize the importance of in situ measurements. This research strongly advocates for collaborations between countries to share in situ river, lake and reservoir data, as well as corresponding socioeconomic data (e.g. water use by sector), and the need to increase investment in constructing more gauging stations globally.

Conversely, with only gauging stations we cannot measure millions of lakes and countless floodplains and wetlands around the world. The most environmentally, socially, and financially effective way to understand the global water system is to establish a comprehensive, continuous, spatially consistent, and long-term hydrological monitoring system based on satellite remote sensing. A web-based application to visualize these global water data should be a pragmatic information source for many communities and individuals to easily understand changes in water resources availability in their environment, learning them better and preparing for future water challenges in a changing climate.

Appendix 1: Supplementary Materials to Chapter 2

This appendix is the supplementary materials to Chapter 2, which was published in the journal Hydrology and Earth System Sciences as:

Hou, J., Van Dijk, A.I.J.M., Renzullo, L.J. and Vertessy, R.A., 2018. Using modelled discharge to develop satellite-based river gauging: a case study for the Amazon Basin. Hydrology & Earth System Sciences, 22, https://doi.org/10.5194/hess-22-6435-2018.

Supplement of

Using modelled discharge to develop satellite-based river gauging: a case study for the Amazon Basin

Jiawei Hou et al.

Correspondence to: Jiawei Hou (jiawei.hou@anu.edu.au)

S1 Daily, 8-day and Monthly Performance of the MODIS and GFDS SGRs, and the Model

We compared daily, 8-day and monthly performance of the MODIS and GFDS SGRs and the model in two river reaches in the lower channel of the Amazon River to evaluate the effect of temporal aggregation on prediction accuracy. The daily streamflow records were derived from Brazil's National Water Agency database by H.E. Beck (Princeton University, pers. comm.). To highlight temporal details, below we compared the different estimates for an arbitrary 13-month period (August, 2006 - August, 2007 for G32; June, 2006 - June, 2007 for G33). The daily and 8-day SGR predictions are noisy (Figure S1a, b, d and e) as the GFDS signal is influenced by many factors such as the weak magnitude of the radiance received at the passive sensor, the changing scanning geometry, footprint size of each swath, and the path of the radiation through the atmosphere (Kugler and De Groeve, 2007), whereas the MODIS signal sometimes appears to be affected by cloud or aerosols. However, both MODIS and GFDS SGRs can reflect monthly and seasonal discharge dynamics reliably (Figure S1c and f).
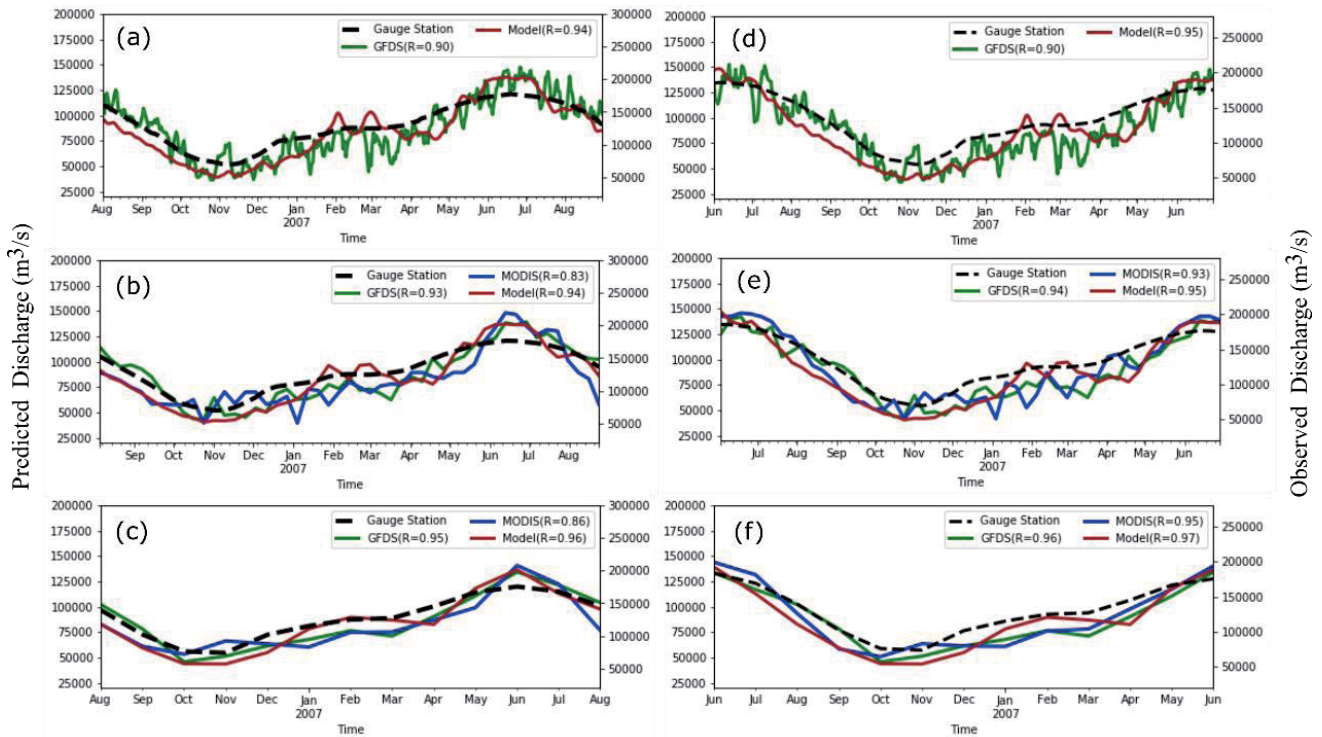
Figure S1 Comparisons between observations (right axis) from gauging stations (black dash) and river discharge estimates (left axis) derived using MODIS SGRs (blue line), GFDS SGRs (green line) and the W3 model (brown line) (top row: daily results; middle row: 8-day results; bottom row: monthly results; left column: gauge station G32 (3.06°S, 59.65°W); right column: gauge station G33 (1.92°S, 55.51°W).

I

Appendix 2: Supplementary Materials to Chapter 3

This appendix is the supplementary materials to Chapter 3, which was published in the journal Remote Sensing of Environment as:

Hou, J., Van Dijk, A.I.J.M. and Beck, H.E., 2020. Global satellite-based river gauging and the influence of river morphology on its application. Remote Sensing of Environment, 239, https://doi.org/10.1016/j.rse.2019.111629.

Supplementary Data and Method

The MSWEP v 1.1 (Beck et al. 2017) precipitation estimates, monthly precipitation and air temperature data from the WorldClim dataset (Hijmans et al. 2005), and other meteorological data from the WFDEI v1 dataset (Weedon et al. 2014) were input as global gridded climate time series in the W3 model. Global land surface types (Bicheron et al. 2008), vegetation (Simard et al. 2011), soil (Shangguan et al. 2014), and aquifers (Beck et al. 2015; Gleeson et al. 2014) datasets were used to parameterize surface, vegetation, soil and groundwater. The Penman-Monteith model was used to simulate the surface energy and water balance. A flow direction based on HydroSheds and HYDRO 1k was used as grid-based rive routing. The estimates of evaporation, total water storage, streamflow, soil moisture, and deep drainage of the AWRA-L and its global implementation model, the W3 model, have been evaluated in several studies (e.g., Beck et al. 2016; Holgate et al. 2016; Tian et al. 2017).

Supplementary Table 1 The list of original sources of gauging data (listed in ascending order of number of stations; collated by co-author Hylke Beck)

National and international sources	The number of gauging data
The United States Geological Survey (USGS) National Water Information System (NWIS: https://waterdata.usgs.gov/nwis) and GAGES-II database (Falcone (2011))	9180
The Global Runoff Data Centre (GRDC: http://grdc.bafg.de; Lehner (2012))	4628
The HidroWeb portal of the Brazilian Agência Nacional de Águas (http://www.snirh.gov.br/hidroweb)	3029
The European Water Archive (EWA) of EURO-FRIEND-Water (http://ne-friend.bafg.de)	2260
Water Survey of Canada (WSC) National Water Data Archive (HYDAT; https://www.canada.ca/en/environment-climate-change)	1479
The National Center for Atmospheric Research (Dai 2016)	925
The Australian Bureau of Meteorology (BoM: http://www.bom.gov.au/waterdata; Zhang et al. (2013))	776
The Chilean Center for Climate and Resilience Research (CR2: http://www.cr2.cl/recursos-y-publicaciones/bases-de-datos/datos-de-caudales)	531

References

Beck, H.E., de Roo, A., & van Dijk, A.I.J.M. (2015). Global Maps of Streamflow Characteristics Based on Observations from Several Thousand Catchments. *Journal of Hydrometeorology, 16*, 1478-1501

Beck, H.E., van Dijk, A.I.J.M., De Roo, A., Miralles, D.G., McVicar, T.R., Schellekens, J., & Bruijnzeel, L.A. (2016). Global-scale regionalization of hydrologic model parameters. *Water Resources Research, 52*, 3599-3622

Beck, H.E., van Dijk, A.I.J.M., Levizzani, V., Schellekens, J., Miralles, D.G., Martens, B., & de Roo, A. (2017). MSWEP: 3-hourly 0.25 global gridded precipitation (1979-2015) by merging gauge, satellite, and reanalysis data. *Hydrology and Earth System Sciences, 21*, 589

Bicheron, P., Defourny, P., Brockmann, C., Schouten, L., Vancutsem, C., Huc, M., Bontemps, S., Leroy, M., Achard, F., & Herold, M. (2008). Globcover: products description and validation report. In. ME, Medias France

Dai, A. (2016). *Historical and future changes in streamflow and continental runoff: a review. In: Tang Q, Oki T (eds), Chapter 2 of Terrestrial water cycle and climate change: natural and human-induced impacts*. American Geophysical Union

Falcone, J.A. (2011). GAGES-II: Geospatial attributes of gages for evaluating streamflow. In: US Geological Survey

Gleeson, T., Moosdorf, N., Hartmann, J., & Van Beek, L.P.H. (2014). A glimpse beneath earth's surface: GLobal HYdrogeology MaPS (GLHYMPS) of permeability and porosity. *Geophysical Research Letters, 41*, 3891-3898

Hijmans, R.J., Cameron, S.E., Parra, J.L., Jones, P.G., & Jarvis, A. (2005). Very high resolution interpolated climate surfaces for global land areas. *International journal of climatology, 25*, 1965-1978

Holgate, C., De Jeu, R., van Dijk, A.I.J.M., Liu, Y., Renzullo, L.J., Dharssi, I., Parinussa, R.M., Van Der Schalie, R., Gevaert, A., Walker, J., McJannet, D., Cleverly, J., Haverd, V., Trudinger, C.M., & Briggs, P.R. (2016). Comparison of remotely sensed and modelled soil moisture data sets across Australia. *Remote Sensing of Environment, 186*, 479-500

Lehner, B. (2012). *Derivation of watershed boundaries for GRDC gauging stations based on the HydroSHEDS drainage network. Report 41 in the GRDC Report Series.* *https://www.bafg.de/GRDC/EN/02_srvcs/24_rprtsrs/report_41.pdf?__blob=publicationFile*.

Shangguan, W., Dai, Y., Duan, Q., Liu, B., & Yuan, H. (2014). A global soil data set for earth system modeling. *Journal of Advances in Modeling Earth Systems, 6*, 249-263

Simard, M., Pinto, N., Fisher, J.B., & Baccini, A. (2011). Mapping forest canopy height globally with spaceborne lidar. *Journal of Geophysical Research: Biogeosciences, 116*

Tian, S., Tregoning, P., Renzullo, L.J., van Dijk, A.I.J.M., Walker, J.P., Pauwels, V.R.N., & Allgeyer, S. (2017). Improved water balance component estimates through joint assimilation of GRACE water storage and SMOS soil moisture retrievals. *Water Resources Research, 53*, 1820-1840

Weedon, G.P., Balsamo, G., Bellouin, N., Gomes, S., Best, M.J., & Viterbo, P. (2014). The WFDEI meteorological forcing data set: WATCH Forcing Data methodology applied to ERA-Interim reanalysis data. *Water Resources Research, 50*, 7505-7514

Zhang, Y., Viney, N., Frost, A., Oke, A., Brooks, M., Chen, Y., & Campbell, N. (2013). Collation of Australian modeller's streamflow dataset for 780 unregulated Australian catchments. *Water for a Healthy Country National Research Flagship. https://publications.csiro.au/rpr/download?pid=csiro:EP113194&dsid=DS4*

Appendix 3: Supplementary Materials to Chapter 5

This appendix is the supplementary materials to Chapter 5, which is under review as follows:

Hou, J., Van Dijk, A.I.J.M., Beck, H.E., Renzullo, L.J., and Wada, Y., 2020. Changes in precipitation a greater threat to global water reservoir security than increased water use, under review.

Materials and Methods

1. Data

Surface water extent

The Landsat-derived Global Surface Water Dataset (GSWD) [25] provides statistics on the extent and change of surface water at the global scale over the past three decades at a spatial resolution of 30 m. Clouds, cloud shadows and terrain shadows cause errors or missing data for individual months, but Zhao and Gao [26] developed an automated method to reduce these issues and enhance the accuracy of reservoir surface water extent estimates. They applied this method to produce a monthly time series of surface water extent dataset for 6,817 reservoirs worldwide, based on mapping of the location and high-water mark as contained in the Global Reservoir and Dam database (GRanD) [24]. The resulting data are available from 1984 to 2015 and were used in this study.

Surface water height

The US Department of Agriculture's Foreign Agricultural Service (USDA-FAS) provides near-real-time surface water height anomaly estimates every ten days for around 280 lakes and reservoirs worldwide. The water surface height product (G-REALM) was produced by a semi-automated process using data from a series of altimetry missions including Topex/Poseidon (1992-2002), Jason-1 (2002-2008), Jason-2 (2008-2016) and Jason-3 (2016-present). The root-mean-square error is expected better than 10 cm for the largest water bodies (e.g., Lake Victoria; 67,166 km^2) and better than 20 cm for smaller ones (e.g., Lake Chad; 18,751 km^2). The G-REALM is currently only available for lakes and reservoirs with an extent greater than 100 km^2.

Auxiliary Data

Daily and monthly *in situ* river discharge observations were collated as part of previous research [27] from different national and international sources including the (i) United States Geological Survey (USGS) National Water Information System (NWIS: https://waterdata.usgs.gov/nwis) and GAGES-II database [28]); (ii) Global Runoff Data Centre (GRDC: http://grdc.bafg.de) [29]; (iii) HidroWeb portal of the Brazilian Agência Nacional de Águas (http://www.snirh.gov.br/hidroweb); (iv) European Water Archive (EWA) of EURO-FRIEND-Water (http://ne-friend.bafg.de); (v) Water Survey of Canada (WSC) National Water Data Archive (HYDAT; https://www.canada.ca/en/environment-climate-change); (vi) Australian Bureau of Meteorology (BoM: http://www.bom.gov.au/waterdata) [30]; (vii) Chilean Centre for Climate and Resilience Research (CR2: http://www.cr2.cl/recursos-y-publicaciones/bases-de-datos/datos-de-caudales); and (viii) National Center for Atmospheric Research [31]. In total, we archived 22,710 river gauging records.

Global monthly surface runoff estimates for 1984–2014 were derived from the eartH2Observe water resources reanalysis version 2 [32], calculated as the mean of an ensemble of eight state-of-the-art global models, including HTESSEL, SURFEX-TRIP, ORCHIDEE,

WaterGAP3, JULES, W3RA, and LISFLOOD. Precipitation data derived from a combination of station, satellite, and reanalysis data (MSWEP v1.1) [33] were used here. The representative maximum storage capacity reported in the GRanD database [24] was used as a reference value to calculate absolute storage changes. The HydroBASINS [34] dataset was used to define basin boundaries.

2. Global reservoir storage estimation

In total, 132 large reservoirs (Group A; Fig. S1) had records of both surface water extent and height for the overlapping period 1993–2015. We estimated the height and area at capacity as the maximum observed surface water height and extent, respectively, and estimated reservoir storage volume storage (V_o in GL or 10^6 m^3) as:

$$V_o = V_c - (h_{max} - h_o)(A_{max} + A_o)/2 \qquad (1)$$

where A_o (km^2) is the satellite-observed water extent, A_{max} the maximum value of A_o, h_o (m) observed water height, h_{max} the maximum value of h_o, and V_c (GL) the storage volume at capacity. For those reservoirs with a meaningful relationship between A_o and V_o for this overlapping period (i.e., Pearson's $R \geq 0.4$, $N=78$), V_0 was estimated going back to 1984 using a linear regression equation based on A_0.

For 6,611 reservoirs with water extent observations only (Group B; Fig. S1), we used the HydroLAKES method [35] to estimate storage. The empirical equations [35] used (Table S1) were applied to observed A and the average slope [35] within a 100 m buffer around the reservoir (S_{100} in degrees).

A bias-corrected average water depth (D^* in m) was calculated by solving D for the maximum estimated depth (D_{max} in m) and extent A_{max} at storage capacity (V_c):

$$D^* = \frac{D}{D_{max}} \times \frac{V_c}{A_{max}} \qquad (2)$$

Storage volume for 1984–2015 was subsequently estimated as:

$$V_o = D^* A_o \qquad (3)$$

Evaluation

Time series of *in situ* reservoir storage volume measurements are publicly available for a subset of reservoirs. They can be used to evaluate the uncertainty in the satellite-based storage estimates. Furthermore, data records for some storages can be found in the published literature, derived from grey literature or proprietary data sources. Given the emphasis in trend analysis was on relative changes between the pre- and post-2000 periods, the evaluation below focuses on Pearson's correlation (R) values as a measure of correspondence. Monthly storage data with at least 20-year time series of 67 reservoirs via the US Army Corps of Engineers (http://www.nwd-mr.usace.army.mil/rcc/projdata/projdata.html) and Australian Bureau of Meteorology (http://www.bom.gov.au/waterdata/) were collected. The R between published and estimated volumes in 67% of reservoirs was above 0.9, and 90% above 0.7. Some validation examples,

including robust, typical, and poor agreement are shown in Fig. S1. Annual average water levels for Lake Aswan, the largest reservoir in the world, were published as a graph [36]; a comparison shows good agreement between the altimetry-derived and in situ measurements with R=0.97 (Fig. S2). Assuming the estimation method for Group A is more accurate than for Group B, the latter can be evaluated against the former. The results show that 25 of the total 39 overlapping estimated reservoirs show robust agreement ($R \geq 0.9$) between the two methods. Some validation examples representing good, typical, and poor agreement are shown in Fig. S3.

3. Trend analysis and attribution

We were able to estimate monthly storage dynamics for 6,743 out of the 6,862 reservoirs reported in the GRanD database [24], accounting for 89.3% of the total 6,197 km^3 reported cumulative capacity (Fig. S1). There were only 132 reservoirs for which both extent and height observations were available (Group A), but this relatively small number already accounted for almost half of global combined capacity (Fig. S1). To analyze long-term changes in reservoir storage between 1984–2015, we removed all reservoirs that were destroyed, modified, planned, replaced, removed, subsumed or constructed after 1984 or for which more than five years of water extent observations needed to be interpolated because of lacking data [26]. This left 4,589 of the initial 6,743 reservoirs available for analysis, *i.e.*, 68% of reservoirs, together accounting for 45.9% of combined global capacity (Fig. S4).

We calculated linear trends in annual reservoir storage, observed streamflow, modelled streamflow, and precipitation for each basin (HydroBASINS Level 3). Trend significance was tested using the Mann-Kendall trend test (p<0.05). The linear trends in modelled streamflow were validated by observed data. We also analysed the correlations between precipitation/streamflow and storage in terms of both time series and linear trend. Net evaporation was calculated for each reservoir as follows:

$$E_n = A(E_0 - P) \qquad (4)$$

where E_n (mm) is cumulative monthly net evaporation loss (or gain, if negative), A is reservoir surface area (km^2) from Zhao and Gao [26], E_0 (mm) open water evaporation (Priestley-Taylor potential evaporation from the W3 model [37], and P precipitation (mm) from MSWEP v1.1 [33]. The reservoir net evaporations sum up in each basin and the ratio of the respective trends in net evaporation and storage were calculated to determine whether the former could explain the later. Trends in storage and observed streamflow for individual reservoir and river were also analysed, which can provide additional information on clusters of trends in detail. But, different from analysis at basin scale above, we do not relate the trend of each reservoir to a corresponding river gauge, because there is limited gauging data upstream.

Changes in annual mean storage, resilience, and vulnerability between 1984–1999 and 2000–2015 were analyzed at the scale of river basins. The reliability, resilience and vulnerability (RRV) criteria can be used to evaluate the performance of a water supply reservoir system [38, 39].

The calculation requires that an unsatisfactory state can be defined in which the reservoir cannot meet all water demands, leading to a failure event. *Reliability* indicates the probability that the system is in a satisfactory state:

$$Reliability = 1 - \frac{\sum_{j=1}^{M} d(j)}{T} \qquad (5)$$

where $d(j)$ is the time length of the jth failure event, T is the total time length, and M is the number of failure events. Unfortunately, a single threshold for failure events is not readily determined: firstly, because we did not have access to water demand and release data for each reservoir, and, secondly, because reservoirs are typically operated in response to more than a single threshold. Instead, we assumed that the reliability of each reservoir is designed to be 90%, leaving it in an unsatisfactory state for the remaining 10% of the time. This assumption made it possible to calculate resilience and vulnerability for each reservoir for the assumed 90% threshold. *Resilience* is a measure of how fast a system can return to a satisfactory state after entering a failure state:

$$Resilience = \{\frac{1}{M}\sum_{j=1}^{M} d(j)\}11^{-1} \qquad (6)$$

Vulnerability describes the likely damage of failure events:

$$Vulnerability = \frac{1}{M}\sum_{j=1}^{M} v(j) \qquad (7)$$

where $v(j)$ is the deficit volume of the jth failure events. We analyzed changes in resilience and vulnerability from the pre-2000 to the post-2000 period. An example is shown for the Toledo Bend Reservoir (Texas, USA) (Fig. S5 and Table S2). Four failure events occurred during 1984–2000 and three during 2000–2015. Before 2000, it took an average of three months to recover from failure with an average deficit volume of 357 GL. In contrast, after 2000, it took an average of 10.5 months with a larger average deficit volume of 498 GL (Fig. S2). It follows that resilience was reduced after 2000 (0.12 vs. 0.33) and vulnerability increased (498 vs. 357 GL) when compared to the years before 2000 (Table S2).

The change of resilience (ΔRes) between 1984–2015 is calculated as:

$$\Delta Res = Res_2 - Res_1 \qquad (8)$$

where Res_1 and Res_2 are the reservoir resilience values calculated for 1984–1999 and 2000–2015, respectively. The change in vulnerability (ΔVul) was expressed relative to the maximum deficit volume V_f observed as follows:

$$\Delta Vul = \frac{Vul_2 - Vul_1}{V_f} \times 100\% \qquad (9)$$

where Vul_1 and Vul_2 are the reservoir vulnerability values for the periods 1984–1999 and 2000–2015, respectively.

The analysis above based on storage, rather than water extent, although the uncertainties in surface water extent observations are likely to be less than those in storage estimates derived from altimetry data or geo-statistical equations. However, storage volume plays a more essential role

in this study, based on which we were able to not only discuss correlations between precipitation/streamflow/resilience/vulnerability and storage but also analyse how much of the change in storage caused by inflow and net evaporation (in volume), and then infer the role of reservoir management.

References:

24.   B. Lehner *et al.*, High-resolution mapping of the world's reservoirs and dams for sustainable river-flow management. *Frontiers in Ecology and the Environment* **9**, 494-502 (2011).

25.   J.-F. Pekel, A. Cottam, N. Gorelick, A. S. Belward, High-resolution mapping of global surface water and its long-term changes. *Nature* 540, 418-422 (2016).

26.   G. Zhao, H. Gao, Automatic correction of contaminated images for assessment of reservoir surface area dynamics. *Geophysical Research Letters* 45, 6092-6099 (2018).

27.   H. E. Beck et al., Bias correction of global high-resolution precipitation climatologies using streamflow observations from 9372 catchments. *Journal of Climate* 33, 1299-1315 (2020).

28.   J. A. Falcone, "GAGES-II: Geospatial attributes of gages for evaluating streamflow.," (US Geological Survey, 2011).

29.   B. Lehner, Derivation of watershed boundaries for GRDC gauging stations based on the HydroSHEDS drainage network. Report 41 in the GRDC Report Series. https://www.bafg.de/GRDC/EN/02_srvcs/24_rprtsrs/report_41.pdf?__blob=publication File. (2012).

30.   Y. Zhang et al., Collation of Australian modeller's streamflow dataset for 780 unregulated Australian catchments. Water for a Healthy Country National Research Flagship. https://publications.csiro.au/rpr/download?pid=csiro:EP113194&dsid=DS4, (2013).

31.   A. Dai, Historical and future changes in streamflow and continental runoff: a review. In: Tang Q, Oki T (eds), Chapter 2 of Terrestrial water cycle and climate change: natural and human-induced impacts. Geophysical Monograph (American Geophysical Union, 2016), pp. 17-37.

32.   J. Schellekens et al., A global water resources ensemble of hydrological models: The eartH2Observe Tier-1 dataset. *Earth System Science Data* 9, 389-413 (2017).

33.   H. E. Beck et al., MSWEP: 3-hourly 0.25 global gridded precipitation (1979-2015) by merging gauge, satellite, and reanalysis data. *Hydrology and Earth System Sciences* 21, 589 (2017).

34.   B. Lehner, G. Grill, Global river hydrography and network routing: baseline data and new approaches to study the world's large river systems. *Hydrological Processes* 27, 2171-2186 (2013).

35. M. L. Messager, B. Lehner, G. Grill, I. Nedeva, O. Schmitt, Estimating the volume and age of water stored in global lakes using a geo-statistical approach. *Nature Communications* 7, 13603 (2016).

36. E. A. El Gammal, S. M. Salem, A. E. A. El Gammal, Change detection studies on the world's biggest artificial lake (Lake Nasser, Egypt). *The Egyptian Journal of Remote Sensing and Space Science* 13, 89-99 (2010).

37. A. I. J. M. Van Dijk et al., Global 5 km resolution estimates of secondary evaporation including irrigation through satellite data assimilation. *Hydrology and Earth System Sciences* 22, 4959-4980 (2018).

38. T. R. Kjeldsen, D. Rosbjerg, Choice of reliability, resilience and vulnerability estimators for risk assessments of water resources systems. *Hydrological Sciences Journal* 49, (2004).

39. T. Hashimoto, J. R. Stedinger, D. P. Loucks, Reliability, resiliency, and vulnerability criteria for water resource system performance evaluation. *Water Resources Research* 18, 14-20 (1982).
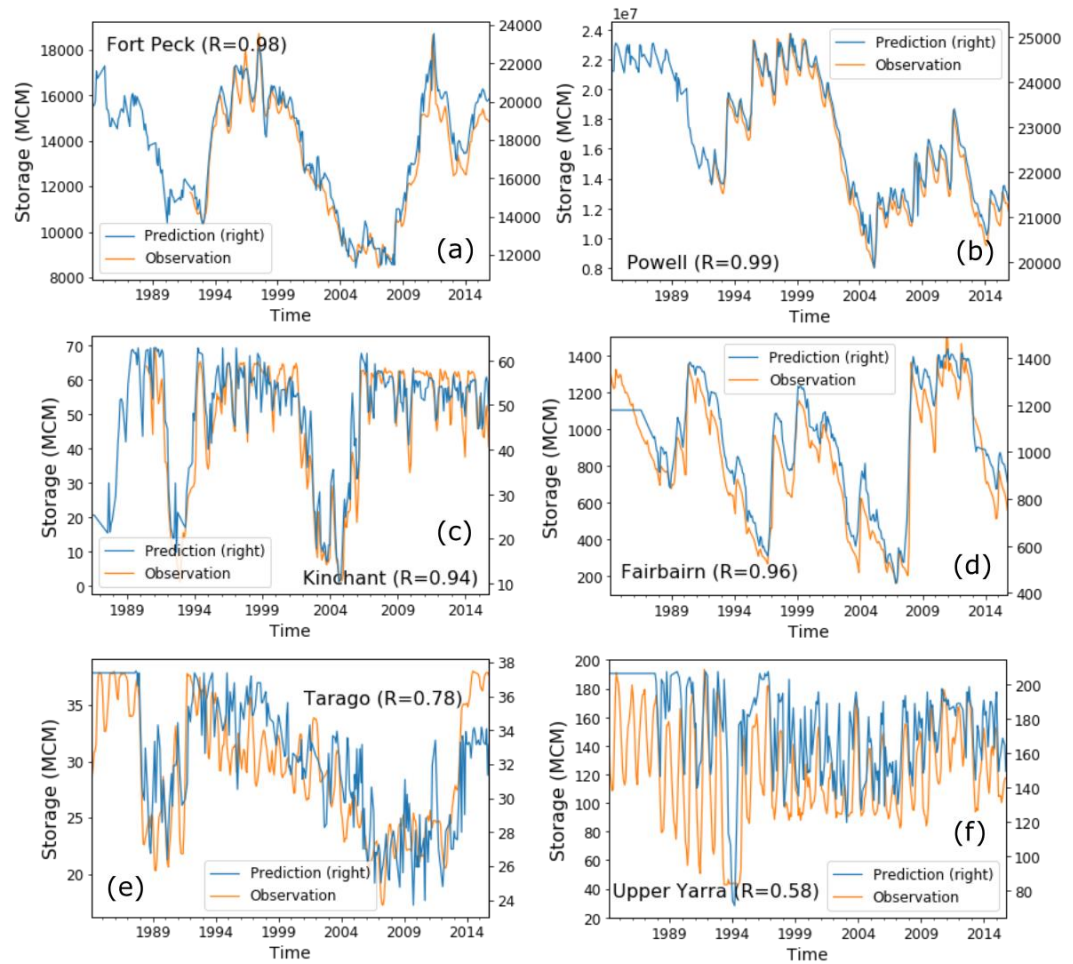
Fig. S1. Validation of reservoir storage reconstruction against in situ data, showing (a, b) robust, (c, d) typical and (e, f) poor results.
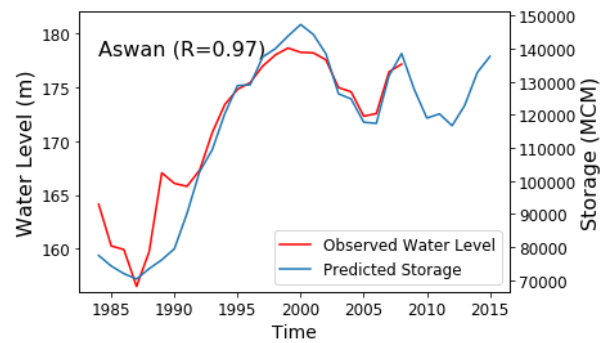
Fig. S2. Validation of reservoir storage reconstruction for Lake Aswan.
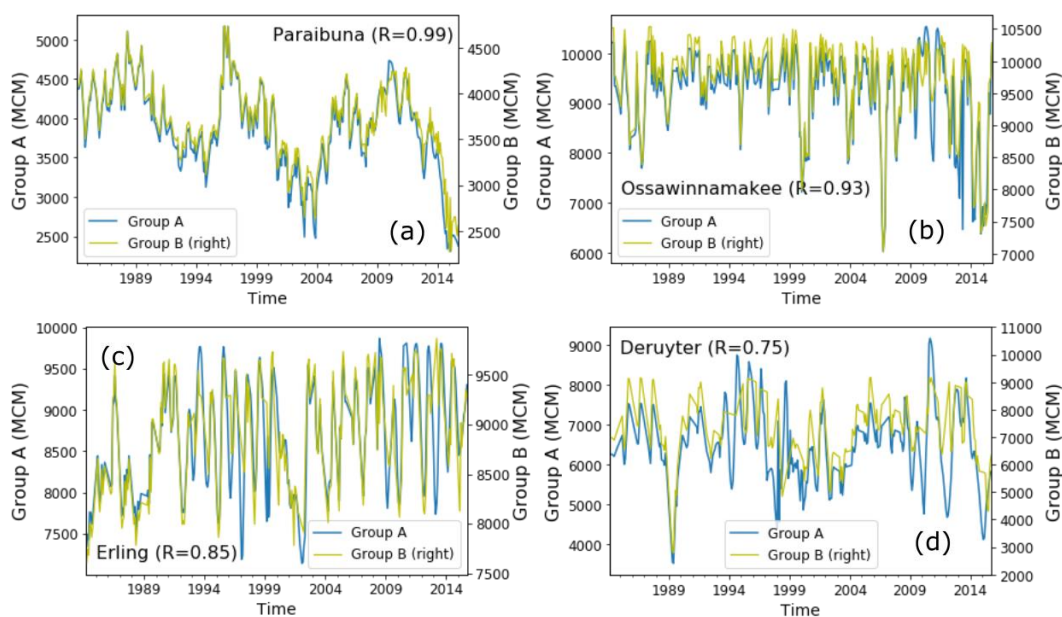
Fig. S3. Validation of reservoir storage reconstruction for Group B against results obtained using the method used for Group A, showing (a) robust, (b and c) typical and (d) poor agreement.
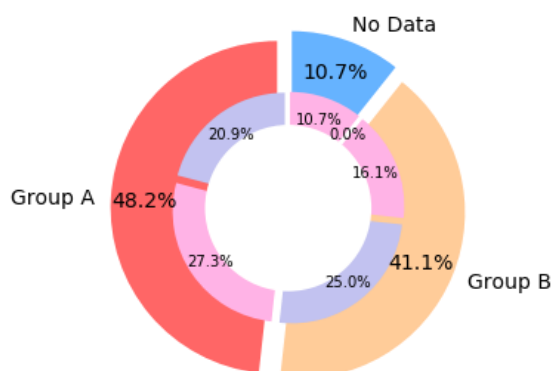
Fig. S4. The total storage capacity in Group A (red) and B (brown) and left unaccounted (blue) and the combined capacity of reservoirs for which the data were suitable (teal) or unsuitable (pink) for long-term analysis.
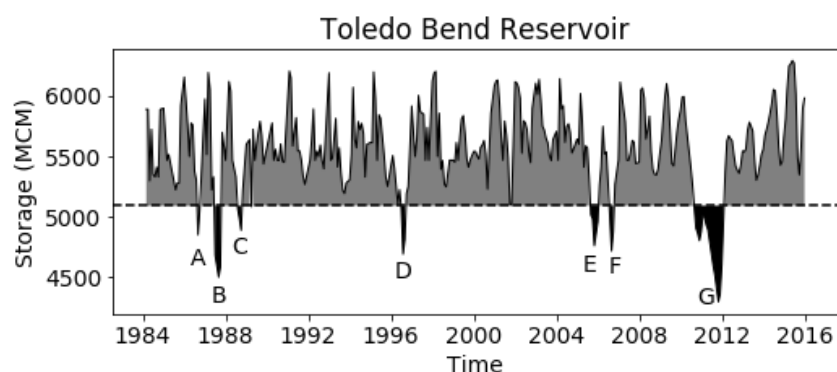
Fig. S5. Example storage time series showing the definition of resilience and vulnerability (black shade: unsatisfactory state; grey shade: satisfactory state, black line: temporal storages; dash line: 10% threshold; letters: failure events).
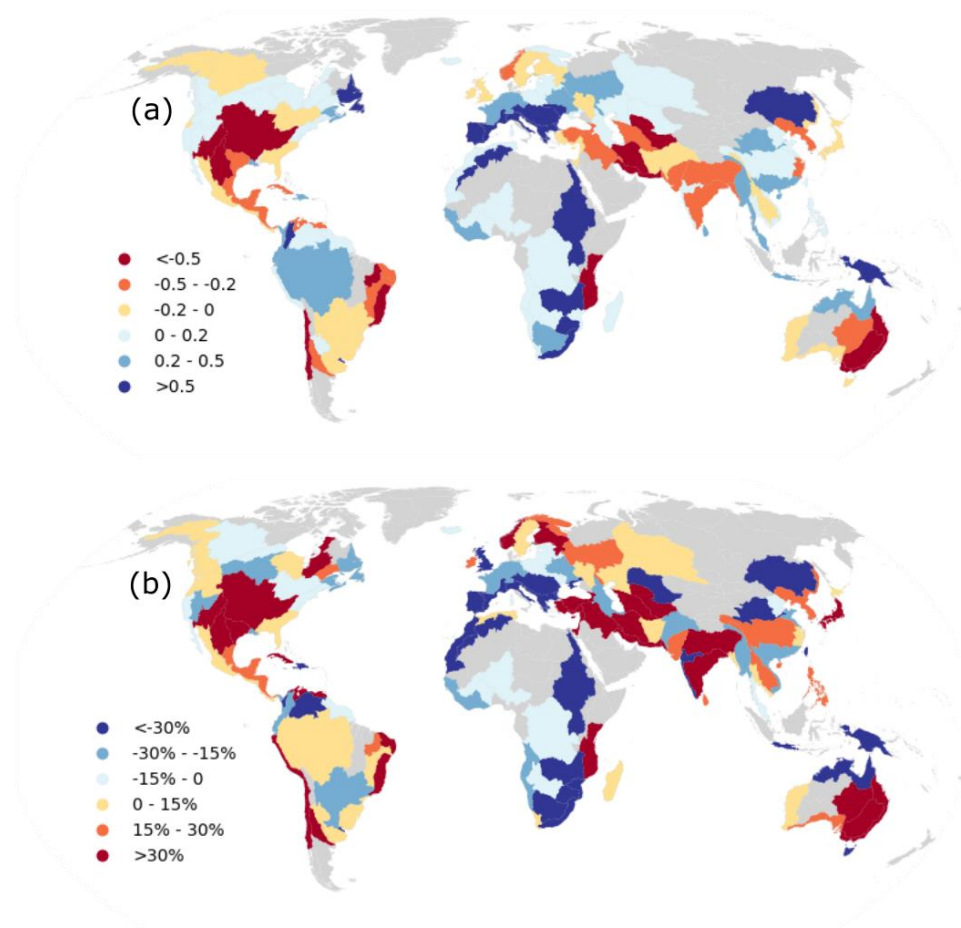
Fig. S6. The change of resilience (a), and vulnerability (b) between pre-2000 and post-2000 (grey shade: no reservoir data).
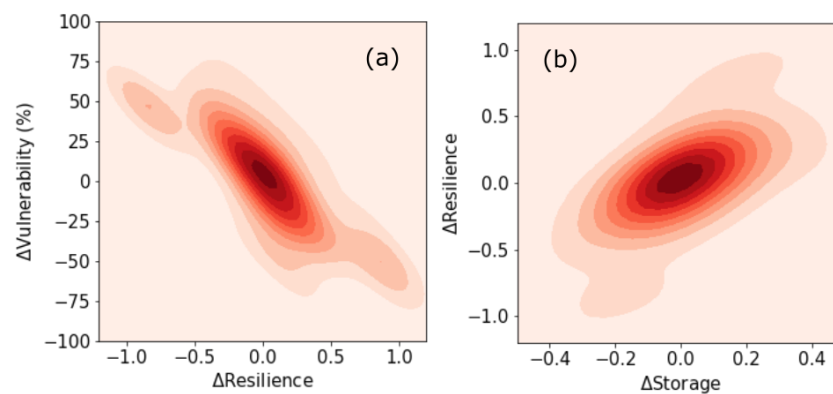
Fig. S7. The relationship between changes from the pre-2000 to the post-2000 period in (a) vulnerability (*ΔVulnerability*) and resilience (*ΔResilience*) and (b) mean storage (*ΔStorage*) and resilience (*ΔResilience*).
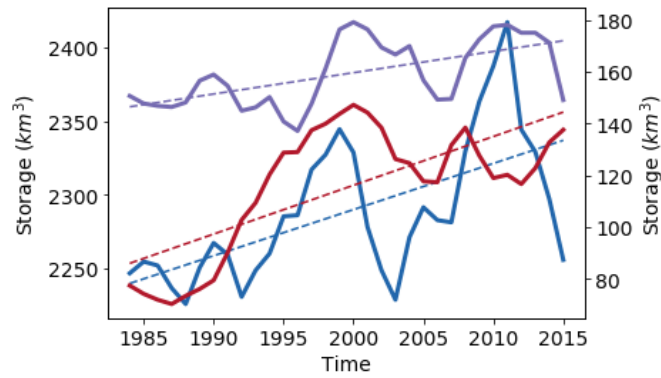
Fig. S8. Annual time series (dash line: significant trends) in combined global reservoir storage (blue line; unit corresponds to left axis), and in storage for Lake Kariba (purple line; unit corresponds to right axis), and Lake Aswan (red line; unit corresponds to right axis).
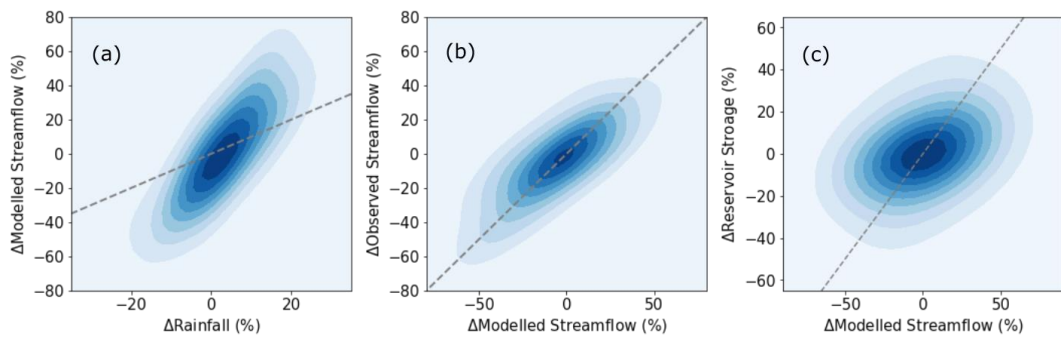
Fig. S9. The relationship (dash grey line: 1: 1 line) between linear change from 1984-2015 in (a) annual precipitation (*ΔRainfall*) and modelled streamflow (*ΔModelled Streamflow*), (b) observed streamflow (*ΔObserved Streamflow*) and modelled streamflow (*ΔModelled Streamflow*) and (c) reservoir storage (*ΔReservoir Storage*) and modelled streamflow (*ΔModelled Streamflow*) corresponding to Figure 2.
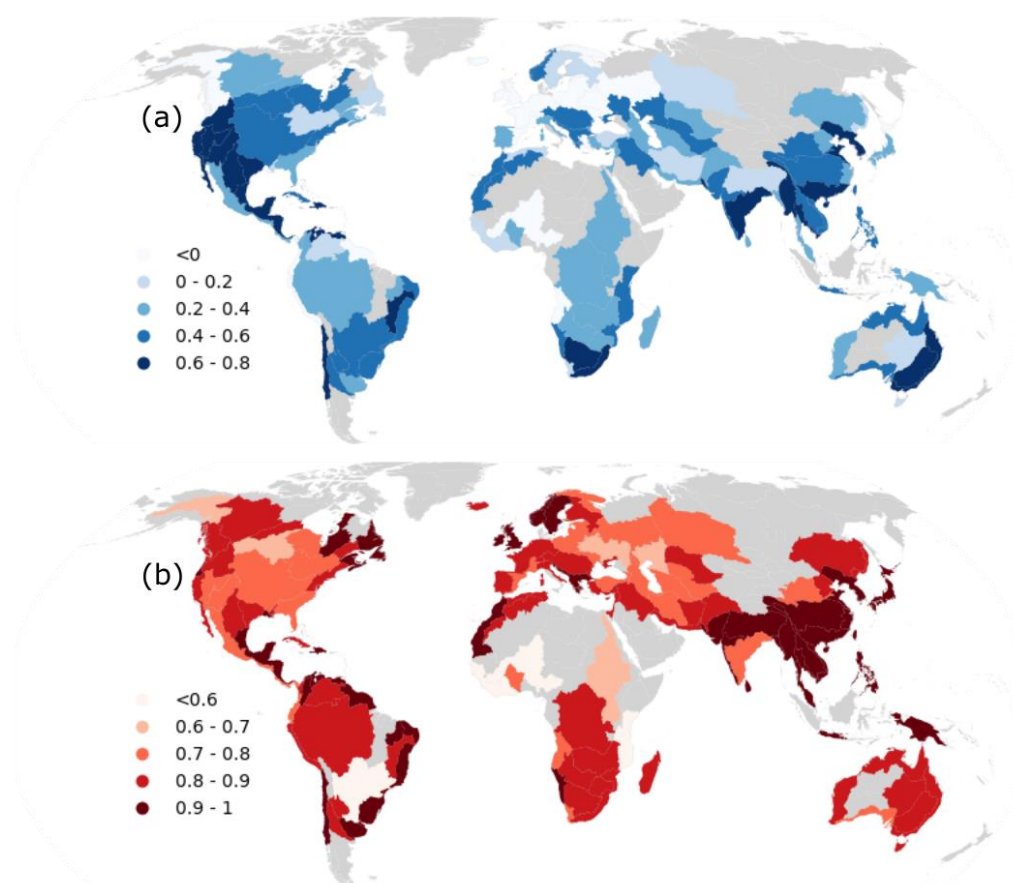
Fig. S10. The correlations of annual storage change and reservoir inflow (as approximated by basin modelled streamflow) (a), and reservoir inflow and precipitation (b) in each basin.
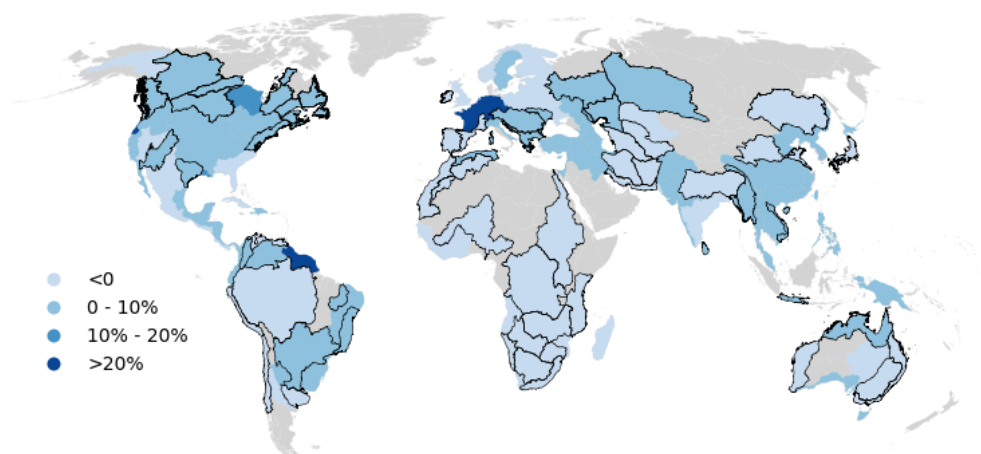
Fig. S11. The ratio of the linear trends in net evaporation and in storage in each basin, showing that net evaporation rarely explains more than a few per cent in observed storage changes.
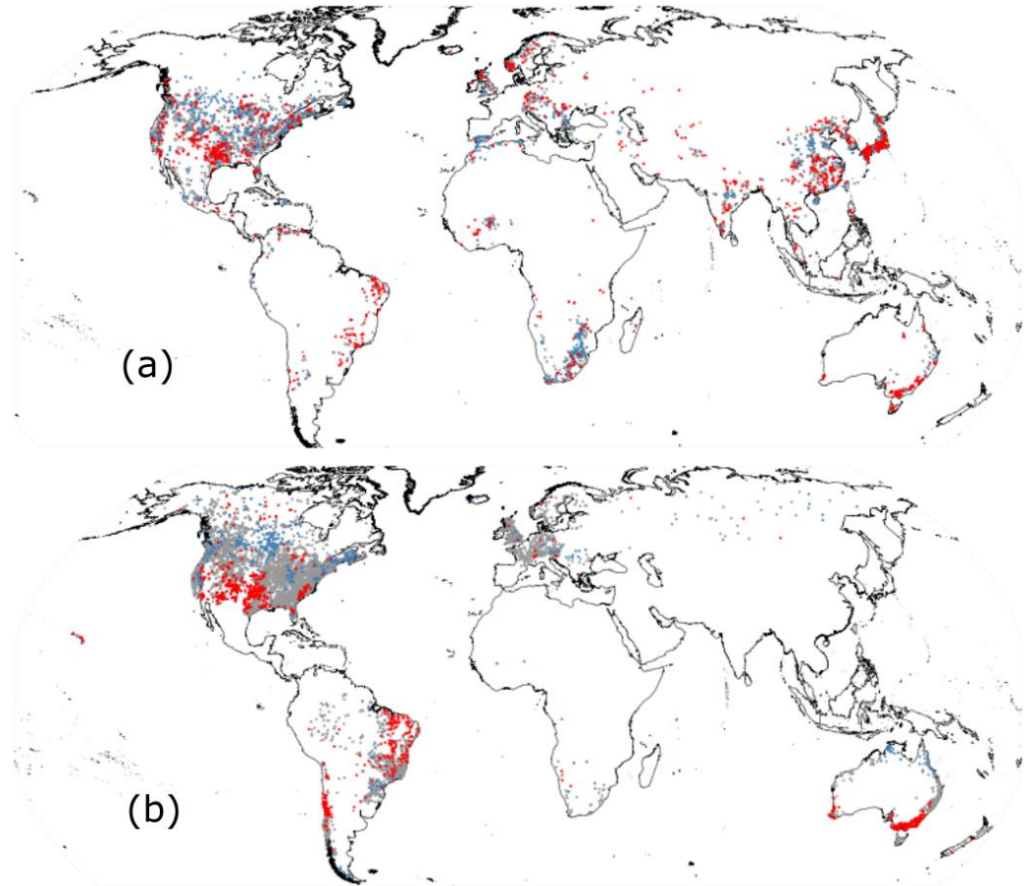
Fig. S12. The trends of storage (a) and observed streamflow (b) for individual reservoir and river globally (p<0.05; increasing: blue; no change: grey; decreasing: red).
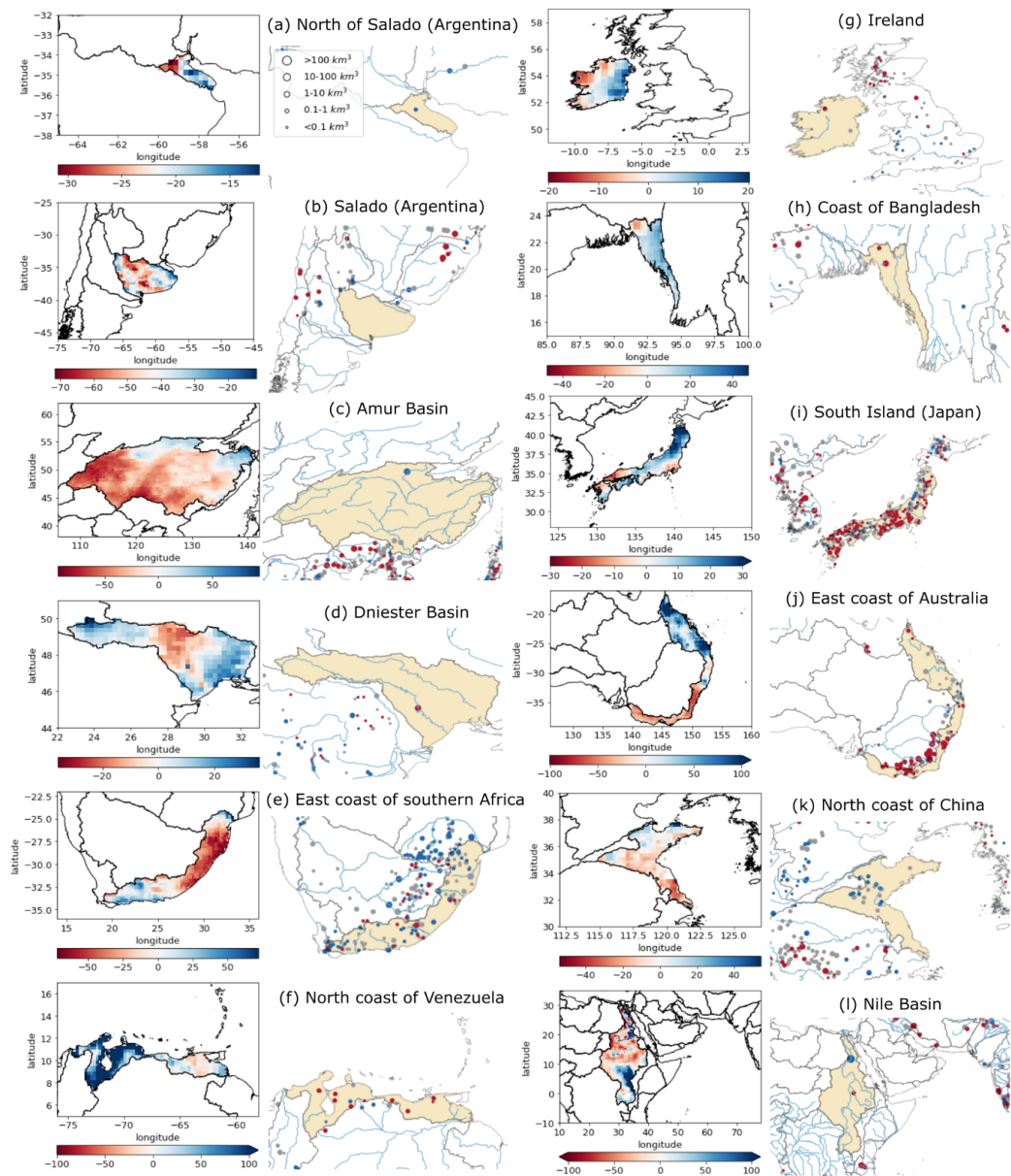
Fig. S13. Trends in reservoir storage (second and fourth column; p<0.05; increasing: blue; no change: grey; decreasing: red; dot sizes correspond to storage capacity; light blue line: main river network; faded yellow shade: selected basins) and grid-based modelled streamflow (first and third column; colour correspond to per cent of linear change overall period) during 1984–2015.
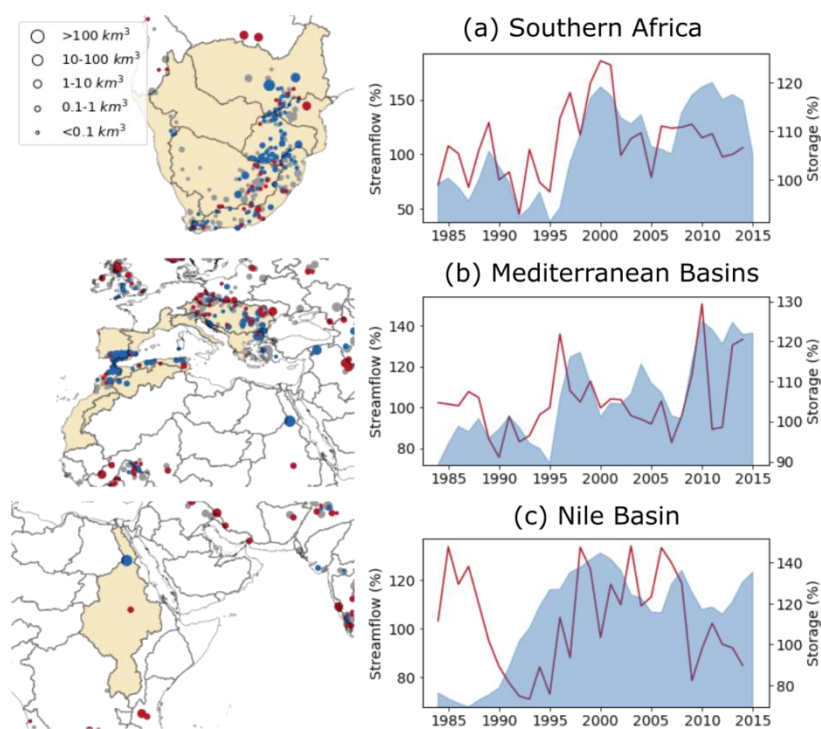
Fig. S14. Trends in reservoir storage (first column; p<0.05; increasing: blue; no change: grey; decreasing: red; dot sizes correspond to storage capacity; faded yellow shade: selected regions) and time series of annual average relative total storage volume (light blue shaded), and modelled streamflow (solid red line) indicated with a base period of 1984–1999 (second column).

Table S1. Statistical models to estimate reservoir depth (D: average depth; A: observed extent; S_{100}: average slope around the reservoir (HydroLAKES)).

Reservoir size class by maximum extent (km^2)	Statistical models
0.1-1	$\log_{10}(D) = 0.3826 + 0.1512 \times \log_{10}(A) + 0.4820 \times \log_{10}(S_{100})$
1-10	$\log_{10}(D) = 0.1801 + 0.2985 \times \log_{10}(A) + 0.8473 \times \log_{10}(S_{100})$
10-100	$\log_{10}(D) = 0.0379 + 0.2445 \times \log_{10}(A) + 1.1517 \times \log_{10}(S_{100})$
100-500	$\log_{10}(D) = 0.0123 + 0.2664 \times \log_{10}(A) + 1.1474 \times \log_{10}(S_{100})$

Table S2. The statistics of resilience and vulnerability for the reservoir in Fig. S2.

Period	1984-2000				2000-2015		
Failure Event	A	B	C	D	E	F	G
Duration Time (month)	2	4	3	3	5	3	18
Resilience (1/average duration)		0.33				0.12	
Deficit Volume (GL)	239	589	202	399	329	373	792
Vulnerability (average deficit volume)		357				498	

Appendix 4: A global, near real-time system measuring river, lake, and reservoir dynamics

This appendix introduced a global near real-time river, lake and reservoir monitoring system, which is published as a conference paper in the 23rd International Congress on Modelling and Simulation (MODSIM2019) as follows:

Hou, J., Van Dijk, A.I.J.M., Beck, H.E., 2019. A global, near real-time system measuring river, lake, and reservoir dynamics. In Elsawah, S. (ed.) MODSIM2019, 23rd International Congress on Modelling and Simulation. Modelling and Simulation Society of Australia and New Zealand.

A global, near real-time system measuring river, lake, and reservoir dynamics

J. Hou[a], A. I. J. M. van Dijk[a] and H. E. Beck[b]

[a] Fenner School of Environment and Society, The Australian National University, Australian Capital Territory, [b] Department of Civil and Environmental Engineering, Princeton University, Princeton, New Jersey, USA
Email: jiawei.hou@anu.edu.au

Abstract: Measuring and predicting the dynamics of discharge in rivers and water storage in lakes and reservoirs can inform water management and policy decisions, flood management and response, and help understand the influence of climate change and anthropogenic activities on hydrological, biogeochemical, and ecological processes. However, water body dynamics are often poorly observed on the ground. Gauging networks are unevenly distributed and in decline globally, and much gauging data is not publicly accessible in near real-time, if at all. Remote sensing technologies provide a unique alternative to monitor changes in water extent, level and volume in space and time. Our aim was to develop a global monitoring system that provides near real-time river discharge and lake and reservoir storage information from satellite observations. To estimate river discharge, we derived global surface water extent fraction from the 8-day 0.05° resolution reflectance data from the Moderate Resolution Imaging Spectroradiometer (MODIS) and used recorded discharge at gauged sites and hydrological model estimates at ungauged sites to train MODIS-based satellite gauging reaches (SGRs) that can be used to estimate river discharge globally. In total, we were able to construct over 2,000 gauge-based and 11,000 model-based SGRs globally (Figure 1). To estimate volume changes in lakes and reservoirs, surface water extent dynamics for over 280 lakes and reservoirs (Figure 1) were derived from a daily 500-m resolution global surface water change dataset. Storage variations were calculated using surface water extent and height time series from the 10-day near real-time global lake and reservoir elevation dataset (G-REALM). As MODIS and G-REALM provide near real-time information, these data similarly allow estimation of river discharge and lake and reservoir storage in near real-time. It is hoped that the global monitoring system provides immediate and relevant information on rivers, lakes, and reservoirs, to inform government, the community and individuals on the current state of water resources in a historical context.
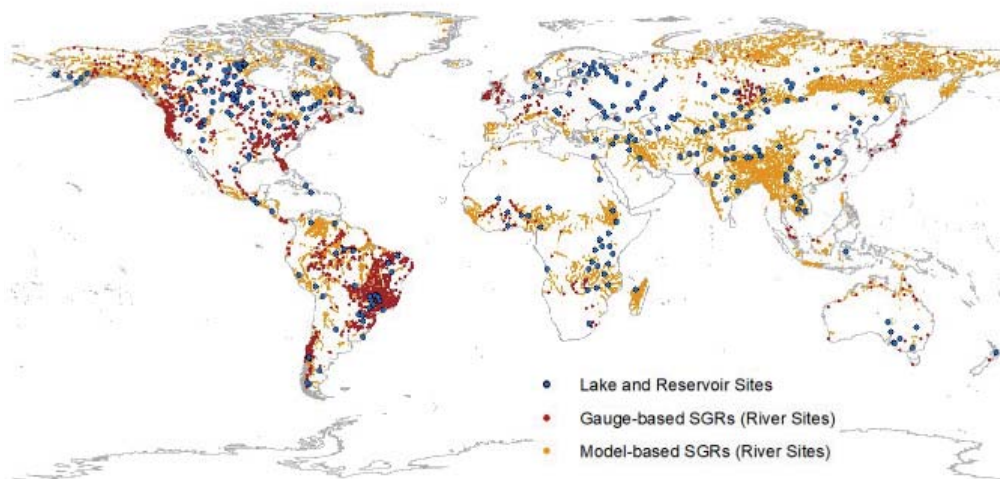
Figure 1. Global distribution of monitoring sites for rivers, lakes and reservoirs.

Keywords: *River discharge, lake and reservoir storage, global monitoring system*

1. INTRODUCTION

Globally, 87% of the earth's liquid surface freshwater is stored in reservoirs and lakes, and more than 50% of the potable water supply is extracted either from rivers directly or from reservoirs (Barnett et al. 2005; Gao 2015). According to the statistics on 1.43 million natural lakes and reservoirs with a surface water area greater than >0.10 km^2 from the HydroLAKES and the Global Reservoir and Dam database (GRanD), there are a total of 2.67×10^6 km^2 of natural lakes and 0.26×10^6 km^2 of human-made reservoirs, covering about 2% of the global land area. The total shoreline length of reservoirs and lakes is approximately four times the global ocean shoreline (Lehner et al. 2011; Messager et al. 2016). Based on the Global River Widths from Landsat (GRWL) database, the total surface area of rivers and streams at mean annual discharge is roughly 7.73×10^5 km^2, which is about 0.58% of Earth's non-glaciated land surface (Allen and Pavelsky 2018).

With ongoing human interventions and climate change, many rivers, lakes and reservoirs have experienced remarkable changes over the last few decades. Understanding the temporal and spatial dynamics of rivers, lakes and reservoirs at a global scale is essential for a sustainable future. However, variations in surface water dynamics are often poorly observed on the ground. Measurement precision, decline in the number of gauges, disparity in the number of gauges across monitoring networks, economic and technical challenges, limitations in terms of spatial coverage, flood monitoring difficulties, and data intermittency all pose challenges to the use of *in-situ* data for the analysis of river, lake and reservoir dynamics (Alsdorf et al. 2007; Gao 2015). For example, there are still technical and operational difficulties to produce bathymetric maps of rivers, lakes, or reservoirs, which currently require time- and cost-intensive survey methods (e.g. acoustic profiling). Remote sensing technology provides a unique alternative opportunity to observe changes in water extent, level and volume in space and time, as it is capable of detecting surface water in areas which are inaccessible, remote, or very large, and is unhindered by transboundary issues.

To estimate river discharge from space, the general approach has been to link remote sensing measurement to discharge observed *in-situ*. Several studies have revealed that river discharge can be estimated based on at-a-station hydraulic geometry (AHG) that relates remote sensing derived hydraulic variables to ground measurements of river discharge at a certain reach (e.g. Papa et al. 2010; Pavelsky 2014). In addition, Gleason and Smith (2014) presented a new method, at-many-stations hydraulic geometry, which can be used to estimate discharge solely from remote sensing derived river widths at multiple cross sections, as they found that the parameters of AHG are log-linearly related along a river. River discharge can be also estimated using open-channel hydraulic equations (e.g. the Manning equation) with remotely sensed data and ground measurements of river depth and roughness coefficient (e.g. LeFavour and Alsdorf 2005). Besides, The ratio of wet and dry pixel from Moderate Resolution Imaging Spectroradiometer (MODIS) near-infrared reflectance or the Advanced Microwave Scanning Radiometer (AMSR-E) passive microwave brightness temperature was demonstrated as a readily automated approach to estimate river discharge at large scale (Brakenridge et al. 2007; Hou et al. 2018; Van Dijk et al. 2016).

Lake and reservoir storage variations can be estimated based on the measurements of surface water level and inundation area, either or both of which can be derived from satellite observation. For example, rating curves relating storage, surface water elevation, and inundation area for Lake Izabal (Guatemala) were developed by combining *in-situ* lake elevation measurements and the ENVISAT Advanced Synthetic Aperture Radar (ASAR) derived inundated areas, and then used to extend volume estimates using the ENVISAT Radar Altimeter (RA-2) data (Medina et al. 2010). Zhang et al. (2014) estimated reservoir storage variations for 21 reservoirs in South Asia using MODIS-derived surface water areas and the ICESat/GLAS altimetry derived surface water elevation measurements. As there are currently several surface water extent and satellite altimetry databases globally, some studies estimated lake and reservoir storage variations derived directly from a combination of these databases (e.g. Busker et al. 2019). To tackle the absence of globally consistent data, Messager et al. (2016) established a geo-statistical model to estimate the volume for lakes with >0.10 km^2 surface area at global scale, based on their surrounding topography.

The aim of this study was to develop a global monitoring system that can provide near real-time river discharge (2000-current) and lake and reservoir storage variations (1992-current) by combining satellite radar altimetry and optical remote sensing. Here, we present the workflow of our global near real-time monitoring system. We discuss the benefits, limitations, and practical applications of the system.

2. WORKFLOW

2.1. Global river discharge prediction

Van Dijk et al. (2016) introduced a simple automated statistical method to construct satellite gauging reaches (SGRs) to use *in-situ* river discharge data to train MODIS optical remote sensing imagery. This is valuable to fill gaps in gauging discharge records and extend river discharge estimates, but the method is limited to gauged river reaches. Hou et al. (2018) expanded the method to both gauged and ungauged reaches using MODIS optical remote sensing and hydrological model simulations. We used the approach developed by Hou et al. (2018) to construct both gauge-based and model-based SGRs at global scale, which can be used to predict river discharge from satellite observation (Figure 2).

The remote sensing data used here to derive river discharge is Moderate Resolution Imaging Spectroradiometer (MODIS) product MCD43C4 version 6, which produces 8-day Nadir BRDF (Bidirectional Reflectance Distribution Function)-Adjusted Reflectance (NBAR) data derived from NASA's Terra and Aqua MODIS instruments. This product provides global 0.05°×0.05° resolution imagery from 2000 to present in near real-time. The MCD43C4's shortwave infrared (SWIR) band 7 (2105-2155 nm) was chosen due to the contrast between water and dry land in this wavelength. A surface water extent fraction (w) for each grid cell of each imagery was estimated as follows:

$$\text{w} = \frac{\rho_M - \rho_{dry}}{\rho_{water} - \rho_{dry}} \quad (1)$$

where ρ_M is the band 7 reflectance of target cell M, ρ_{dry} is the fifth percentile highest reflectance in a 7×7 cell window around M, and ρ_{water} is the reflectance of surface water (assumed equal to 0.008; refer to Van Dijk et al., 2016 for further details).

Daily and monthly *in-situ* river discharge observations were collated from different national and international sources (i.e., the United States Geological Survey, the Global Runoff Data Centre, the Brazilian Agência Nacional de Águas, the European Environment Agency, the Water Survey of Canada, the Australian Bureau of Meteorology, the Chilean Center for Climate and Resilience Research, and the National Center for Atmospheric Research). In total, this yielded 22,808 gauging records. For ungauged river reaches, daily river discharge for the period 2000-2014 was simulated by the World-Wide Water model (W3) version 2, which is a 0.05°×0.05° grid-based, one-dimensional water balance model that has a semi-distributed representation of the surface water, soil, groundwater stores and is coupled to a grid-based routing scheme (Van Dijk et al. 2018).

We constructed over 2,000 gauge-based and 11,000 model-based SGRs globally, which are able to predict river discharges with Pearson correlations above 0.6 against *in-situ* or modeling data. For each site, a search window of 0.55° × 0.55° centers on a gauging station (gauge-based SGRs) or W3 model grid cell with a river flowing through it (model-based SGRs). Observed or modelled discharge time series for the target reach are compared with each MODIS-derived surface water extent fraction time series within the search window. The MODIS pixel that has the strongest correlation with discharge data is selected as the best pixel to reflect river discharge variations. The relationship (Q-W) between discharge and water extent time series is established for the years 2000-2014 using cumulative

Figure 2. Workflow of river discharge prediction through satellite observation.

distribution function (CDF) matching; river discharge is then predicted based on the developed relationship (Q-W) using MODIS-derived surface water extent fraction time series for the years 2000-present for filling the gaps in gauging data and providing near real-time data (Figure 2).

2.2. Global lake and reservoir storage measurement

Sufficiently high-resolution remote sensing is needed to measure lake and reservoir volume variations. A 500-m resolution global surface water change dataset (Ji et al. 2018) was used in this study. It provides daily surface water mapping derived from MODIS surface reflectance product, MOD09GA version 6, for the period of 2001 to 2016. The product achieved accuracy of over 93% compared with classification results derived from Landsat. In addition, the U.S. Department of Agriculture's Foreign Agricultural Service (USDA-FAS) 10-day near real-time global lake and reservoir elevation dataset (G-REALM) was used. This surface water height product for more than 290 lakes and reservoirs around the world was produced by a semi-automated process developed by the NASA Ocean Altimeter Pathfinder Project, using near real-time data from the Jason-3 mission (2016-current) and archive data from the Topex/Poseidon (1992-2008), Jason-1 (2002-2008), and Jason-2 (2008-2016) missions. The accuracy is expected to better than 10 cm root-mean-square (rms) error for the largest water bodies (e.g. Lake Victoria, Africa), and better than 20 cm rms for smaller ones (e.g. Lake Chad, Africa).
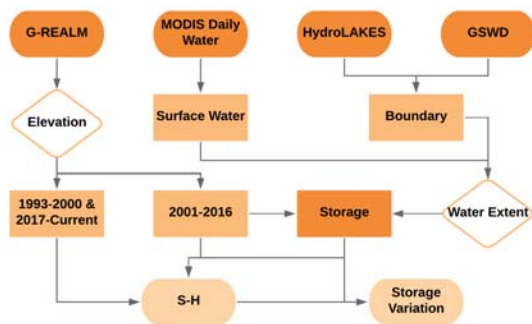
Figure 3. Workflow of lake and reservoir storage measurement from satellite observations.

For each lake or reservoir, we selected surface water images from one MODIS tile or combined tiles, depending on the size of water body, of the 500-m resolution global surface water change dataset (Ji et al. 2018) at the dates with surface water height records between 2001 and 2016. The maximum boundary for each lake or reservoir was delineated based on the HydroLAKES database (Messager et al. 2016), which provides the shoreline polygons of lakes and reservoirs with surface extent above >0.10 km^2, and the maximum surface water product from the Global Surface Water Dataset (GSWD) of the European Commission Joint Research Centre (Pekel et al. 2016). The lake or reservoir surface water extent was derived for all selected surface water images within the maximum boundary. Lake and reservoir storage variations for 2001-2016 were calculated using surface water height records and surface water extents as follows:

$$\Delta S = \Delta h \times (A_1 + A_2)/2 \quad (2)$$

where ΔS is the change of storage from time 1 to time 2, Δh is the surface water height variation with respect to the average height, A_1 is the surface water area at time 1, and A_2 is the surface water area at time 2. The (S-H) relationship, between surface water height records and calculated storage variations, was established for all lakes and reservoirs using data for 2001–2016. Next, storage variations for 1992–2000 and 2017–current were estimated based on the developed (S-H) relationship and combined with estimates for 2001-2016 (Figure 3).

2.3. The operation of the global near real-time monitoring system

The SGRs-derived historical river discharge (Q_h) and the (Q-W) relationship between discharge and water extent for each SGRs site were stored on the National Computational Infrastructure (NCI), in Australia. The NCI also provides a copy of the MODIS MCD43C4 version 6 imagery required that is kept updated with the NASA Land Processes Distributed Active Archive Center (LP DAAC) Distribution Server at the USGS Earth Resources Observation and Science (EROS) Center (https://e4ftl01.cr.usgs.gov/MOTA/MCD43C4.006/).
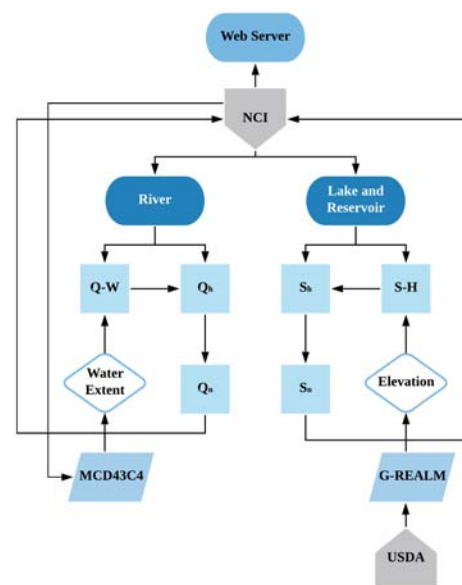
Figure 4. The overall workflow of the global near real-time monitoring system.

Therefore, we are able to derive up to date surface water extent fraction data from the updated MCD43C4 imagery on NCI directly. Next, the near real-time river discharge is calculated from water extent based on the developed (Q-W) relationship. Finally, the updated river discharge time series (Q_n) are stored on NCI. Similar to river discharge, storage variation time series (S_h) and the (S-H) relationship for each lake and reservoir are stored. The updated surface water elevations are retrieved from the USDA's web server. Next, the up-to-date volume changes are derived from the new surface water height observations based on the (S-H) relationship and the new storage variations (S_n) are stored (Figure 4). All data used and produced are stored on the Australian National Computational Infrastructure (NCI) and exposed via THREDDS web services.

All dynamic river discharge and lake and reservoir storage information is displayed online through a web application using the NCI web services. The statistics for rivers are also provided, including real-time streamflow compared to historical streamflow for the time of year, the river discharge hydrograph showing different flood return periods, and recent river discharge plotted over the long-term statistics of discharge for each day of the year. River morphology data (e.g. Hou et al. 2019) may also present useful information that can be assigned to each river reach and may be added in future.

3.   DISCUSSION AND CONCLUSION

This study presents the workflow of a global monitoring system that measures river discharge and lake and reservoir storage variations from satellite observations in near real-time. The algorithm developed by Hou et al. 2018 was used here to predict river discharge, and we extended this approach to a global application and made the best use of the near real-time merit of MCD43C product. The global surface water change dataset (Ji et al., 2018) and G-REALM surface water height product provide basic elements to measure lake and reservoir storages, and G-REALM product makes it possible to both reproduce historical storage records back to 1992 and provide valuable near real-time information. Errors in forcing data (e.g., precipitation, radiation, temperature), a lack of model parameter optimization or model structural deficiencies from the hydrological model can propagate to model-based SGRs. But some model-based SGRs did outperform the model itself, which provide opportunities to improve model estimates through assimilation of SGR discharge estimates. Wide channels and broad floodplains provide the best conditions for SGRs, and lake and reservoir storage measurement targets at water bodies with water extent above 100 km^2, limited by G-REALM product. Higher temporal and spatial input remote sensing data could enhance the capabilities of the monitoring system to observe more rivers, lakes, and reservoirs and to improve the accuracy of the measurements.

Surface water area can also be measured with alternative passive and active satellite sensors, which could be incorporated into the monitoring system. Active microwave sensors (e.g. synthetic aperture radar) are able to observe water regardless of cloud and vegetation cover, but can require complex image processing that is currently not easily automated (Gao, 2015). Passive microwave sensors (e.g., AMSR-E, AMSR2, SMAP) can be used to estimate inundation extent, but their spatial resolution is too coarse to detect narrow or small water bodies, including many rivers, lakes and reservoirs. The most common way to estimate the surface water area of rivers, lakes and reservoirs at global scale has been to use passive visible/infrared bands of satellite sensors such as MODIS and Landsat. The main advantage of MODIS (2000-current) is that it provides daily observations with medium spatial resolution (250 m or 500 m) that are readily available from NASA. Similar observations are available from Sentinel-3 and VIIRS. Landsat (1972-current) provides a higher spatial resolution (ca. 30 m) but is available with much lower frequency (i.e. 16 days). Both are affected by cloud contamination. The Sentinel-2A and B instruments provide potential to improve revisit time for most of the world to 5 days or better with a spatial resolution of 10-60 m. However, they were launched in or after 2015, and hence currently only cover a relatively short period of observation.

There are several satellite radar altimeters commonly used to estimate surface water elevation of large inland water bodies at global scale. These satellites include GEOSAT (1985-1989), Topex/Poseidon (1992-2002), ERS-1 and 2 (1992-2003), GFO (2000-2008), ENVISAT (2002-2010), Jason-1, 2 and 3 (2002-current), and Sentinel-3A and B (2016-current). Their return period ranges from 10 to 35 days. The main limitations of radar altimeters are their low spatial resolution and the influence of the target's surrounding topography (Gao, 2015). In contrast, satellite laser altimeters (e.g. ICESat) are able to measure elevation of water bodies even at smaller sizes or in mountainous regions, as they have higher spatial resolution and smaller cross track spacing (Zhang, et al., 2014). However, they have quite a long return period (e.g. 91 days for ICESat), which makes them unsuitable for operational monitoring. There are other satellite altimetry databases, including the Database for Hydrological Time Series of Inland Waters (DAHITI), the European Space Agency's (ESA) River and Lake data set and the French Space Agency Centre National d'Etudes Spatiales' (CNES)

Hydrology by Altimetry. These datasets, as well as available near real-time *in-situ* water level records (e.g. from the United State Army Corps of Engineers and the United States Geological Survey) could also be implemented in this global monitoring system and this will be the focus of future research.

Long-term records are the basis for designing flood control, irrigation and hydropower systems, and transboundary water agreements, while real-time data are needed to operate water infrastructure, and manage and reduce flood and drought risk (García et al. 2016; Sheffield et al. 2018). They are valuable to make better connections between researchers, policy-makers, and the society for a deeper understanding of the changes that are occurring in our environment due to climate change and anthropogenic activities. Our goal was to contribute global, near real-time information on river, lake and reservoir dynamics to make it easier for government, the community and individuals to access current information on the state of water resources in their region of interest and in a historical context.

ACKNOWLEDGMENTS

REFERENCES

Allen, G.H., & Pavelsky, T.M. (2018). Global extent of rivers and streams. *Science, 361*, 585-588

Alsdorf, D.E., Rodriguez, E., & Lettenmaier, D.P. (2007). Measuring surface water from space. *Reviews of Geophysics, 45*

Barnett, T.P., Adam, J.C., & Lettenmaier, D.P. (2005). Potential impacts of a warming climate on water availability in snow-dominated regions. *Nature, 438*, 303

Brakenridge, G.R., Nghiem, S.V., Anderson, E., & Mic, R. (2007). Orbital microwave measurement of river discharge and ice status. *Water Resources Research, 43*

Busker, T., de Roo, A., Gelati, E., Schwatke, C., Adamovic, M., Bisselink, B., Pekel, J.-F., & Cottam, A. (2019). A global lake and reservoir volume analysis using a surface water dataset and satellite altimetry. *Hydrology and Earth System Sciences, 23*, 669-690

Gao, H. (2015). Satellite remote sensing of large lakes and reservoirs: From elevation and area to storage. *Wiley Interdisciplinary Reviews: Water, 2*, 147-157

García, L.E., Rodríguez, D.J., Wijnen, M., & Pakulski, I. (2016). *Earth observation for water resources management: Current use and future opportunities for the water sector.* Washington, DC: World Bank Group.

Gleason, C.J., & Smith, L.C. (2014). Toward global mapping of river discharge using satellite images and at-many-stations hydraulic geometry. *Proceedings of the National Academy of Sciences, 111*, 4788-4791

Hou, J., Van Dijk, A.I.J.M., Renzullo, L.J., & Vertessy, R.A. (2018). Using modelled discharge to develop satellite-based river gauging: a case study for the Amazon Basin. *Hydrology and Earth System Science, 22*, 6435-6448

Hou, J., Van Dijk, A.I.J.M., Renzullo, L.J., Vertessy, R.A., & Mueller, N. (2019). Hydromorphological attributes for all Australian river reaches derived from Landsat dynamic inundation remote sensing. *Earth System Science Data, 11*, 1003-1015

Ji, L., Gong, P., Wang, J., Shi, J., & Zhu, Z. (2018). Construction of the 500‐m Resolution Daily Global Surface Water Change Database (2001‐2016). *Water Resources Research, 54*, 10,270-210,292

LeFavour, G., & Alsdorf, D. (2005). Water slope and discharge in the Amazon River estimated using the shuttle radar topography mission digital elevation model. *Geophysical Research Letters, 32*

Lehner, B., Liermann, C.R., Revenga, C., Vörösmarty, C., Fekete, B., Crouzet, P., Döll, P., Endejan, M., Frenken, K., & Magome, J. (2011). High‐resolution mapping of the world's reservoirs and dams for sustainable river‐flow management. *Frontiers in Ecology and the Environment, 9*, 494-502

Medina, C., Gomez-Enri, J., Alonso, J.J., & Villares, P. (2010). Water volume variations in Lake Izabal (Guatemala) from in situ measurements and ENVISAT Radar Altimeter (RA-2) and Advanced Synthetic Aperture Radar (ASAR) data products. *Journal of Hydrology, 382*, 34-48

Messager, M.L., Lehner, B., Grill, G., Nedeva, I., & Schmitt, O. (2016). Estimating the volume and age of water stored in global lakes using a geo-statistical approach. *Nature communications, 7*, 13603

Papa, F., Durand, F., Rossow, W.B., Rahman, A., & Bala, S.K. (2010). Satellite altimeter‐derived monthly discharge of the Ganga‐Brahmaputra River and its seasonal to interannual variations from 1993 to 2008. *Journal of Geophysical Research: Oceans, 115*

Pavelsky, T.M. (2014). Using width‐based rating curves from spatially discontinuous satellite imagery to monitor river discharge. *Hydrological Processes, 28*, 3035-3040

Pekel, J.-F., Cottam, A., Gorelick, N., & Belward, A.S. (2016). High-resolution mapping of global surface water and its long-term changes. *Nature, 540*, 418-422

Sheffield, J., Wood, E.F., Pan, M., Beck, H., Coccia, G., Serrat‐Capdevila, A., & Verbist, K. (2018). Satellite remote sensing for water resources management: potential for supporting sustainable development in data-poor regions. *Water Resources Research, 54*, 9724-9758

Van Dijk, A.I.J.M., Brakenridge, G.R., Kettner, A.J., Beck, H.E., De Groeve, T., & Schellekens, J. (2016). River gauging at global scale using optical and passive microwave remote sensing. *Water Resources Research, 52*, 6404-6418

Van Dijk, A.I.J.M., Schellekens, J., Yebra, M., Beck, H.E., Renzullo, L.J., Weerts, A., & Donchyts, G. (2018). Global 5 km resolution estimates of secondary evaporation including irrigation through satellite data assimilation. *Hydrology and Earth System Science, 22*, 4959-4980

Zhang, S., Gao, H., & Naz, B.S. (2014). Monitoring reservoir storage in South Asia from multisatellite remote sensing. *Water Resources Research, 50*, 8927-8943

References

The International Commission on Large Dams. (2020). *https://www.icold-cigb.org/GB/world_register/general_synthesis.asp*.

ALLEN, G. H. & PAVELSKY, T. M. 2015. Patterns of river width and surface area revealed by the satellite‐derived North American river width data set. *Geophysical Research Letters,* 42**,** 395-402.

ALLEN, G. H. & PAVELSKY, T. M. 2018. Global extent of rivers and streams. *Science,* 361**,** 585-588.

ALSDORF, D. E., RODRIGUEZ, E. & LETTENMAIER, D. P. 2007. Measuring surface water from space. *Reviews of Geophysics,* 45.

BARNETT, T. P., ADAM, J. C. & LETTENMAIER, D. P. 2005. Potential impacts of a warming climate on water availability in snow-dominated regions. *Nature,* 438**,** 303.

BARNETT, T. P., PIERCE, D. W., HIDALGO, H. G., BONFILS, C., SANTER, B. D., DAS, T., BALA, G., WOOD, A. W., NOZAWA, T. & MIRIN, A. A. 2008. Human-induced changes in the hydrology of the western United States. *Science,* 319**,** 1080-1083.

BIANCAMARIA, S., LETTENMAIER, D. P. & PAVELSKY, T. M. 2016. The SWOT mission and its capabilities for land hydrology. *Surveys in Geophysics,* 37**,** 307-337.

BIRKINSHAW, S. J., O'DONNELL, G. M., MOORE, P., KILSBY, C. G., FOWLER, H. J. & BERRY, P. A. M. 2010. Using satellite altimetry data to augment flow estimation techniques on the Mekong River. *Hydrological Processes,* 24**,** 3811-3825.

BJERKLIE, D. M., DINGMAN, S. L., VOROSMARTY, C. J., BOLSTER, C. H. & CONGALTON, R. G. 2003. Evaluating the potential for measuring river discharge from space. *Journal of Hydrology,* 278**,** 17-38.

BRAKENRIDGE, G. R., COHEN, S., KETTNER, A. J., DE GROEVE, T., NGHIEM, S. V., SYVITSKI, J. P. M. & FEKETE, B. M. 2012. Calibration of satellite measurements of river discharge using a global hydrology model. *Journal of Hydrology,* 475**,** 123-136.

BRAKENRIDGE, G. R., NGHIEM, S. V., ANDERSON, E. & MIC, R. 2007. Orbital microwave measurement of river discharge and ice status. *Water Resources Research,* 43.

BUSKER, T., DE ROO, A., GELATI, E., SCHWATKE, C., ADAMOVIC, M., BISSELINK, B., PEKEL, J.-F. & COTTAM, A. 2019. A global lake and reservoir volume analysis using a surface water dataset and satellite altimetry. *Hydrology and Earth System Sciences,* 23**,** 669-690.

CHAO, B. F., WU, Y. & LI, Y. 2008. Impact of artificial reservoir water impoundment on global sea level. *Science,* 320**,** 212-214.

COE, M. T. & BIRKETT, C. M. 2004. Calculation of river discharge and prediction of lake height from satellite radar altimetry: Example for the Lake Chad basin. *Water Resources Research,* 40.

CRÉTAUX, J.-F., JELINSKI, W., CALMANT, S., KOURAEV, A., VUGLINSKI, V., BERGÉ-NGUYEN, M., GENNERO, M.-C., NINO, F., DEL RIO, R. A. & CAZENAVE, A. 2011. SOLS: A lake database to monitor in the Near Real Time water level and storage variations from remote sensing data. *Advances in space research,* 47**,** 1497-1507.

FRASSON, R. P. D. M., SCHUMANN, G. J. P., KETTNER, A. J., BRAKENRIDGE, G. R. & KRAJEWSKI, W. F. 2019. Will the Surface Water and Ocean Topography (SWOT) satellite mission observe floods? *Geophysical Research Letters,* 46**,** 10435-10445.

FROST, A. J., RAMCHURN, A. & SMITH, A. 2018. The Australian Landscape Water Balance model (AWRA-L v6). Technical Description of the Australian Water Resources Assessment Landscape model version 6. Bureau of Meteorology, http://www.bom.gov.au/water/landscape/assets/static/publications/AWRALv6_Model_Description_Report.pdf.

GAO, H., BIRKETT, C. & LETTENMAIER, D. P. 2012. Global monitoring of large reservoir storage from satellite remote sensing. *Water Resources Research,* 48.

GLEASON, C. J. & SMITH, L. C. 2014. Toward global mapping of river discharge using satellite images and at-many-stations hydraulic geometry. *Proceedings of the National Academy of Sciences,* 111**,** 4788-4791.

GLEASON, C. J. & WANG, J. 2015. Theoretical basis for at‐many‐stations hydraulic geometry. *Geophysical Research Letters,* 42**,** 7107-7114.

ISIKDOGAN, F., BOVIK, A. & PASSALACQUA, P. 2017. RivaMap: An automated river analysis and mapping engine. *Remote Sensing of Environment,* 202**,** 88-97.

JI, L., GONG, P., WANG, J., SHI, J. & ZHU, Z. 2018. Construction of the 500‐m Resolution Daily Global Surface Water Change Database (2001‐2016). *Water Resources Research,* 54**,** 10,270-10,292.

KLEIN, I., GESSNER, U., DIETZ, A. J. & KUENZER, C. 2017. Global WaterPack–A 250 m resolution dataset revealing the daily dynamics of global inland water bodies. *Remote Sensing of Environment,* 198**,** 345-362.

KOURAEV, A. V., ZAKHAROVA, E. A., SAMAIN, O., MOGNARD, N. M. & CAZENAVE, A. 2004. Ob'river discharge from TOPEX/Poseidon satellite altimetry (1992–2002). *Remote Sensing of Environment,* 93**,** 238-245.

LEFAVOUR, G. & ALSDORF, D. 2005. Water slope and discharge in the Amazon River estimated using the shuttle radar topography mission digital elevation model. *Geophysical Research Letters,* 32.

LEHNER, B., LIERMANN, C. R., REVENGA, C., VÖRÖSMARTY, C., FEKETE, B., CROUZET, P., DÖLL, P., ENDEJAN, M., FRENKEN, K. & MAGOME, J. 2011. High‐resolution mapping of the world's reservoirs and dams for sustainable river‐flow management. *Frontiers in Ecology and the Environment,* 9**,** 494-502.

LEOPOLD, L. B. & MADDOCK, T. 1953. *The hydraulic geometry of stream channels and some physiographic implications,* Washington, D.C., U.S. Government Printing Office.

MEDINA, C., GOMEZ-ENRI, J., ALONSO, J. J. & VILLARES, P. 2010. Water volume variations in Lake Izabal (Guatemala) from in situ measurements and ENVISAT Radar Altimeter (RA-2) and Advanced Synthetic Aperture Radar (ASAR) data products. *Journal of Hydrology,* 382**,** 34-48.

MESSAGER, M. L., LEHNER, B., GRILL, G., NEDEVA, I. & SCHMITT, O. 2016. Estimating the volume and age of water stored in global lakes using a geo-statistical approach. *Nature Communications,* 7**,** 13603.

NIJSSEN, B., O'DONNELL, G. M., LETTENMAIER, D. P., LOHMANN, D. & WOOD, E. F. 2001. Predicting the discharge of global rivers. *Journal of Climate,* 14**,** 3307-3323.

PAPA, F., DURAND, F., ROSSOW, W. B., RAHMAN, A. & BALA, S. K. 2010a. Satellite altimeter‐derived monthly discharge of the Ganga‐Brahmaputra River and its seasonal to interannual variations from 1993 to 2008. *Journal of Geophysical Research: Oceans,* 115.

PAPA, F., PRIGENT, C., AIRES, F., JIMENEZ, C., ROSSOW, W. & MATTHEWS, E. 2010b. Interannual variability of surface water extent at the global scale, 1993–2004. *Journal of Geophysical Research: Atmospheres,* 115.

PAPA, F., PRIGENT, C. & ROSSOW, W. 2008. Monitoring flood and discharge variations in the large Siberian rivers from a multi-satellite technique. *Surveys in Geophysics,* 29**,** 297-317.

PAVELSKY, T. M. 2014. Using width‐based rating curves from spatially discontinuous satellite imagery to monitor river discharge. *Hydrological Processes,* 28**,** 3035-3040.

PAVELSKY, T. M. & SMITH, L. C. 2008. RivWidth: A software tool for the calculation of river widths from remotely sensed imagery. *IEEE Geoscience and Remote Sensing Letters,* 5**,** 70-73.

PEKEL, J. F., COTTAM, A., GORELICK, N. & BELWARD, A. S., 2016. High-resolution mapping of global surface water and its long-term changes. *Nature*, 540, 418-422.

REVILLA-ROMERO, B., BECK, H. E., BUREK, P., SALAMON, P., DE ROO, A. & THIELEN, J. 2015. Filling the gaps: Calibrating a rainfall-runoff model using satellite-derived surface water extent. *Remote Sensing of Environment,* 171**,** 118-131.

SCHELLEKENS, J., DUTRA, E., LA TORRE, A. M.-D., BALSAMO, G., VAN DIJK, A., WEILAND, F. S., MINVIELLE, M., CALVET, J.-C., DECHARME, B., EISNER, S., FINK, G., FLÖRKE, M., PEßENTEINER, S., VAN BEEK, R., POLCHER, J., BECK, H., ORTH, R., CALTON, B., BURKE, S., DORIGO, W. & WEEDON, G. P. 2017. A global water resources ensemble of hydrological models: The eartH2Observe Tier-1 dataset. *Earth System Science Data,* 9**,** 389-413.

SHEFFIELD, J., WOOD, E. F., PAN, M., BECK, H., COCCIA, G., SERRAT‐CAPDEVILA, A. & VERBIST, K. 2018. Satellite remote sensing for water resources management: potential for supporting sustainable development in data-poor regions. *Water Resources Research,* 54**,** 9724-9758.

SHEN, C., WANG, S. & LIU, X. 2016. Geomorphological significance of at‐many‐stations hydraulic geometry. *Geophysical Research Letters,* 43**,** 3762-3770.

SMITH, L. C., ISACKS, B. L., BLOOM, A. L. & MURRAY, A. B. 1996. Estimation of discharge from three braided rivers using synthetic aperture radar satellite imagery: Potential application to ungaged basins. *Water Resources Research,* 32**,** 2021-2034.

SMITH, L. C., ISACKS, B. L., FORSTER, R. R., BLOOM, A. L. & PREUSS, I. 1995. Estimation of discharge from braided glacial rivers using ERS 1 synthetic aperture radar: First results. *Water Resources Research,* 31**,** 1325-1329.

SMITH, L. C. & PAVELSKY, T. M. 2008. Estimation of river discharge, propagation speed, and hydraulic geometry from space: Lena River, Siberia. *Water Resources Research,* 44.

SMITH, L. C., SHENG, Y., MACDONALD, G. & HINZMAN, L. 2005. Disappearing arctic lakes. *Science,* 308**,** 1429-1429.

SOLANDER, K. C., REAGER, J. T. & FAMIGLIETTI, J. S. 2016. How well will the Surface Water and Ocean Topography (SWOT) mission observe global reservoirs? *Water Resources Research,* 52**,** 2123-2140.

TAO, S., FANG, J., ZHAO, X., ZHAO, S., SHEN, H., HU, H., TANG, Z., WANG, Z. & GUO, Q. 2015. Rapid loss of lakes on the Mongolian Plateau. *Proceedings of the National Academy of Sciences,* 112**,** 2281-2286.

TARPANELLI, A., BROCCA, L., LACAVA, T., MELONE, F., MORAMARCO, T., FARUOLO, M., PERGOLA, N. & TRAMUTOLI, V. 2013. Toward the estimation of river discharge variations using MODIS data in ungauged basins. *Remote Sensing of Environment,* 136**,** 47-55.

TONG, X., PAN, H., XIE, H., XU, X., LI, F., CHEN, L., LUO, X., LIU, S., CHEN, P. & JIN, Y. 2016. Estimating water volume variations in Lake Victoria over the past 22 years using multi-mission altimetry and remotely sensed images. *Remote Sensing of Environment,* 187**,** 400-413.

TOURIAN, M. J., SNEEUW, N. & BÁRDOSSY, A. 2013. A quantile function approach to discharge estimation from satellite altimetry (ENVISAT). *Water Resources Research,* 49**,** 4174-4186.

VAN DIJK, A. I. J. M. 2010. The Australian Water Resources Assessment System. Technical Report 3. Landscape Model (version 0.5) Technical Description. CSIRO: Water for a Healthy Country National Research Flagship, http://www.clw.csiro.au/publications/waterforahealthycountry/2010/wfhc-aus-water-resources-assessment-system.pdf.

VAN DIJK, A. I. J. M., BRAKENRIDGE, G. R., KETTNER, A. J., BECK, H. E., DE GROEVE, T. & SCHELLEKENS, J. 2016. River gauging at global scale using optical and passive microwave remote sensing. *Water Resources Research,* 52**,** 6404-6418.

VÖRÖSMARTY, C. J., MCINTYRE, P. B., GESSNER, M. O., DUDGEON, D., PRUSEVICH, A., GREEN, P., GLIDDEN, S., BUNN, S. E., SULLIVAN, C. A. & LIERMANN, C. R. 2010. Global threats to human water security and river biodiversity. *Nature,* 467**,** 555.

WANG, J., SONG, C., REAGER, J. T., YAO, F., FAMIGLIETTI, J. S., SHENG, Y., MACDONALD, G. M., BRUN, F., SCHMIED, H. M. & MARSTON, R. A. 2018. Recent global decline in endorheic basin water storages. *Nature Geoscience,* 11**,** 926-932.

WURTSBAUGH, W. A., MILLER, C., NULL, S. E., DEROSE, R. J., WILCOCK, P., HAHNENBERGER, M., HOWE, F. & MOORE, J. 2017. Decline of the world's saline lakes. *Nature Geoscience,* 10**,** 816.

YAMAZAKI, D., O'LOUGHLIN, F., TRIGG, M. A., MILLER, Z. F., PAVELSKY, T. M. & BATES, P. D. 2014. Development of the global width database for large rivers. *Water Resources Research,* 50**,** 3467-3480.

ZHANG, S., GAO, H. & NAZ, B. S. 2014. Monitoring reservoir storage in South Asia from multisatellite remote sensing. *Water Resources Research,* 50**,** 8927-8943.